PRODUCTION AND ADSORPTION OF VOLATILE TELLURIUM HEXAFLUORIDE

A Dissertation Presented for the
Doctor of Philosophy
Degree
The University of Tennessee, Knoxville

Stephanie Holbrook Bruffey
December 2021

Copyright © 2021 by Stephanie Holbrook Bruffey
All rights reserved.

ACKNOWLEDGEMENTS

The author is grateful to Jason Richards for sharing his knowledge of fluorine chemistry and for his hands-on contributions to the experimental portion of this work. The contributions of Tara Davis, Tamara Keever, and Alicia Raftery are also appreciated.

Many thanks are owed to my committee members and to my committee Chair, Dr. Steven Skutnik. They displayed patience with my non-traditional matriculation path and provided valuable scientific input throughout the development of this dissertation.

I am especially indebted to my husband for his enthusiastic support of my academic pursuits and his unwavering commitment to the wellbeing of our family.

ABSTRACT

Research and development supporting the management of off-gases from nuclear fuel reprocessing has historically been focused on the off-gas streams that arise from aqueous reprocessing technology. With the advent of advanced reactor designs off-gas streams arising from advanced reprocessing methodology, such as that of FV [fluoride volatility] processing, also merit consideration. This work focuses on TeF_6 [tellurium hexafluoride], one of the most volatile radioactive compounds produced during FV, and investigates TeF_6 production, measurement, and abatement technologies.

To assist in on-line monitoring of TeF_6 by Fourier-transformed infrared spectroscopy, this work systematically used the ideal gas law and Beer's Law to report a new molar absorptivity coefficient for TeF_6 at 752 cm^{-1} of 28.51 ± 1.35 cm^2 $Torr^{-1}$.

TeF_6 was produced by the fluorination of Te metal across a temperature range of 100-250°C (degrees Celsius) with a fluorine pressure of 20 Torr. Reaction progress was very fast above 250°C. Two particle sizes of Te metal were used in testing and no significant change in reaction rate was observed for these different particle sizes under the experimental conditions used. When fluorine partial pressure was increased to 40 Torr, the reaction rate was too quick to be measured by this experimental system. It was observed that about 80% of the starting Te metal was converted and that this conversion rate was independent of reaction temperature.

Sorption of TeF_6 in the presence of F_2 [fluorine] by activated alumina was very fast and complete. No practical differences in TeF_6 sorption were observed across the two F_2 pressures used. TeF_6 was observed to be fully removed by copper when the sorbent was heated above 300°C and when fluorine was not present in the gas stream. Sorption was slow, requiring 50 minutes for full TeF_6 removal. SEM [scanning electron microscopy] of the discharged copper sorbent confirmed that Te was present on the copper surface.

TABLE OF CONTENTS

Chapter One Introduction and Research Aims 1
Tellurium Hexafluoride Released during Fluoride Volatility Processing 4
Research Aims 6
Chapter Two Flouride Volatility Processing and Off-gas Management 7
Fluoride Volatility Processing 7
Off-gas Management within Fluoride Volatility Processing 8
Chapter Three Materials and Methods 11
Test Matrix 11
Test System 11
General Test Method 13
FTIR Measurements 16
FTIR Methodology 16
FTIR Error Estimation 19
Materials 19
Sorbent Bed Design 19
Preliminary Work 21
Preliminary Testing with TeO_2 21
Preliminary Testing with Te metal 22
Chapter Four Measurement of Tellurium Hexafluoride Molar Absorptivity Coefficient 25
Background 25
Determination of Molar Absorptivity Coefficient 28
Analysis of Determined Absorptivity Coefficient 30
Deconvolution of TeF_6 and Te_2F_{10} spectral overlap 30
Comparison of Analytical Methodology 34
Technical Notations on Absorptivity Coefficient 36
Chapter Five Tellurium Hexafluoride Production 39
Classical Kinetic Study of Gas-Solid Reactions 39
Experimental Approach 40
Tellurium Hexafluoride Production Characteristics 42
TeF_6 Production Rate as a Function of Temperature 42
TeF_6 Production as a Function of Particle Size 49
TeF_6 Production as a Function of Fluorine Partial Pressure 51
Te Conversion Fraction 51
Analysis of Reaction Curves 53
Chapter Six Tellurium Hexafluoride Sorption 57
Identification of Potential Sorbent Materials 57
Sorption by Activated Alumina 58
Sorption by Copper 60
Scoping Test 1 64
Scoping Test 2 64
Scanning Electron Microscopy of Copper Material 68

Chapter Seven Conclusions 75
List of References 77
Chapter Eight Appendix A: Reaction Data 80
Vita 91

LIST OF TABLES

Table 1-1: Composition of process gas discharged from the fluorination of reference spent fuel. 5
Table 1-2. Boiling points of key fluorinated compounds (Haynes, 2016). 5
Table 3-1: Summary of completed tests. 12
Table 3-2: Volume of test loop components used in TeF_6 extinction coefficient determination. 17
Table 3-3: Sequential F_2 additions during Test 3. 24
Table 4-1: Infrared-active vibrations for TeF_6 and Te_2F_{10}. 26
Table 4-2: Maximum absorbance of TeF_6 as a function of system pressure. 32
Table 4-3: Fraction of Te volatilized based on the mass of recovered solids. 37
Table 4-4: Comparison of calculated gas-phase TeF_6 concentrations 37
Table 5-1: Initial rate of reaction at varied test temperatures. 47
Table 5-2: Fitted parameters for selected tests. 54
Table 6-1: Free energies of reaction for selected TeF_6 and F_2 interactions with Cu. 61
Table 6-2: Tellurium surface concentration on copper sorbent material recovered from Scoping Test 2. 72

LIST OF FIGURES

Figure 1-1: Processing uranium oxide fuel by FV. 2
Figure 1-2. Processing uranium fuel salt by FV. 3
Figure 2-1: UF_6 purification processes as envisioned by Fukasawa, et al. 2020. 10
Figure 3-1: Interconnectivity of research objectives. 12
Figure 3-2: Test loop schematic. 14
Figure 3-3. Laboratory test loop. 14
Figure 3-4. Reaction vessel. 15
Figure 3-5: Te metal and Ni plate post-test. 17
Figure 3-6. Te residue post-test. 18
Figure 3-7: FTIR spectrum of TeF_6. 20
Figure 3-8: Absorbance at 752 cm^{-1} during Test 3. 24
Figure 4-1: Infrared spectra of TeF_6 (The product of pressure and path length is indicated by the numbers associated with each curve). Reproduced from Vissers and Steindler, 1966. 26
Figure 4-2: Infrared spectra of Te_2F_{10} between 450 and 950 cm^{-1} (numbers denote pressure in mm vapor in 10-cm cell). Reproduced from Vissers and Steindler, 1966. 27
Figure 4-3: U-tube equilibrated in liquid nitrogen. 29
Figure 4-4: System Pressure during TeF_6 condensation. 31
Figure 4-5: System pressure during intermittent release of TeF_6. 32
Figure 4-6: Absorption of TeF_6 at 752 cm^{-1} as a function of TeF_6 concentration. 33
Figure 4-7: Infrared spectra of TeF_6 highlighting minor peaks attributable to Te_2F_{10}. 35
Figure 5-1. Ingrowth of TeF_6 as shown by successive FTIR scans. The legend indicates the time of each scan. 41
Figure 5-2: Monitoring of TeF_6 absorbance as a function of reaction time. TeF_6 produced at 200°C using 20% F_2 gas mixture. 43
Figure 5-3: Absorbance measured at 752 cm^{-1} for Test 4 displayed oscillation attributable to poor gas mixing. 44
Figure 5-4: Initial TeF_6 production at varying temperatures. 45
Figure 5-5. Initial reaction rate as a function of temperature. 47
Figure 5-6: Dependence of initial rate of reaction on temperature. 48
Figure 5-7: Two sizes of Te metal particles located on nickel reaction support plate (10-25 µm, L; 37–74µm, R). 50
Figure 5-8. Production of TeF_6 from different particle size fractions. 50
Figure 5-9. Effect of increased F_2 partial pressure on the initial reaction rate. 52
Figure 5-10: Curve fitting for Tests 6-11. 56
Figure 5-11: Correlation of conversion coefficient with reaction temperature. 56
Figure 6-1: Production, steady-state, and sorption phases of Test 10. 59
Figure 6-2. Sorption of TeF_6 by activated alumina at two different F_2 pressures. 61
Figure 6-3: Predominance diagram for the Cu-Te-F system at 200°C. 62

Figure 6-4. Predominance diagram for the Cu-Te-F system at 325°C. 63
Figure 6-5: Predominance diagram for Cu-F-Te system at 365°C. 63
Figure 6-6. Temperature profiles of test 12 with each sorbent temperature hold noted as the letters A–K. 65
Figure 6-7. Comparison of TeF_6 absorbances during sorption phases A and K. 66
Figure 6-8: Temperature and absorption monitoring for Test 13. 67
Figure 6-9: Observe the difference between fresh copper (L), copper exposed to a mixed F_2/TeF_6 stream (middle), and a pure TeF_6 stream (R)..... 69
Figure 6-10: Scanning electron microscopy of fresh copper and fluorine-exposed copper..... 70
Figure 6-11: Granules formed on copper surface having an average composition of CuF. 70
Figure 6-12: SEM of copper sorbent material recovered from Scoping Test 2. .. 71
Figure 6-13: SEM of mapped areas for Scoping Test 2, samples 3 and 4. 74
Figure 8-1: Test 3 measured absorbance at 752 cm^{-1} across test duration. 81
Figure 8-2: Test 4 measured absorbance at 752 cm^{-1} across test duration. 82
Figure 8-3: Test 5 measured absorbance at 752 cm^{-1} across test duration. 83
Figure 8-4: Test 6 measured absorbance at 752 cm^{-1} across test duration. 84
Figure 8-5: Test 7 measured absorbance at 752 cm^{-1} across test duration. 85
Figure 8-6: Test 8 measured absorbance at 752 cm^{-1} across test duration. 86
Figure 8-7: Test 9 measured absorbance at 752 cm^{-1} across test duration. 87
Figure 8-8: Test 10 measured absorbance at 752 cm^{-1} across test duration. 88
Figure 8-9: Test 11 measured absorbance at 752 cm^{-1} across test duration. 89
Figure 8-10: Test 12 measured absorbance at 752 cm^{-1} across test duration. ... 90

CHAPTER ONE INTRODUCTION AND RESEARCH AIMS

Removing radionuclides from facility off-gas streams is important in the deployment of advanced nuclear technology. Limiting gaseous radiological emissions from reactors and fuel cycle facilities is critical for minimizing environmental contamination from a facility, ensuring that the dose received by the general public is not harmful, and supporting the safe long-term disposition of radiological material associated with advanced fuel cycles.

Research and development that supports the management of off-gases from nuclear fuel reprocessing has historically focused on the off-gas streams that arise from aqueous reprocessing technology. However, as Gen-IV reactor development pathways move toward deployment, alternative spent nuclear fuel (SNF) processing and disposition pathways have been considered more actively. Although proposed processing technologies vary widely, several historical SNF processing concepts continue to merit consideration and these technologies could be correlated to specific reactor designs. Most notably, the electrochemical processing of SNF is well-matched with the metallic fuel deployed in fast reactors, and the irradiated metal fuel is easily dissolved into the processing salt and the final metal product suited for fabrication as recycled metal fuel. Salt-fueled reactors, such as the molten chloride fast reactor or a fluoride salt-based thermal reactor, naturally lend themselves to volatility processing methods, recovering uranium from the fuel as either gaseous UCl_x or UF_6.

The subject of this work is tellurium hexafluoride removal from the off-gas streams generated by fluoride volatility (FV) processing. FV methods were used successfully to defuel the spent fuel salt used in the Molten Salt Reactor Experiment at Oak Ridge National Laboratory (ORNL). Beyond that, FV has been a subject of international research and development for several decades as a processing technology that could be used to recycle irradiated uranium oxide fuel (Collins, et al. 2018). The versatility of this method in deployment against multiple types of spent fuel encourages the continued advancement of both the primary separations processes and the secondary supporting processes that include waste treatment, material control and accountability, and engineering designs. Figure 1-1 shows the concept of FV used to recover uranium from irradiated uranium oxide fuel assemblies and Figure 1-2 shows the concept of FV used to recover uranium from irradiated uranium-bearing molten fuel salt.

Volatility processing is especially interesting when considering the management of radioactive off-gas wastes as the product itself (UCl_x or UF_6) resides in the vapor phase with the contaminants of concern. Thus, off-gas treatment flowsheets will both purify the product and reduce radioactive emissions.

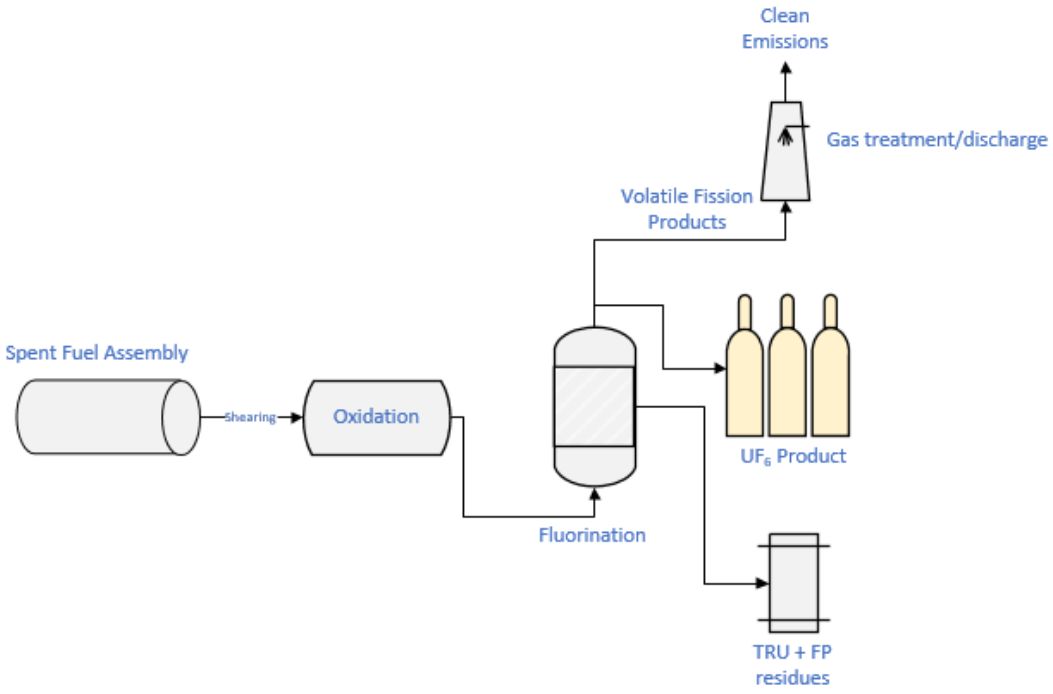


Figure 1-1: Processing uranium oxide fuel by FV.

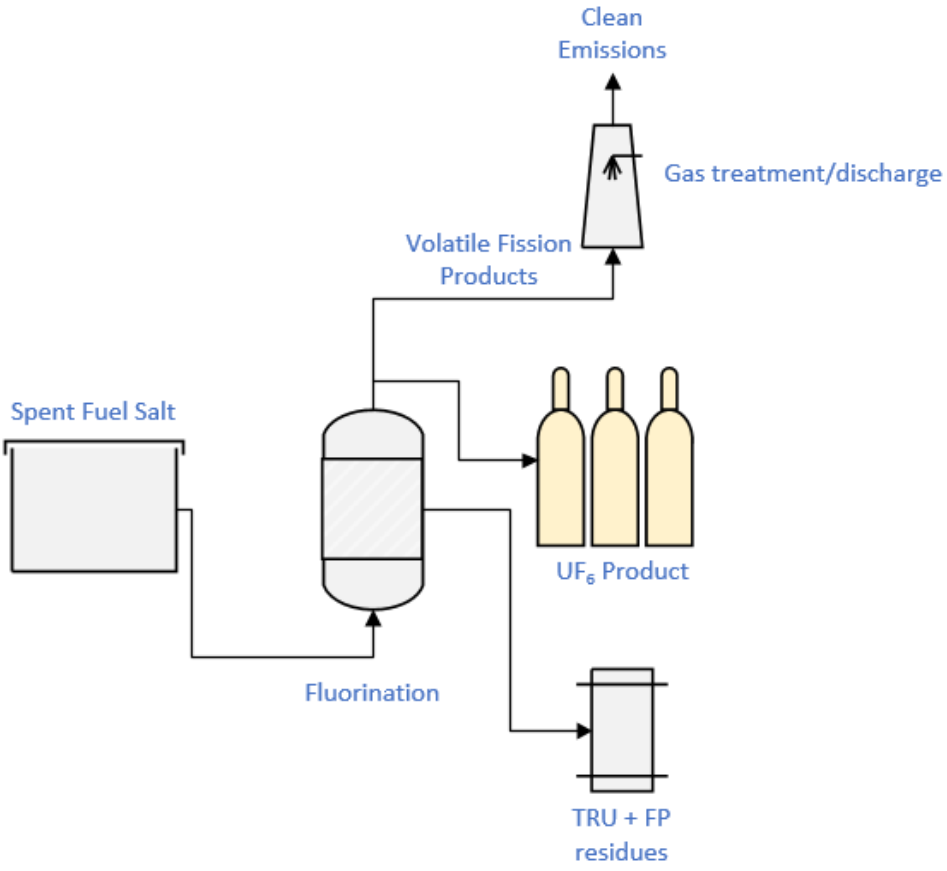


Figure 1-2. Processing uranium fuel salt by FV.

Tellurium Hexafluoride Released during Fluoride Volatility Processing

Recent work performed a series of detailed mass balances for the FV process represented in Figure 1-1. To start, an ORIGEN simulation of pressurized water reactor fuel (Catawba I type) was completed. The peak assembly discharge burnup was 50 GWd/tU, and the average assembly discharge burnup was 40.2 GWd/tU. Three cycles of 395 days each were simulated with 20-day cycle downtimes. The selected cooling time was 15 years. The initial ^{235}U enrichment of the UO_2 fuel was set at 4.0%. The dataset was generated based on uranium fission only; no impurities were assumed to be present in the fuel. The results of this simulation and the associated mass balance identified the gaseous effluent from the fluorination step as being composed as described in Table 1-1.

During the development of these mass balances, gaseous abatement technology that could be used against the radionuclides of concern was also reviewed. With the exception of UF_6, the capture technologies needed to support the management of gaseous components that arise from FV processing had very low technological maturity. Notably, the literature review did not identify any agreement as to the best capture methodology for TeF_6.

With an activity of 21.5 Ci/assembly at 15 years after reactor discharge, ^{125m}Te is formed from the decay of the fission product ^{125}Sb and is in transient and/or secular equilibrium with this parent, indicating that the activity will remain roughly constant until the Sb is sufficiently depleted (^{125}Sb $t_{1/2}$ = 2.76 years). The radiological half-life of ^{125m}Te is 57.4 days and it undergoes internal transition, transforming to stable ^{125}Te.

Of the fluorinated compounds formed in FV, TeF_6 possesses the highest volatility, as shown in Table 1-2.

The lack of validated abatement technology and the high activity of $^{125}TeF_6$, even after 15 years of cooling, prompted the decision to conduct a few scoping tests using common sorbent materials to remove TeF_6 from a gas stream. This work was intended to help understand the magnitude of effort required to fully develop TeF_6 abatement technology. As test design progressed, it became clear that there are very few scientific studies focused on TeF_6 and that there are many unknowns regarding its production, analysis, and adsorption.

Table 1-1: Composition of process gas discharged from the fluorination of reference spent fuel.

Component	**Mass of component present in off-gas stream (g/assembly)**
CF_4	2.79E-03
N_2	5.80E-05
Ne	7.87E-04
Br_2	9.08E+00
Kr	6.44E+01
MoF_6	3.70E+03
TcF_6	8.15E+02
RuF_5	2.06E+03
TeF_6	4.47E+02
I_2	8.45E+01
Xe	9.69E+02
At_2	4.46E-20
Rn	4.76E-12
UF_6	5.81E+05
F_2	Process gas

Table 1-2. Boiling points of key fluorinated compounds (Haynes, 2016).

Compound	**Boiling point (°C)**
TeF_6	−38.9 (sublimation point)
MoF_6	34.0
TcF_6	55.3
UF_6	56.5 (sublimation point)
RuF_5	227

Research Aims

The experimental effort described here addressed several of these unknowns. **The overarching aim of this work was to advance the management of fluoride volatility off-gases through development of TeF_6 production, measurement, and abatement technologies.** Three primary goals were achieved. **First**, online quantitative measurement of TeF_6 by Fourier-transform infrared spectroscopy (FTIR) was advanced through the determination of the TeF_6 molar absorptivity coefficient. **Second**, the production of TeF_6 from Te metal in the temperature range of 100-250°C was characterized as a function of temperature, particle size, and fluorine concentration. **Third**, copper and alumina sorbent materials were tested for their ability to remove TeF_6 from a flowing gas stream.

CHAPTER TWO FLOURIDE VOLATILITY PROCESSING AND OFF-GAS MANAGEMENT

Some of the earliest references in peer-reviewed literature to fluoride volatility processes are from the Oak Ridge National Laboratory and were published in the 1950's (Bresee, J.C. 1957, Milford 1957). In these early processing concepts, used nuclear fuel (typically metal-alloy fuels, rather than UOx fuels) were dissolved into molten salts and the uranium was then removed through fluorination-volatilization and subsequent distillation. The fluorination was performed at 600°C. (Milford 1957). More recently, research interest has been driven by government-sponsored studies in Japan, the Czech Republic, and Russia. Disclosures also indicate that research from these countries is supplemented by commercial interests as well (Fukasawa et al. 2020). Implementation processes currently under study include the FLUOREX process in Japan (a hybrid FV-solvent extraction flowsheet) and a more traditional FV process from the Czech Republic that is kept completely gas-phase.

Fluoride Volatility Processing

Using a FV process to recover resources from LWR UO_x SNF assemblies would require several upfront unit operations. The first is to segment the fuel rods, which is traditionally done through mechanical shearing. This exposes irradiated UO_2 pellets contained within the fuel rods in preparation for the second unit operation, voloxidation. Voloxidation is the oxidation of UO_2 to U_3O_8 at high temperature. The primary purpose of voloxidation in this flowsheet is to pulverize the fuel into a fine powder (<20 µm particle diameter) that can be more easily fluorinated. Voloxidation has the secondary benefit of releasing several important volatile radionuclides (including ^3H and the noble gases) in a controlled manner that facilitates their subsequent abatement.

The fuel powder produced during voloxidation can then be fluorinated according to Equation 1.

Equation 1 $U_3O_8(s) + 9F_2(g) = 3UF_6(g) + 4O_2(g)$

This is a highly exothermic reaction and initiates around 250°C (Uhlir, 2012). The enthalpy of reaction is tabulated as -955.8 kJ/mol U at 298K. The reaction can be controlled by metering either the powder feed or the fluorine gas to maintain a desired reaction temperature. The use of fluorine gas results in highly efficient conversion of U_3O_8 to UF_6. Of course, all other spent fuel components present in

the voloxidized fuel powder will also have the ability to form fluorides. Indeed, fluorination is favorable for almost all of these components, but any non-volatile fluorine species will remain in the chemical reaction vessel as waste. The volatile species will have the potential to travel with the UF_6 product stream into the purification processes. These will typically include: SbF_5, NbF_5, TcF_6, TeF_6, SeF_6, MoF_6, RuF_5. Some oxyfluorides could also be present, depending on conditions.

The temperature of the process will be dependent on the specific equipment designs, although recent advancements have suggested the use of a flame fluorination (Fukasawa, 2020, Uhlir, 2012) which would imply reaction temperatures greater than 1000°C. However, given the thermodynamic favorability of the fluorination above 250°C, flame fluorination is not required. Drivers for lower temperature fluorination include: (1) impure uranium feeds (impurities can complicate flame fluorination and impure feeds are likely in SNF), (2) corrosion or degradation of reaction vessels could be reduced through lower operating temperatures, (3) alternative feeds (such as U_3O_8 powder feed outside of size specification or irradiated molten fuel salts) will not be suitable for flame fluorination.

Of especial interest to the field of nuclear safety and security is the behavior of plutonium within any spent fuel processing operation. In the case of fluorination with F_2, Pu will be fluorinated to non-volatile PuF_4 under typical conditions. If F_2 is present in substantial excess, volatile PuF_6 may be produced but it is thermally unstable and is likely to decompose back to the non-volatile species and be retained in the waste residue. Nevertheless, research efforts have been devoted to the use of alternative fluorinating agents for use in the FV process. These alternative reagents are proposed to decrease the likelihood that volatile PuF_6 would be formed. The most commonly investigated alternative fluorinating reagents have included SF_6, NF_3, and ClF.

Following fluorination, the gaseous UF_6 product stream must be purified, and this purification is discussed in more detail in Section 2.2. The goals of this operation are to remove volatile contaminants and adjust the UF_6 product stream to the desired concentration. The UF_6 product stream may be stored as-received or the uranium can be converted to a more stable oxide storage form, depending on the ultimate destination of the material.

Off-gas Management within Fluoride Volatility Processing

It is an interesting feature of the FV process that gaseous emissions will be controlled somewhat through the same processes as are used to purify the product. For this reason, the treatment sequence used in UF_6 purification and emissions control.

Fukasawa et al. (2020) has the most comprehensive description of a UF_6 purification/emissions sequence. This sequence (Figure 2-1) includes the following chemical traps: (1) UO_2F_2 *(150°C)*, (2) NaF *(350°C)*, (3) MgF_2 *(125°C)*, (4) BaF *(200°C)*, and (5) activated alumina *(ambient temperature)*. Fukasawa recorded a capture efficiency of 99.95 for TeF_6. Work by Watanabe et al. (2016) utilizes a similar treatment approach without the final alumina trap. In that work, TeF_6 was not effectively captured, indicating that the first four chemical traps have limited interactions with TeF_6 and that the bulk of the decontamination reported by Fukasawa et al. 2020 was associated with the activated alumina trap.

For several reasons, this treatment process may not be reflective of the treatment process eventually deployed industrially. First, there may be a desire to recycle excess fluorine present in the off-gas streams back into the fluorination process or even back into the off-gas treatment process to ensure that uranium absorbed on NaF traps remains fully fluorinated. The use of alumina, which will effectively remove all halogens, would prevent fluorine recycle. Second, the required purity of the UF_6 product stream could vary. If UF_6 is intended for recycle back into fast reactor fuel, the tolerances for impurities are high (excluding neutron poisons) and a simple condensation and recovery step may be envisioned for UF_6 purification. In this case, TeF_6 and other higher volatility compounds may not be condensed efficiently and could remain in the off-gas stream. Finally, there is indication in the literature that alumina may not be an effective sorbent for TeF_6 in the presence of high fluorine concentrations. This aspect of TeF_6 sorption will be discussed more fully in Section 6, as will TeF_6-specific sorption studies.

For the purposes of this dissertation, the term *sorption* is used to reflect a non-specific interaction between a solid material and a gaseous compound. *Sorption* could refer to processes such as classical absorption via chemical or physical interactions, reductive decomposition, or catalytic conversion of the gaseous component to a non-volatile species.

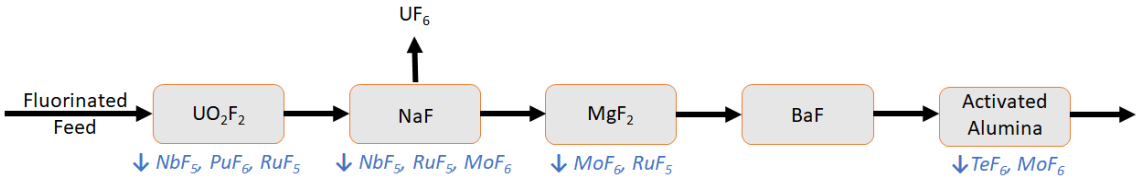


Figure 2-1: UF_6 purification processes as envisioned by Fukasawa, et al. 2020.

CHAPTER THREE MATERIALS AND METHODS

The three primary objectives outlined in Section 1 were achieved through a series of 13 tests. All tests began with fluorination of tellurium to produce TeF_6 as described by Equation 2. After TeF_6 production, the material was either discharged, sorbed, or condensed as required to support the specific objectives.

Equation 2 $Te(s) + 3F_2(g) \rightarrow TeF_6(g)$

The objectives of this work (to improve quantification of TeF_6, to understand TeF_6 production, and to characterize potential TeF_6 sorbents) were closely connected, as reflected in Figure 3-1. All parametric kinetic tests were continuously monitored by Fourier-transform infrared spectroscopy (FTIR), and determination of the molar absorptivity coefficient was intended to support that monitoring. Understanding how TeF_6 was sorbed by two common materials was enabled through continuous FTIR monitoring and drew upon kinetic studies to ensure that the sorbate stream was produced and steady prior to sorption by copper or alumina.

Test Matrix

Completed tests are shown in Table 3-1 with test conditions and notes.

Test System

Handling F_2 gas necessitates specialized experimental equipment, an understanding of safe F_2 handling practices, and a fundamental understanding of corrosion, hydrolysis, and other common F_2 operational challenges. Additionally, TeF_6 is more toxic to humans than F_2 and has very low exposure limits. The equipment used supported the safe handling of all reagents. It is constructed primarily of stainless steel that has been passivated for use in F_2 handling. Stainless steel is not compatible with fluorine at high temperatures, so for higher temperature operations (>125℃), high nickel alloys (H-276 or Inconel-625) or Ni-coated reactors were required.

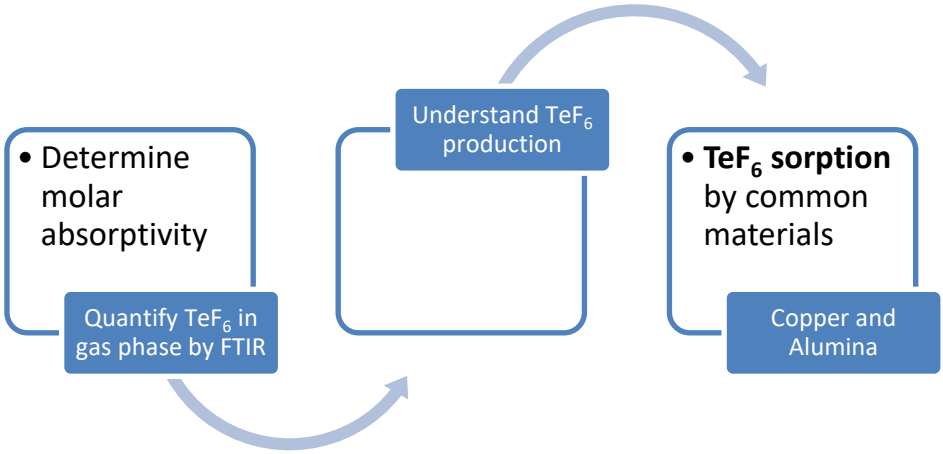


Figure 3-1: Interconnectivity of research objectives.

Table 3-1: Summary of completed tests.

Test	Reaction temperature (°C)	Sorbent (temperature, °C)	Particle size of Te (µm)	F_2 pressure (Torr)	Comments
1	250	n/a	n/a	20	TeO_2
2	250	n/a	n/a	20	TeO_2
3	250	n/a	10–25	20	Unsieved Te metal
4	200	n/a	10–25	20	F_2/N_2 not well-mixed
5	100	n/a	10–25	20	
6	150	n/a	10–25	20	
7	150	n/a	37–74	20	
8	125	n/a	10–25	20	
9	200	Alumina (35)	10–25	20	Non-activated alumina
10	200	Alumina (35)	10–25	20	
11	200	Alumina (35)	10–25	40	
12	200	Copper (50–335)	10–25	40	Used 60 mg Te
13	200	Copper (25-365)	10-25	20	

The test loop is represented in Figure 3-2. Primary components included a heated reactor used to produce TeF_6 from Te metal, a sorbent test column, a metal bellows recirculation pump, a vacuum pump, a flowmeter, pressure gauges with measurement uncertainties of 0.01 Torr, a mass flow meter, thermocouples within the reaction vessel, and a Fourier-transform infrared (FTIR) spectrometer. A picture of the entire test loop is shown in Figure 3-3, and the reaction vessel is shown in more detail in Figure 3-4. Figure 3-3 does not show the sorbent beds that were connected to the loop during tests 9–13. When the inlet-side and effluent-side valves of the sorbent bed were open, the sorbent bed was in line with the test loop.

This work relied heavily on the use of the ideal gas law and measured pressures to calculate the amount of TeF_6 in the test loop. To support this, precise volumes of the test loop components were determined. The main loop was determined through previous work to have a known calibrated volume of 0.551 L. The entire test system was evacuated and all loops were closed. The main loop was filled with 99.55 Torr N_2 (2.98×10^{-3} mols, based on a system volume of 0.551 L and a system temperature of 21.5°C). Each test system side loop was sequentially opened and the system pressure, which decreased with each sequential addition, was monitored. From this, precise measurements of each test system component could be determined. The data for this determination is shown in Table 3-2.

General Test Method

Each test followed a similar experimental method. First, approximately 30 mg of Te powder was transferred to a nickel plate and placed inside the reaction vessel and in the heating zone. If a sorbent bed was in use, then it was filled with adsorbent and placed in line with the test loop. The system was tested for large leaks and then evacuated and refilled with N_2 three times to remove any residual moisture. The system was then evacuated, and a formal leak check was performed. The system was assumed to be leak-tight if the leak rate was less than 0.01 Torr/min.

The reaction vessel and sorbent bed were brought to temperature, filled with 100 Torr N_2, and isolated from the recirculation loop. The recirculation loop was evacuated, filled with a 20% F_2 mixture made by combining 20 Torr F_2 with 80 Torr N_2. Tests 11 and 12 used a 40% F_2 mixture while maintaining the same overall pressure. The gases were poorly mixed during early tests, so a 45–60 min recirculation period was added after the gas was added to the test loop to ensure that the gas was well mixed before introducing it to the reaction vessel.

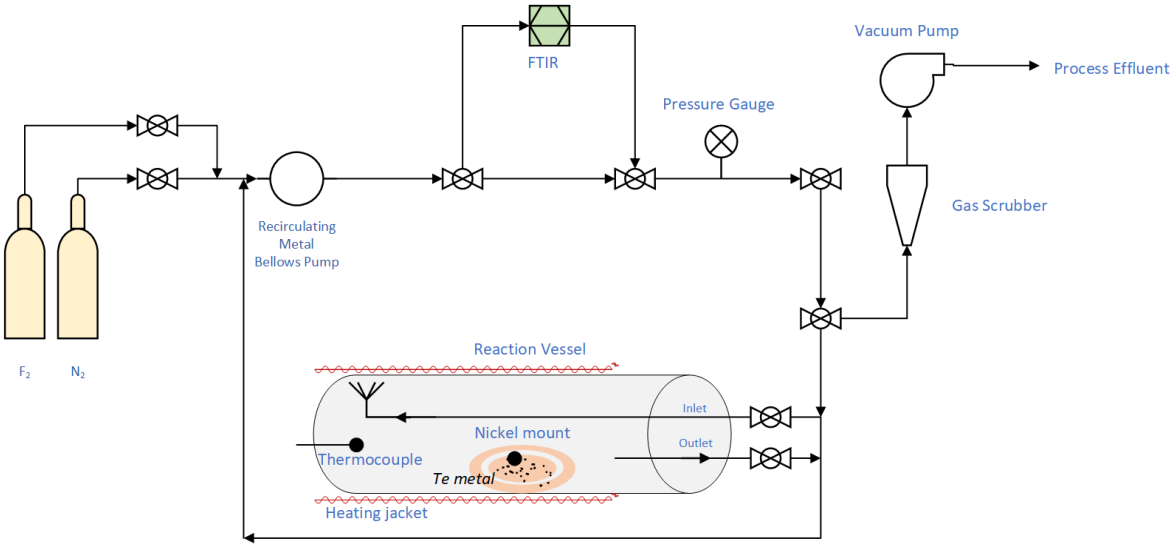


Figure 3-2: Test loop schematic.



Figure 3-3. Laboratory test loop.



Figure 3-4. Reaction vessel.

After gas mixing, the reaction vessel was opened to the recirculation loop. The reaction was monitored by FTIR with scans conducted as frequently as every 14 s. When FTIR measurements indicated that TeF_6 production was complete or plateaued, the gas flow was the circulated through the sorbent bed. FTIR monitored decreases in the TeF_6 concentration. When TeF_6 sorption was complete, the gas was discharged into a trapping bed, and the system was evacuated and refilled with N_2 three times before bringing to ambient pressure with N_2 and breaking the system. During testing, the reactor temperature and system pressures were continuously monitored.

The nickel plate located inside the reactor was retrieved, along with any unreacted Te metal. Images of the nickel plate and Te residue are shown in Figures 3-5 and 3-6. The orange coloring is attributed to possible silver fluoride compounds on the surface of the plate; Ag residue could be present on the plate post-manufacturing, and the plates were used as-received. Silver fluorides are hygroscopic, and some liquid was observed on the plate after removing it from the reactor, as shown in Figure 3-6. The residue was dissolved into 2% HNO_3. Drops of HF were added to each sample to promote the dissolution of any partially reacted Te, which could be in the form of TeF_x. This solution was analyzed by inductively coupled plasma–mass spectrometry (ICP–MS) to quantify the amount of Te unreacted in each test.

The sorbent beds were poured out in aliquots directly into glass vials. The copper materials were analyzed by scanning electron microscopy-electron dispersive spectroscopy (SEM-EDS) using a Phenom XL Desktop SEM.

FTIR Measurements

The infrared spectra were taken with an ABB MB3000 FTIR fitted with a 12.16 cm stainless-steel gas cell with ZnSe windows.

FTIR Methodology

All spectra were taken with a resolution of 4 cm^{-1} and were the average of five scans. For each run, a background spectrum was collected while the system was under vacuum. A spectrum of the mixed F_2/N_2 was also collected before reaction initiation. After reaction initiation, TeF_6 is easily monitored by a strong peak at 752 cm^{-1}, as shown in Figure 3-7. Other absorption bands of note are bands associated with trace HF (4,000 cm^{-1}) resulting from trace water within the test system and trace CO_2 (2,300–2,200 cm^{-1}). More detailed discussion of collected TeF_6 spectra is provided in Section 4.

Table 3-2: Volume of test loop components used in TeF_6 extinction coefficient determination.

Test System Component	Pressure (Torr)	Total Volume (L)	Component Volume (L)
Main loop	99.55 ± 0.01	0.551[a]	0.551[a]
V1 - FTIR	78.28 ± 0.01	0.701 ± 0.007	0.150 ± 0.007
V2 - alumina trap	74.36 ± 0.01	0.738 ± 0.010	0.037 ± 0.012
V3 - copper trap	67.79 ± 0.01	0.809 ± 0.011	0.071 ± 0.015
V4 - metal bellows pump	59.11 ± 0.01	0.928 ± 0.012	0.119 ± 0.016
V5 - U-tube	53.06 ± 0.01	1.034 ± 0.014	0.106 ± 0.019
V7 - production reactor	36.03 ± 0.01	1.522 ± 0.018	0.489 ± 0.023
[a]*Benchmarked value*			

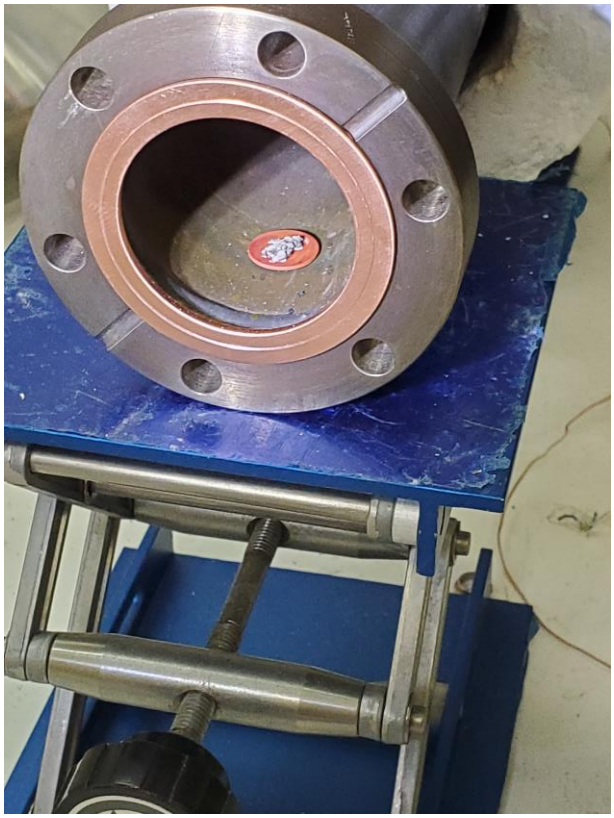


Figure 3-5: Te metal and Ni plate post-test.



Figure 3-6. Te residue post-test.

FTIR Error Estimation

A conservative estimation of instrumental error was performed by analyzing the measured absorption at 752 cm^{-1} for 31 replicate spectra obtained during Test 7. The absorbance values averaged 1.953 with a standard deviation of 0.031. Using values centered near an absorbance of 2 introduces conservativism into the error estimation, as the instrument is most accurate with values from 0–1.5. The 95% confidence interval for this data set was 1.953 ± 0.011. This translates to a relative percent error of 0.55%. This relative percent error was assumed to apply to all FTIR data and was used in error propagation when required.

Materials

Te metal was from CERAC chemicals with a purity of >99.99%. It was sieved with commercially available sieves to separate particle size fractions of 10–25, 25–37, and 37–74 µm. F_2 gas was used as-received from Linde plc. Copper was purchased from Sigma-Aldrich as -20-+30 mesh shot with 99.95% purity. Technical grade TeO_2 was procured from Beantown Chemical and was sieved to establish that the particle size of the material was <38 µm.

The alumina was Delta F200 3/16 in. γ-alumina pellets. Prior to use, the alumina was dried at 100℃ under flowing dry air before being crushed and ground in a mortar and pestle (this was not done for the test using non-activated alumina). Particle size was variable with no particles larger than 1 mm in diameter.

Sorbent Bed Design

Throughout the experiments described here, efforts were taken to minimize the amount of TeF_6 produced and thus reduce any potential exposure risk if system failures are encountered. For this reason, the sorbent beds themselves were sized relatively small. Each bed was 6 in. deep and held in passivated Inconel tubing with an inner diameter of ¼ in. Sorbent particle sizes were also small to minimize channeling and to maintain an appropriate sorbent particle diameter to bed diameter ratio. The sorbent tubes were heated with heat tape external to the tube. The sorbent material was supported by copper wool plugs at the effluent side of the column. The columns were held vertically with a downflow configuration.

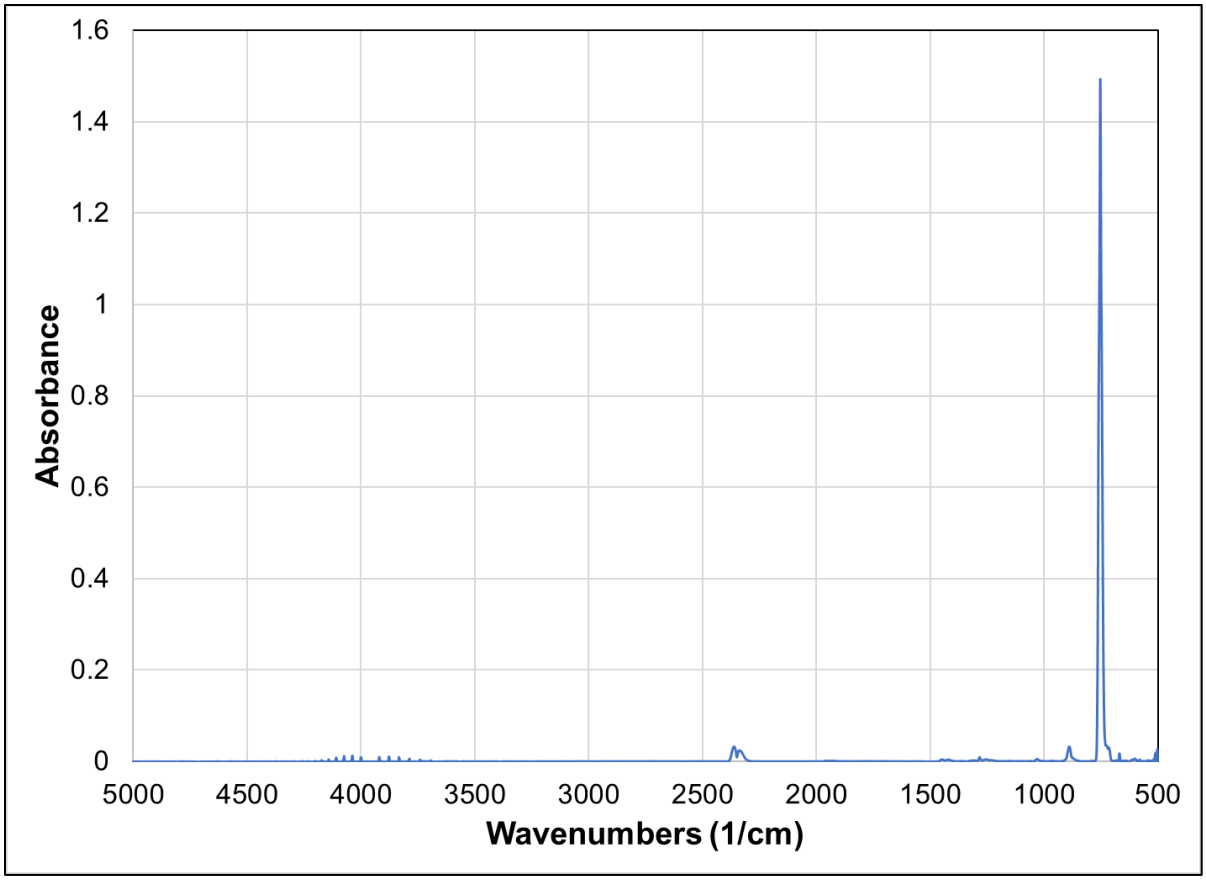


Figure 3-7: FTIR spectrum of TeF_6.

Preliminary Work

Several preliminary tests laid the groundwork for the experimental protocols used in Tests 5–13.

Preliminary Testing with TeO_2

An examination of the literature showed that both Te metal and TeO_2 have been successfully fluorinated to produce TeF_6. As described in Table 3-1, two tests were performed with the intention of fluorinating TeO_2 to form TeF_6. This reaction is shown in Equation 3.

Equation 3 $TeO_2(s) + 3F_2(g) \rightarrow TeF_6(g) + O_2(g)$

HSC Chemistry calculates this reaction to be thermodynamically favorable in the temperature range of 0–1000°C, with a ΔG of -238 kcal/mol at 100°C and -231 kcal/mol at 300°C.

Two studies reported successful fluorination of TeO_2 to produce TeF_6.The first, Campbell and Robinson (1956), reports formation of TeF_6 from TeO_2 at temperatures from 100–200°C. In those experiments, flow rates of 0.5–10 L/h of F_2 were used, with F_2 diluted with 0–5 L/min of N_2. The reactor design appears to have been a flow-through design.

The second study (Clark, et al. 2015) shows the fluorination of both Te and TeO_2 using NF_3 as the fluorinating agent. The experiments were conducted using 5% NF_3 in argon and the temperature of the reactor was ramped, with TeF_6 formation observed beginning at 350°C.

Given that F_2 is a more powerful fluorinating agent than NF_3, it was assumed that fluorination of TeO_2 using F_2 would initiate at lower temperatures, as was documented by Campbell and Robinson (1956).

Test 1 was conducted by placing 30.9 mg of TeO_2 in the reactor on a nickel support plate. 12.03 Torr of F_2 was added to the system, followed by N_2 addition to bring the total pressure to about 100 Torr. The reaction vessel temperature was ramped from ambient temperature to 200°C over the course of 90 minutes while continuously monitoring the IR spectra to observe any production of TeF_6. No TeF_6 was observed. An additional 50 Torr of F_2 was then added to the system and the temperature was increased to 250°C with additional hold time. No TeF_6 was observed. The reaction vessel has a maximum temperature limit of 250°C, which prevented additional temperature increases. The test was discontinued. After cooling and evacuating the system, the nickel support plate was recovered and no physical change in the appearance of the TeO_2 was observed.

Test 2 was conducted very similarly to Test 1, but the decision was made to forego the temperature ramp and bring the reaction vessel to temperature prior to introducing F_2. 22.8 mg of TeO_2 was added to the reaction vessel and the reaction vessel was brought to 250°C. 25.10 Torr F_2 was introduced into the main test loop and was balanced to about 100 Torr with N_2. This gas mixture was then introduced into the heated reaction vessel and the IR spectra of the recirculating gas was continuously monitored for evidence of TeF_6. The mixture was allowed to circulate for 60 min and no TeF_6 was observed on the IR spectra. After Test 2 was concluded and all F_2 was evacuated from the system, the reaction vessel was opened and the TeO_2 powder did not show any visual changes.

The failure of Test 1 and Test 2 to produce TeF_6 was unexpected based on the results described in Campbell and Robinson (1956) and Clark et al. (2015) and unexpected due to the favorable thermodynamics of the reaction. It is unclear what could have prevented the formation of TeF_6, but possible causes include (1) that the reaction required a greater stoichiometric excess of F_2 than was present in these tests, (2) the source material was hydrated or in some other way prevented from reacting with F_2, or (3) that TeO_2 was partially fluorinated to a non-volatile form that did not transport to the FTIR (for example, TeF_4 is described as a white non-volatile solid and could look very similar to the white non-volatile TeO_2 powder used). As the objective of this testing was to produce a source of TeF_6 for use in sorption testing, no further testing was conducted with TeO_2 once Te metal was found to be easily fluorinated to TeF_6.

Preliminary Testing with Te metal

Test 3 (Table 3-1) was a preliminary test designed to determine whether TeF_6 could be produced from Te metal by fluorination with F_2 at 250°C. The general test method was followed with one key exception: fluorine gas was introduced intermittently (Table 3-3). This was intended to assess how much excess fluorine would be required during each test. At the time, system volumes were not known. 29.4 mg of unsieved Te metal was placed into the reactor (2.304×10^{-4} mols Te). The system was configured during F_2 addition to have the main loop, IR, and MBP loop in-line, generating a system volume of 823 cm^3. 10.17 Torr F_2 was added to the system in this configuration, corresponding to an addition of 4.56×10^{-4} mols F_2. FTIR scans immediately indicated TeF_6 production with a peak growing in at 752 cm^{-1}. After 5 min, the measured absorbance of this peak began to decay. An additional 7.28×10^{-4} mol of F_2 was added to the system and the absorbance of the primary peak began to increase again, plateaued, and remained steady for 8 minutes. A third F_2 addition (7.21×10^{-4} mol) was performed, but no further changes in the measured absorbance of the primary

peak were observed. (Figure 3-8). The TeF_6 was held recirculating in the test loop for an additional hour and the measured absorbance remained steady.

Several key conclusions were drawn from this preliminary test. First, that TeF_6 could be produced by fluorinating Te metal with F_2. Second, that roughly 20 Torr of F_2 would be sufficient to bring the reaction to completion. This corresponds to a stoichiometric ratio of 2.76 F_2:Te and indicates that some Te will remain unreacted (as Equation 2 prescribes a stoichiometric ratio of 3 F_2:Te). Third, no decay of the TeF_6 peak was observed over the hour following the final F_2 addition. This indicates that there is no deposition or loss of TeF_6 to the system and that it is stable in the test system over the time periods studied here.

As a note, pure F_2 gas is no longer available in laboratory-scale quantities so operating under a large excess of F_2 was not desirable in terms of conservation of resources.

Table 3-3: Sequential F_2 additions during Test 3.

Fluorine Addition (Torr)	Addition time (min)	System volume (cm^3)	F_2 added (mol)	F_2 (total mol)	System configuration
10.17	0	823 ± 18	4.56×10^{-4}	4.56×10^{-4}	Main, V1, V4
10.20	14	1312 ± 29	7.28×10^{-4}	1.18×10^{-3}	Main, V1, V4, V7
10.10	22	1312 ± 29	7.21×10^{-4}	1.95×10^{-3}	Main, V1, V4, V7

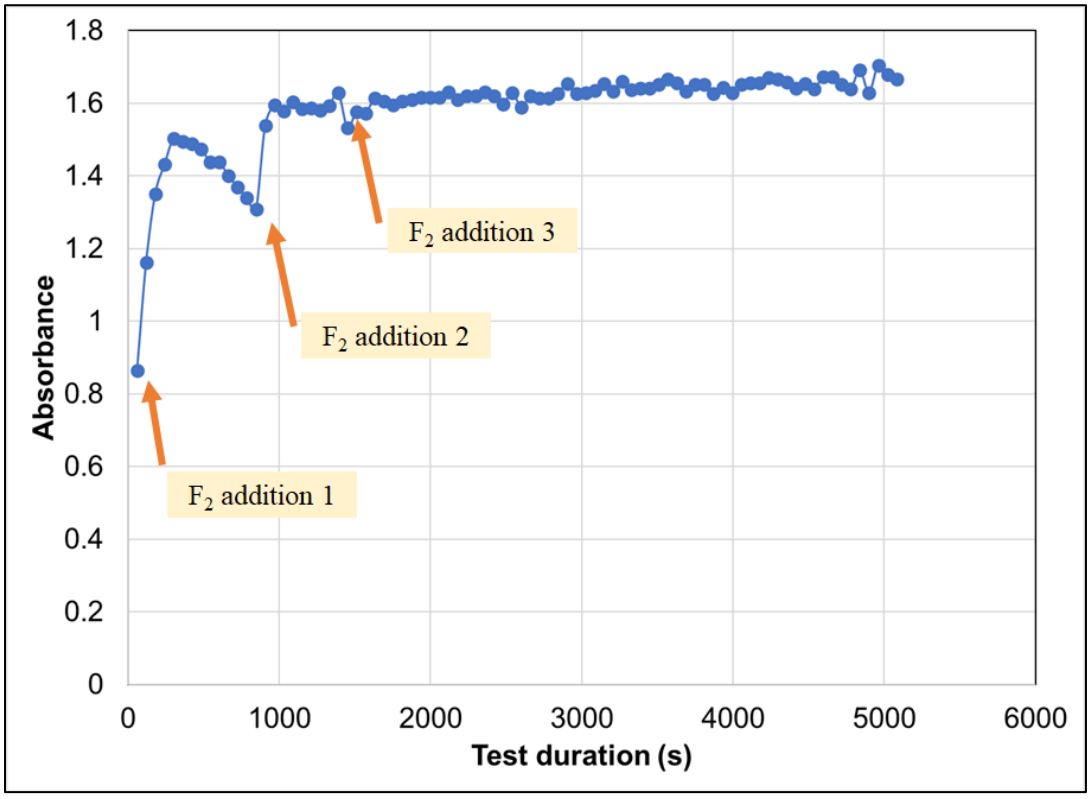


Figure 3-8: Absorbance at 752 cm^{-1} during Test 3.

CHAPTER FOUR MEASUREMENT OF TELLURIUM HEXAFLUORIDE MOLAR ABSORPTIVITY COEFFICIENT

In order to support FTIR measurements the molar absorptivity of the TeF_6 primary peak was determined.

Background

There is very limited spectroscopic information available on TeF_6, except for the assignment of primary vibrational bands. A collection of TeF_6 spectra obtained at different pressures is shown in Figure 4-1.

The infrared active bands for TeF_6 and Te_2F_{10} are shown in Table 5. McDowell et al. (1986) reported an absorptivity coefficient (ε) of 1,751 cm^2 atm^{-1} (2.3 cm^2 $Torr^{-1}$), for the primary TeF_6 peak at 752 cm^{-1}. This peak arises from the v_3 stretching band. McDowell et al. (1986), Vissers and Steindler (1966), and Shimanouchi (1972) contain the only spectroscopic information found during a review of available literature.

Vissers and Steindler (1966) include Te_2F_{10} in their discussion of tellurium fluoride species. Te_2F_{10} is a dimer species that can be coincident with TeF_6 and it has a fundamental band that overlaps the 752 cm^{-1} infrared active band of TeF_6 (Table 4-1). Te_2F_{10} also has 714, 734, and 890 cm^{-1} infrared bands (Figure 4-2). It is a colorless liquid at room temperature. This dimer species has been reported to be present in TeF_6 at abundances of 5-10% and can be purified through distillation. Since the most intense Te_2F_{10} and TeF_6 bands overlap directly, the presence of Te_2F_{10} must be confirmed through the presence of the secondary 734 $cm^{-1}$and 714 cm^{-1} bands. Vissers and Steindler (1966) indicate that Te_2F_{10} may be more absorptive than TeF_6. Intuitively, Te_2F_{10} will be less abundant in fluorine-rich environments where the equilibrium described by Equation 4 favors TeF_6.

Equation 4 $2TeF_6(g) \leftrightarrow Te_2F_{10}(l) + F_2(g)$

HSC Chemistry (Outotec, 2018) calculates that Equation 4 has a free energy of reaction (ΔG) of 69 kcal/mole, favoring the formation of TeF_6.

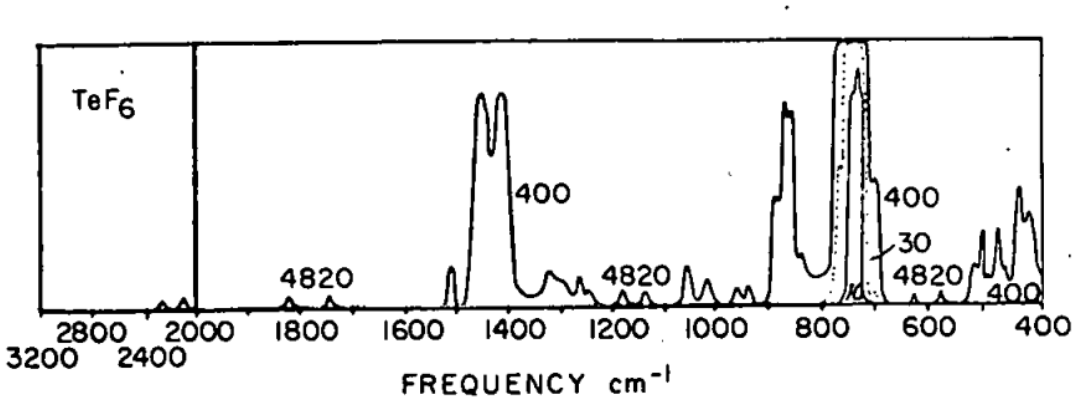


Figure 4-1: Infrared spectra of TeF_6 (The product of pressure and path length is indicated by the numbers associated with each curve). Reproduced from Vissers and Steindler, 1966.

Table 4-1: Infrared-active vibrations for TeF_6 and Te_2F_{10}.

TeF_6 infrared active bands	**Wavenumber (cm^{-1})**
$v_2 + v_6$	871[b]
v_3 (stretching)	751[a]
v_4 (deformation)	327[a]
Te_2F_{10} infrared active bands	**Wavenumber (cm^{-1})**
resonance	890[b]
v_6	752[b]
v_7	734[b]
v_9	714[b]
[a]Shimanouchi, 1972	
[b]Vissers and Steindler, 1966	

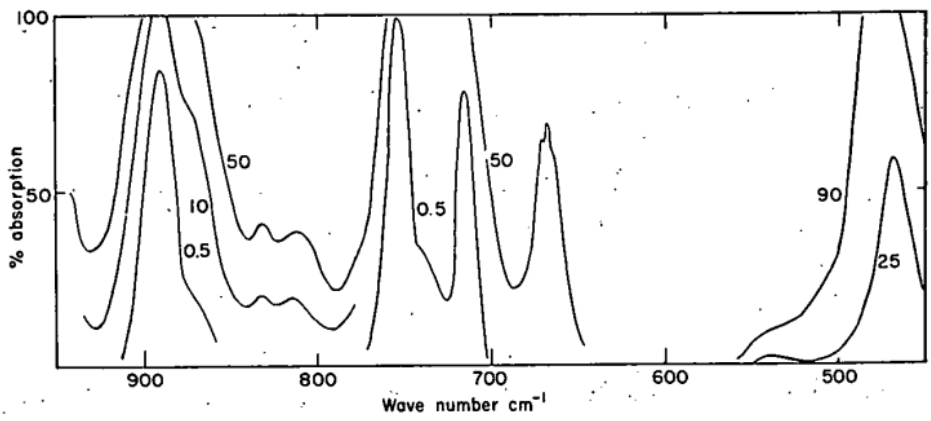


Figure 4-2: Infrared spectra of Te_2F_{10} between 450 and 950 cm^{-1} (numbers denote pressure in mm vapor in 10-cm cell). Reproduced from Vissers and Steindler, 1966.

Determination of Molar Absorptivity Coefficient

Beer's Law was used to determine the molar absorptivity coefficient of the primary TeF_6 peak at 752 cm^{-1}.

Equation 5 $A = \varepsilon bc$

where A = measured absorbance (unitless); ε = absorptivity coefficient (cm^2 $Torr^{-1}$); b = cell path length (cm); c = concentration (Torr cm^3)

The methodology to perform the absorptivity coefficient determination is described here in detail and broadly involved (1) the determination of test loop volume, (2) the generation of a pure TeF_6 condensate, (3) release of pure TeF_6 into the test loop to generate known pressures, and finally, (4) measurement of the absorbance of a known pressure of TeF_6. This approach provides known gas pressures and a known gas volume, allowing calculation of TeF_6 concentration by the Ideal Gas Law.

First, the volume of the test loop was determine as described in Section 3.

Second, TeF_6 was produced at 200°C by the method described in Section 3.1. TeF_6 was then condensed into a U-tube by allowing a mixed $F_2/TeF_6/N_2$ gas stream to pass through the U-tube while the U-tube was equilibrated in a liquid nitrogen (LN2) bath (Figure 4-3). The boiling point of N_2 is -195.8°C and the boiling point of fluorine (F_2) is –188.11°C. The boiling point of TeF_6 is -38.9°C and it is easily condensed by LN2. The condensation of TeF_6 was tracked qualitatively by FTIR and when the spectrum was not distinguishable from a background spectrum, the U-tube was isolated from the main system and the main system was evacuated. The U-tube was burped to allow the headspace (which contained F_2 and N_2) to transfer to the evacuated main loop, which was again evacuated. This burping was repeated until the headspace of the vessel was evacuated, leaving only TeF_6 condensate under vacuum in the U-tube. The pressure of the system was monitored during TeF_6 condensation and decreased from 103 Torr to 91 Torr, with the residual pressure comprised of F_2 and N_2. The residual F_2 and N_2 were discharged from the loop and the loop was fully evacuated.

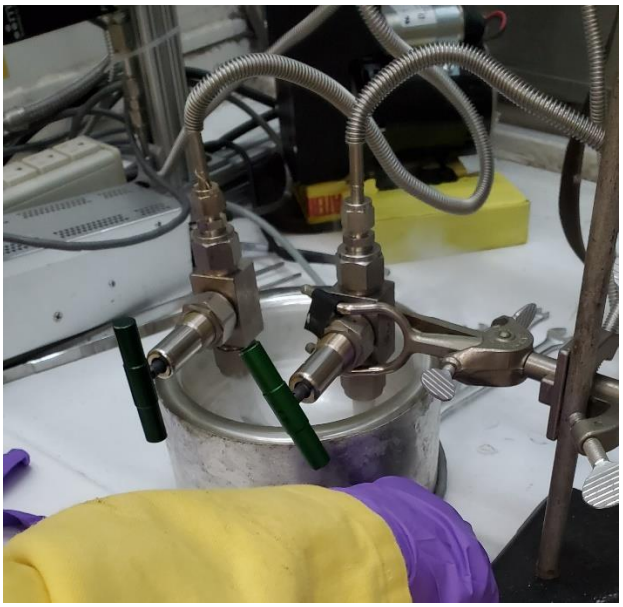


Figure 4-3: U-tube equilibrated in liquid nitrogen.

Third, the U-tube was then brought to roughly room temperature in a water bath. The U-tube was opened to allow some TeF_6 to transfer to the evacuated main loop. The pressure change in the main loop, the known volume of the main loop, and the known temperature of the test system can then used to determine the mols of TeF_6 in the test system. Then, an additional aliquot of TeF_6 was added, the pressure change was noted, and a second spectrum was taken, where the absorbance was the sum of the first and second aliquots. In total, five aliquots of TeF_6 were transferred to the main loop and the measured absorbances ranged from 0.266 to 1.80 AU. The pressure of the system during condensation is shown in Figure 4-4 and the pressure of the system during TeF_6 addition is shown in Figure 4-5.

The measured absorbances at each pressure are tabulated in Table 4-2, along with mols of TeF_6 (calculated via the Ideal Gas Law) and the calculated concentration.

The data in Table 4-2 was used to generate a Beer's Law plot (Figure 4-6) and a linear regression was used to determine the slope of the line. The slope is equal to ε*path length (b). **Using a path length of 12 cm, the molar absorptivity was determined via this linear regression to be 28.51 ± 1.35 cm^2 $Torr^{-1}$.**

Analysis of Determined Absorptivity Coefficient

The determined value of ε (28.51 ± 1.35 cm^2 $Torr^{-1}$) is significantly larger than that of the single reported literature value of 2.3 cm^2 $Torr^{-1}$ (McDowell et al. 1986). For this reason, a careful examination of the procedures and methods used in this determination was performed.

Deconvolution of TeF_6 and Te_2F_{10} spectral overlap

The only potential source of error identified was the presence of the Te_2F_{10} dimer. Reviewing the spectra reveals that several low-absorbance peaks indicative of the dimer are present (Figure 4-7).

There are many approaches that can be used to resolve two overlapping components within a spectrum. However, these methods almost universally require the use of extinction coefficients for at least one (but often several) peak of each component. That is not available in this case. Furthermore, interactions between components can lead to amplification or depression of absorbances and this can further complicate spectral deconvolution.

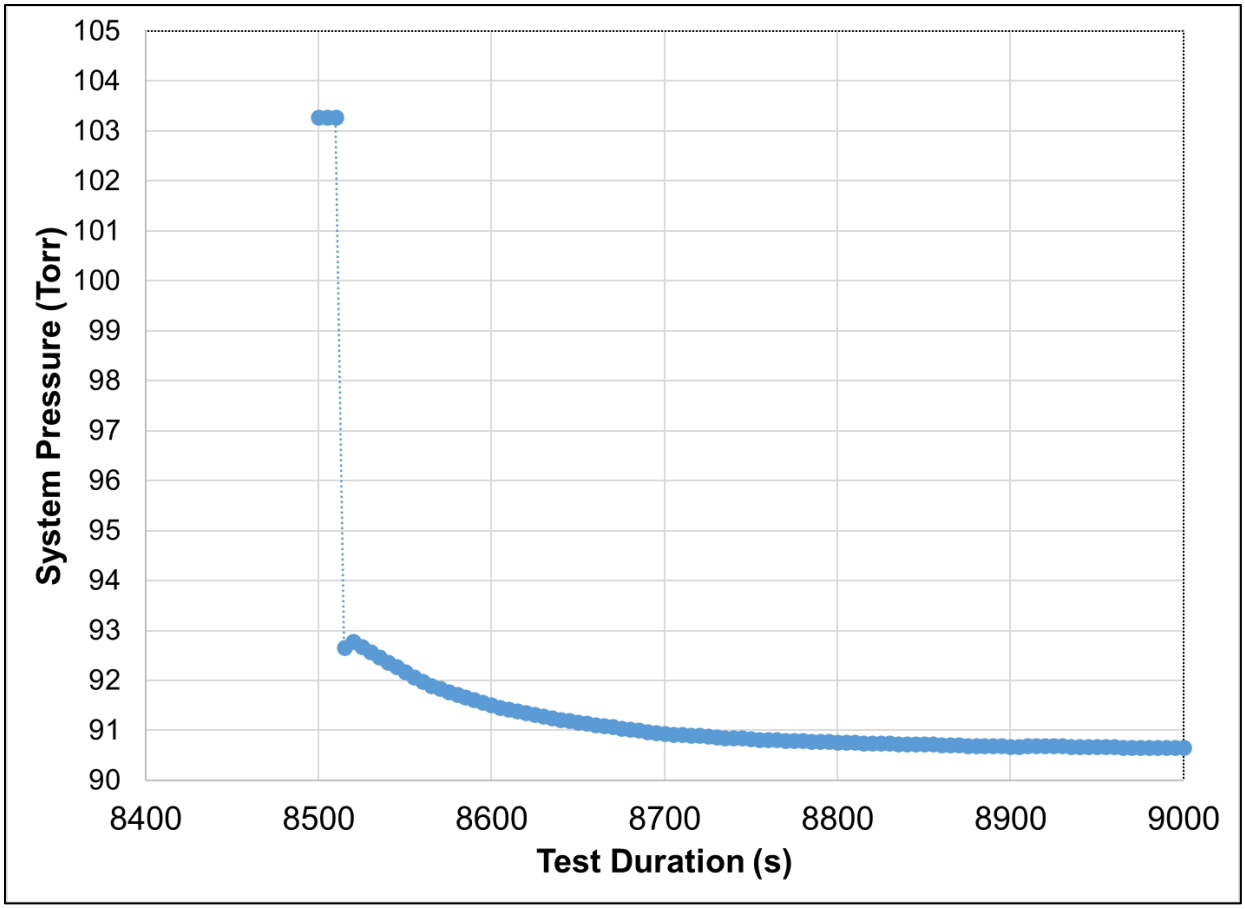


Figure 4-4: System Pressure during TeF_6 condensation.

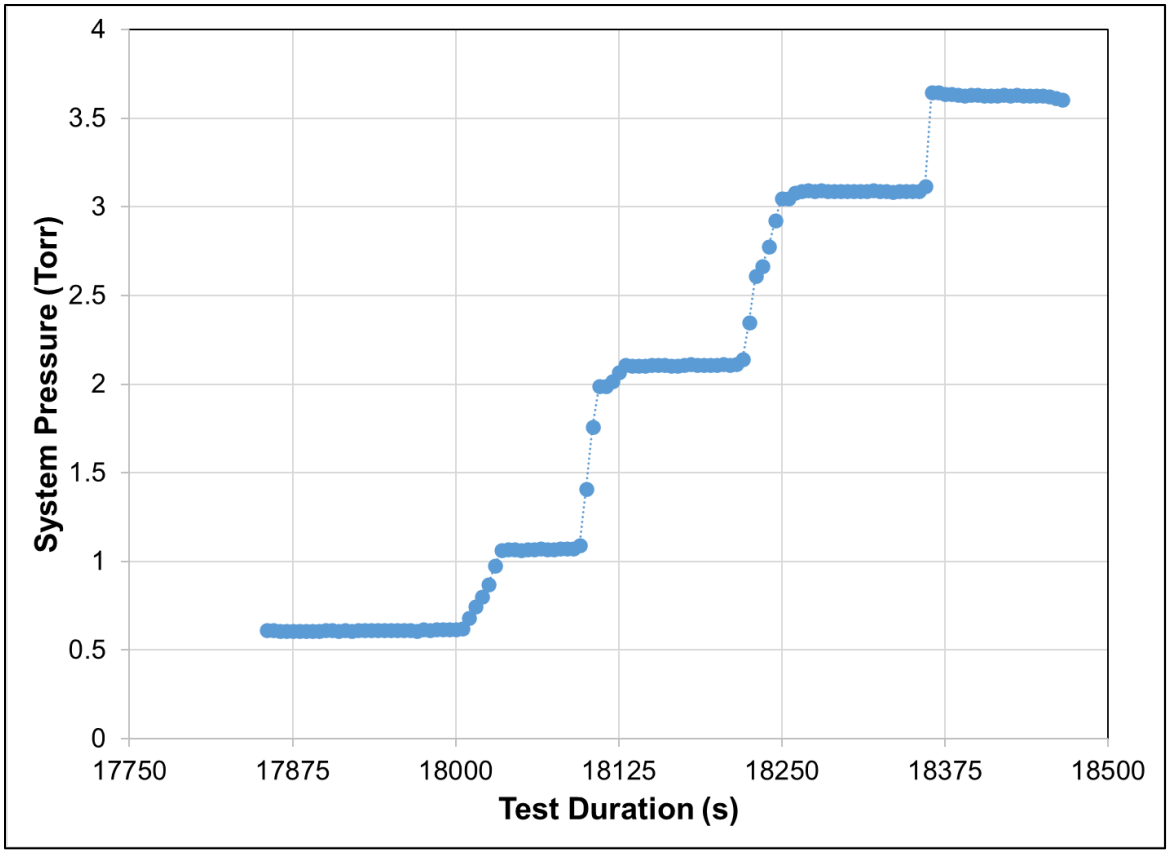


Figure 4-5: System pressure during intermittent release of TeF_6.

Table 4-2: Maximum absorbance of TeF_6 as a function of system pressure.

System Pressure (Torr)	Absorbance (752 cm^{-1})	TeF_6 (mol)	$[TeF_6]$ ($Torr/cm^3$)
0.61 ± 0.01	0.266 ± 0.001	$(2.33 \pm 0.45) \times 10^{-2}$	$(8.73 \pm 0.19) \times 10^{-4}$
1.07 ± 0.01	0.449 ± 0.002	$(4.08 \pm 0.06) \times 10^{-2}$	$(1.53 \pm 0.26) \times 10^{-3}$
2.11 ± 0.01	1.010 ± 0.006	$(8.04 \pm 0.09) \times 10^{-2}$	$(3.01 \pm 0.45) \times 10^{-3}$
3.09 ± 0.01	1.518 ± 0.008	$(1.18 \pm 0.01) \times 10^{-1}$	$(4.41 \pm 0.64) \times 10^{-3}$
3.63 ± 0.01	1.802 ± 0.010	$(1.38 \pm 0.01) \times 10^{-1}$	$(5.18 \pm 0.75) \times 10^{-3}$

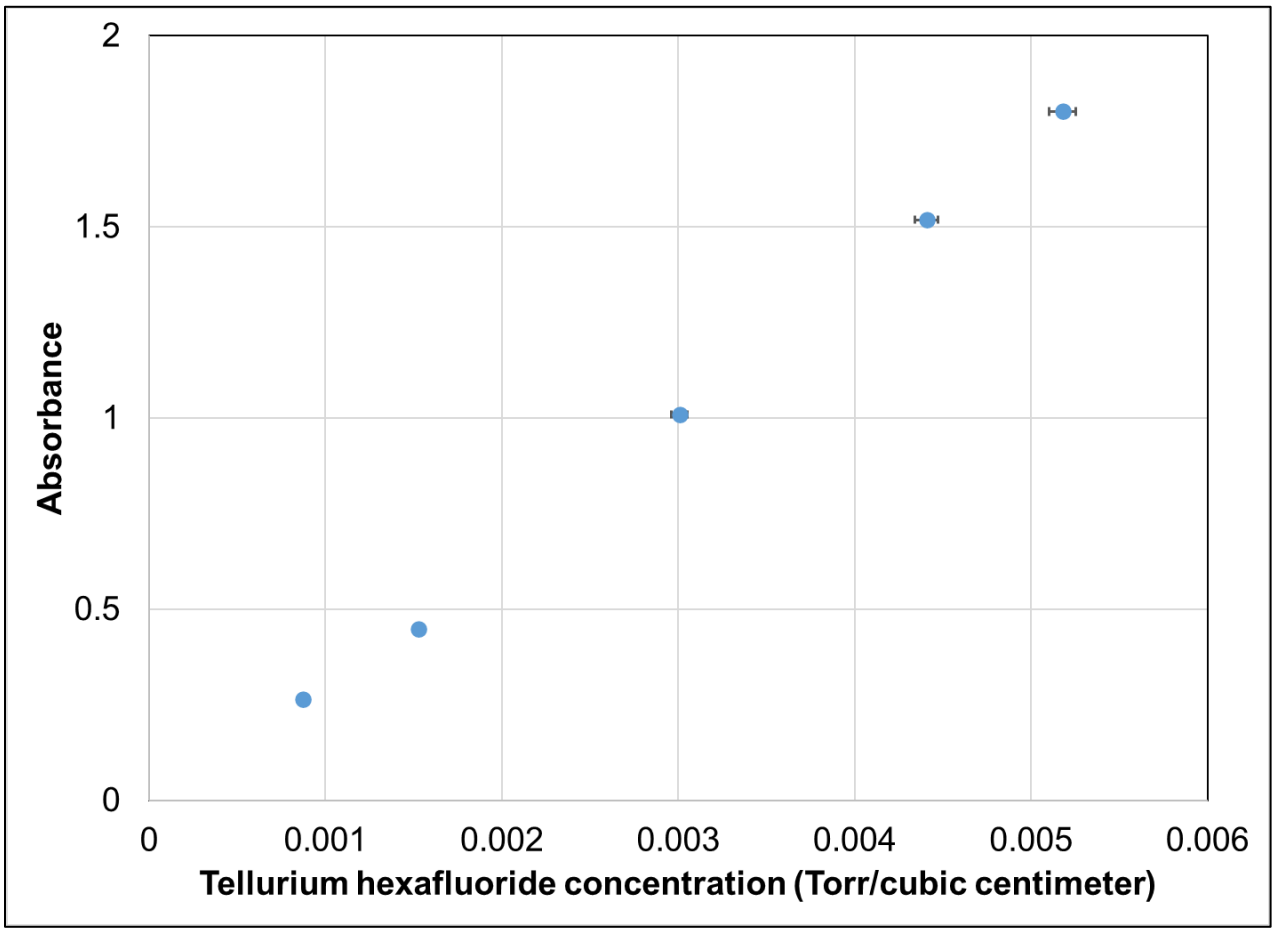


Figure 4-6: Absorption of TeF_6 at 752 cm^{-1} as a function of TeF_6 concentration.

Despite these difficulties, a retroactive attempt was made using the spectral data collected to understand the potential effect of Te_2F_{10} presence on the absorbance of TeF_6.

Vissers and Steindler provide the relative intensities of the Te_2F_{10} peaks present in the infrared region. This data shows that the 890 cm^{-1} Te_2F_{10} peak is roughly 40% as absorptive as the 752 cm^{-1} peak in a pure Te_2F_{10} spectrum. To describe the correction, Figure 4-7 is used as an example. In Figure 4-7, the intensity of the Te_2F_{10} peak is 0.033 AU at 890 cm^{-1}. This would imply a peak height of 0.082 AU at 752 cm^{-1} for Te_2F_{10}. The total absorbance of the 752 cm^{-1} peak in Figure 4-7is 1.490, and subtracting out what is perceived to be attributable to Te_2F_{10} would provide a peak height of 1.408 for TeF_6 at 752 cm^{-1}. Using revised peak heights based on this correction, the calculated molar absorptivity of the TeF_6 peak is 26.76 ± 2.61 cm^2 $Torr^{-1}$ (as compared to 28.51 ± 1.35 cm^2 $Torr^{-1}$ for the uncorrected work).

For the purposes of this work, the uncorrected 28.51 ± 1.35 cm^2 $Torr^{-1}$ value will be reported as the determined extinction coefficient. This is because although the correction just described can provide a general understanding of the magnitude of Te_2F_{10} effects on the measured TeF_6 peak, there is not enough data to perform a formal spectral deconvolution. Additionally and importantly, the potential error of the reported extinction coefficient exceeds the estimate of Te_2F_{10} contribution to measurement error.

Comparison of Analytical Methodology

The unreacted solids were recovered from each test and the mass of Te in these solids was determined by the dissolution of the solids and analysis of the solution by ICP-MS for tests 3–10. The amount of Te volatilized as TeF_6 was inferred from the amount of Te recovered from the reaction vessel at the conclusion of each test and is shown in Table 4-3. The maximum observed absorbance for each test is also tabulated.

Using the maximum absorbance at 752 cm^{-1} and the experimentally determined molar absorptivity coefficient, the concentration of TeF_6 in the gas phase for each test was calculated (and designated as $[TeF_6]_{\mathbf{exp}}$). This was compared to the concentration that would result from the amount of TeF_6 volatilized as measured by ICP-MS of the recovered solid (designated as $[TeF_6]_{\mathbf{mass}}$). Finally, a third concentration was calculated using the literature value of 2.3 cm^2 $Torr^{-1}$ for the molar absorptivity coefficient (McDowell, et al. 1986) (designated as $[TeF_6]_{\mathbf{lit}}$). These three calculated concentrations are shown in Table 4-4.

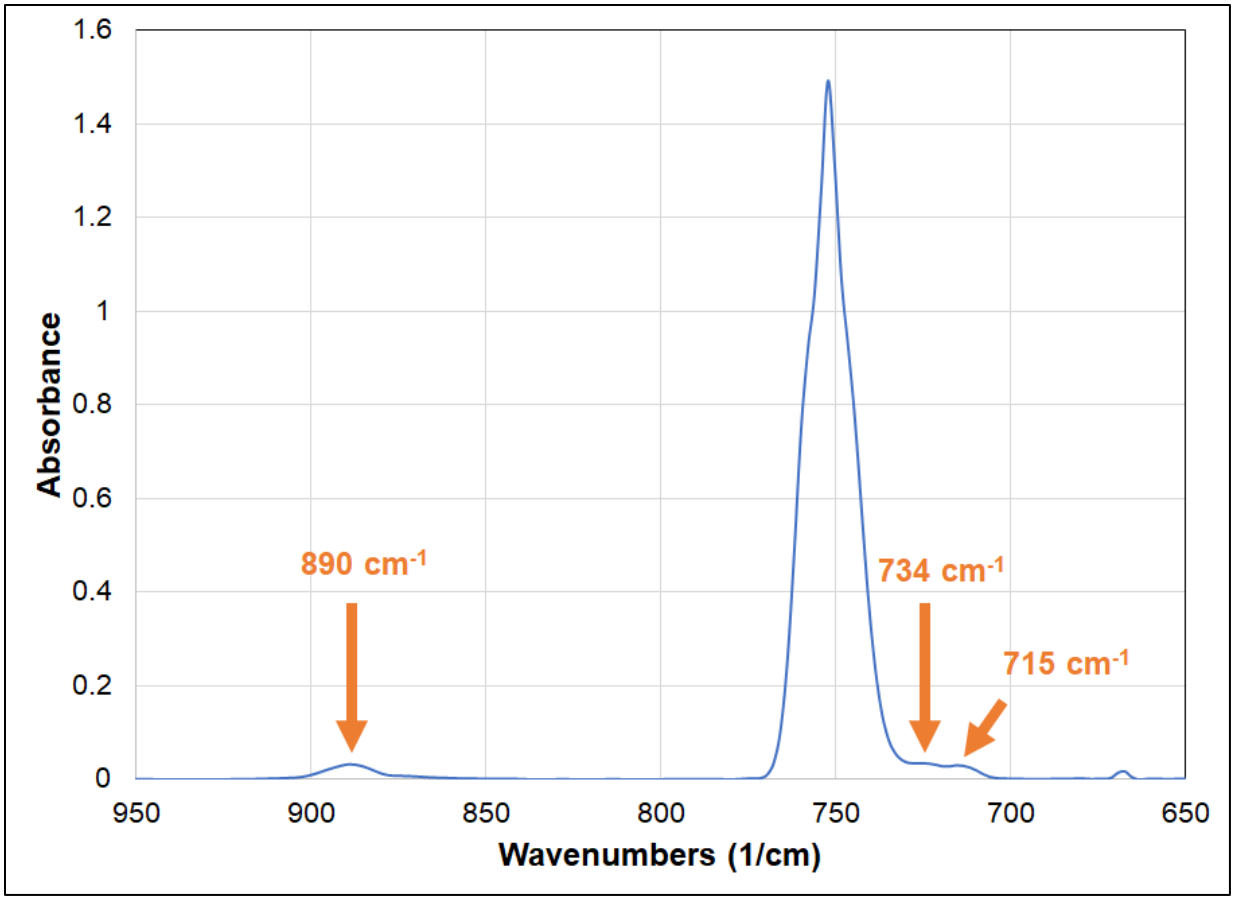


Figure 4-7: Infrared spectra of TeF_6 highlighting minor peaks attributable to Te_2F_{10}.

From these numbers, it can be observed neither $[TeF_6]_{exp}$ or $[TeF_6]_{lit}$ directly correlated with $[TeF_6]_{mass}$. However, $[TeF_6]_{exp}$, calculated using the experimentally determined molar absorptivity coefficient of 28.51 cm^2 $Torr^{-1,}$ is along the same order of magnitude as that of $[TeF_6]_{mass}$, differing by a factor of 4 in many cases. In contrast, the gas-phase concentrations indicated by using a ε of 2.3 cm^2 $Torr^{-1}$ are a factor of roughly 50× higher than that indicated by $[TeF_6]_{mass}$. Using the literature value of 2.3 cm^2 $Torr^{-1}$ would further indicate that a mass of 600–700 mg of Te was used in each experiment.

Thus, it was concluded that although there is not complete agreement between the $[TeF_6]_{mass}$ and $[TeF_6]_{exp}$, that the molar absorptivity coefficient determined in this work is likely more accurate than that previously reported by MacDowell, et al. 1986.

Technical Notations on Absorptivity Coefficient

In reviewing literature on the spectroscopy of TeF_6 and of other Group 16 hexafluorides such as SF_6 and SeF_6, it was observed that there is limited data that can be used to benchmark the determined molar absorptivity coefficient. Specifically, in trying to attempt to convert reported values there was often not enough information about the test system (including the pressures and volumes) to allow for conversion of reported values to values with units comparable to those used here.

Throughout the reporting of this work, every effort was made to provide as much descriptive detail regarding the specifics of testing methodology and test systems such that any external source would easily be able to manipulate or transform the data for their specific objective.

Two additional observations were made in the course of reviewing spectroscopic information of SF_6 and SeF_6. First, one of the more common approaches to understanding the absorptivity of a gas-phase molecule is the use of absorption cross-section at a given wavelength (σ). The absorption cross-section can be used for quantitation through a relationship of pressure, temperature, and the Boltzmann constant. The absorption cross-section is reported as cm^2 $molecule^{-1}$ and can be provided for an entire IR spectrum, as is shown by Harrison (2020) for SF_6. This type of work is commonly performed with very high-resolution spectrometers that have resolutions better than the instrument used in this work. Future work should attempt to duplicate the test described here using a high-resolution spectrometer such that the absorption cross-section could be determined with high precision across a spectral range.

Table 4-3: Fraction of Te volatilized based on the mass of recovered solids.

Test	Te mass (mg)	Te recovered (mg)	Te volatilized (%)	Maximum Absorbance (at 752 cm^{-1})
3	29.4	5.67 ± 0.57	80.7 ± 8.1	1.704
4	29.3	5.28 ± 0.53	82.0 ± 8.2	1.991
5	28.0	*Not recovered*	–	*Did not reach steady state*
6	~30[a]	5.97 ± 0.60	~ 80	1.350
7	30.0	0.81 ± 0.08	97.3 ± 9.7	2.170
8	~30[a]	5.18 ± 0.52	~83	1.201
9	29.0	3.05 ± 0.31	89.5 ± 8.6	1.380
10	32.6	3.32 ± 0.33	89.8 ± 9.0	1.790
[a]This number was not accurately entered in the experimental log.				

Table 4-4: Comparison of calculated gas-phase TeF_6 concentrations

Test	$[TeF_6]_{mass}$	$[TeF_6]_{exp}$	$[TeF_6]_{lit}$
	$(Torr/cm^3)$		
3	1.05×10^{-3}	4.98×10^{-3}	6.17×10^{-2}
4	1.07×10^{-3}	5.82×10^{-3}	7.21×10^{-2}
5	1.24×10^{-3}	2.35×10^{-3}	2.92×10^{-2}
6	–	4.74×10^{-3}	5.88×10^{-2}
7	1.30×10^{-3}	6.33×10^{-3}	7.85×10^{-2}
8	–	4.87×10^{-3}	6.04×10^{-2}
9	1.15×10^{-3}	4.38×10^{-3}	5.43×10^{-2}
10	1.30×10^{-3}	5.32×10^{-3}	6.59×10^{-2}
$[TeF_6]_{mass}$ based on ICP-MS analysis of recovered Te ash; $[TeF_6]_{exp}$ based on maximum absorbance and ε of 28.51 cm^2 $Torr^{-1}$; $[TeF_6]_{lit}$ based on maximum absorbance and ε of 2.3 cm^2 $Torr^{-1}$.			

Second, it was noted that quantitation can be performed through the use of integrated absorption coefficients, where the entire peak area is used in generating a Beer's law relationship. For this work, only the maximum peak absorbance was utilized due to an unfortunate data loss. Given the strong correlation between maximum absorbance and concentration for this work, and the purity of the collected spectra, this approach was judged acceptable.

CHAPTER FIVE TELLURIUM HEXAFLUORIDE PRODUCTION

In order to understand what conditions would be required to produce a gaseous stream of TeF_6 for use in sorption studies, the fluorination of Te was examined as a function of temperature, Te particle size, and F_2 concentration.

Classical Kinetic Study of Gas-Solid Reactions

The progression of a reaction (i.e. the conversion of a reactant to a product) can usually be described according to fundamental rate expressions. In the case of tellurium fluorination, the potential rate law *could* be as expressed in Equation 6.

Equation 6 Reaction Rate $(dx/dt) = k[Te][F_2]^3$, where k = rate constant

However, each rate expression must be validated to determine the rate order and to determine the rate constant. To perform this validation, studies are completed in which the concentrations of the reactants are measured as a function of time. Their decay provides the reaction rate and by varying experimental conditions (for example, making the reaction pseudo first-order by keeping one reagent in excess) the order of the reaction and the rate constant can be determined.

In the case of gas-solid reactions, specific kinetic theories have been established to allow for development of rate expressions. A good summary of gas-solid kinetic theory is provided in Fedunik-Hofman et al. (2019) and some key principles from that review are summarized here and are supplemented by information from Wright (2004) and Davis and Davis (2003).

Conversion of the reactant to the product (dx/dt) is typically, for gas-solid reactions, monitored through weight loss or weight gain of the solid reactant. Weight loss would occur in the case of tellurium fluorination, where Te metal is fluorinated and the resultant product species is volatile. The extent of conversion (α) is an important parameter in gas-solid kinetic analyses and is defined for a mass-loss process as in Equation 7, with the extent of conversion at a given time (α_t) dependent on the initial mass of the solid ($mass_0$), the final mass of the solid at complete conversion ($mass_{final}$), and the mass of the solid at the given time ($mass_t$).

Equation 7 $\alpha_t = (mass_0 - mass_t)/(mass_0 - mass_{final})$

The extent of conversion, α, is an interesting parameter that typically varies over the course of a reaction based on the mechanism of the gas-solid reaction with f(α) defined as the variance in α as a function of time. For example, f(α) will look different for a shrinking-core adsorption reaction vs. a nucleation reaction

(Vyazovkin and Wight 1997). After defining α and f(α) the rate expression for a gas-solid reaction is then rewritten as Equation 8.

Equation 8 $d\alpha/dt = kf(\alpha)h_P$, where h_P is a pressure dependence term

In evaluating the possible mechanisms involved in TeF_6 production, the most likely mechanism is a shrinking particle mechanism in which the radius (and available surface area) of a solid non-porous material continually decreases as it is reacted and the product is removed. A very nice description of this model as it relates to the fluorination of UO_2 is described in Homma, et al. (2005) and is validated using weight measurements of the reacting solid UO_2.

For the purposes of this discussion, the key takeway is that there must be some way to continuously measure α (dependent on the mass of the solid reactant) over the course of a reaction. Almost universally, this is performed through the use of a thermogravimetric analyzer (TGA) that facilitates exposure of a solid to a flowing gas while continuously measuring the weight of the solid. This type of measurement could not be easily performed using the test systems available. In fact, a TGA that can both maintain a sealed inert environment and be able to handle fluorine gas (corrosive and converted to HF if released into ambient air) is a highly specialized instrument.

As an alternative, sometimes a rate expression can be determined by changing the conditions of the rate to pseudo first order. This refers to operating with one reactant in large excess such that it's concentration can be assumed to be unchanged, thus reducing one term of Equation 6 to a constant. This cannot be performed here due to the need to minimize TeF_6 generation (due to its toxicity) and due to the F_2 shortage experienced nationally. These very practical limitations in reagents and instrumentation mean that a formalized rate expression cannot be derived from the data obtained over the course of these experiments and findings regarding reaction progression will be more qualitative in nature.

Experimental Approach

FTIR data were used effectively to monitor the progression of Te fluorination for the test matrix outlined in Table 3-1. and TeF_6 sorption in real time. The ingrowth of the TeF_6 peak is shown in Figure 4-1.

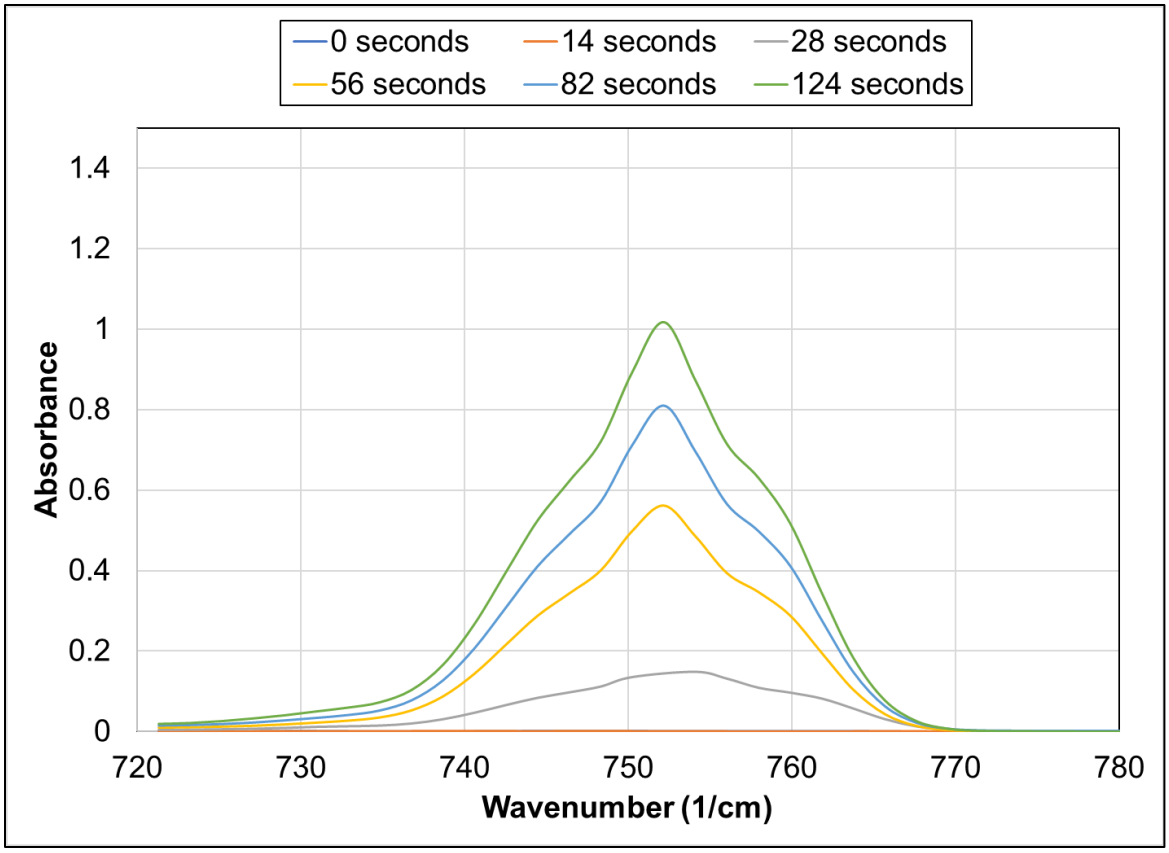


Figure 5-1. Ingrowth of TeF_6 as shown by successive FTIR scans. The legend indicates the time of each scan.

The maximum absorbance at 752 cm^{-1} was plotted as a function of reaction time, as shown in Figure 5-2, to determine the initial rate of reaction and whether the reaction was complete. Figure 5-2 also highlights the results of replicate testing at 200°C, showing that the initial rates of reaction are highly reproducible but that the total amount of TeF_6 produced varies, as reflected by the maximum absorbance. The total amount of Te reacted (and TeF_6 produced) may correlate with the available surface area of the metal, but additional data would be required to support this hypothesis.

It is important to note that in early testing (Tests 3 and 4) the amount of time required to successfully equilibrate the F_2/N_2 blend was underestimated. As a result, the gas contacting the reaction vessel during the initial reaction period was believed to have variable F_2 concentration. This is illustrated in Figure 5-3, where the measured absorbance of the primary TeF_6 was observed to oscillate and eventually equilibrate to a final absorbance. Tests 5 through 13 all incorporated a 45-min equilibration time where the F_2/N_2 blend was pumped through the test system and allowed to mix. The result of this process change was that the oscillation disappeared and smooth curves rising to maximum, such as those in Figure 5-2, were obtained.

Tellurium Hexafluoride Production Characteristics

Reaction Equation 2 was examined to understand the effects of temperature (100–200°C), F_2 partial pressure (20 and 40 Torr), and Te particle size (10–25 and 37–74 µm) on the reaction rate and total TeF_6 produced.

TeF_6 Production Rate as a Function of Temperature

As shown in Figure 5-2, the production rate of TeF_6 plateaus less than 15 min after reaction initiation. The period ranging from 0 to 15 min is shown in Figure 5-4 for tests at temperatures in the range of 100-200°C. From this graph, it is evident that the test completed at 100°C did not produce TeF_6 at a rate similar to those of other temperatures.

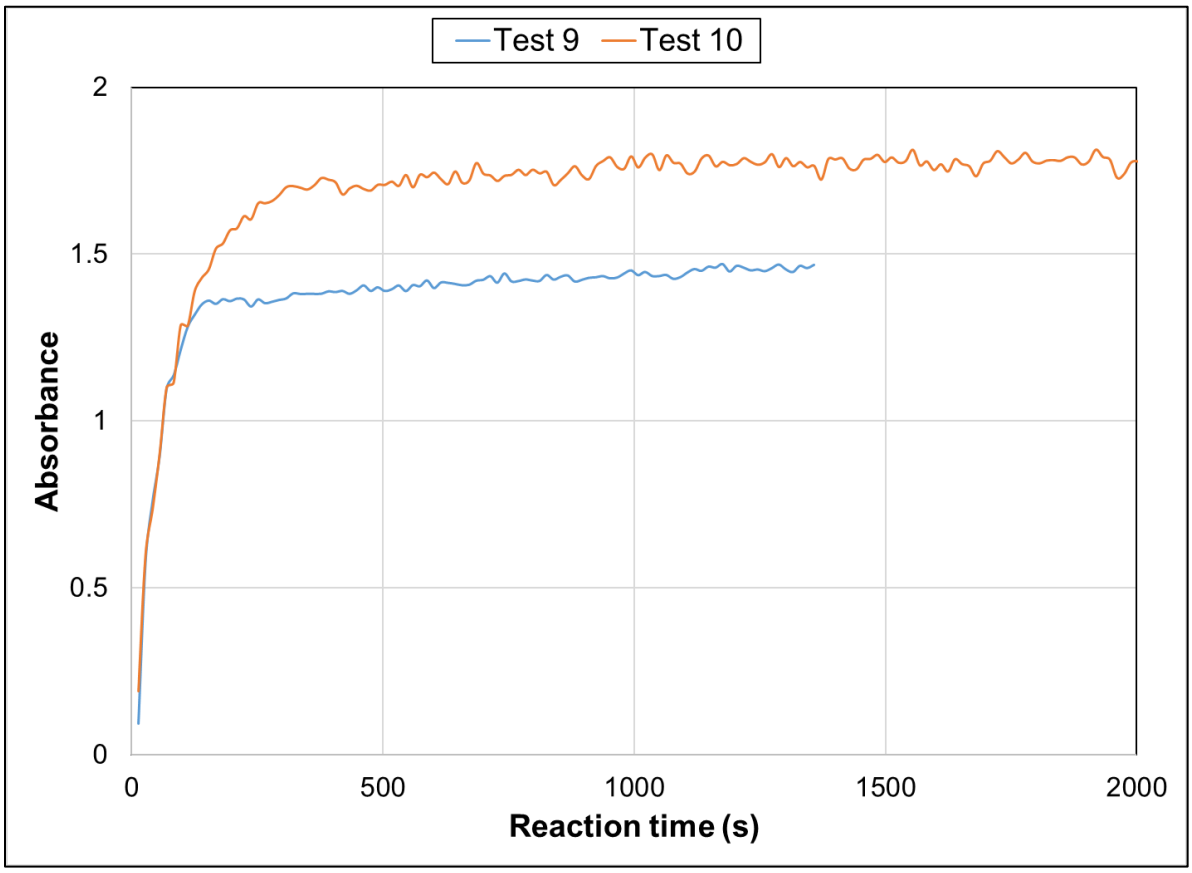


Figure 5-2: Monitoring of TeF_6 absorbance as a function of reaction time. TeF_6 produced at 200°C using 20% F_2 gas mixture.

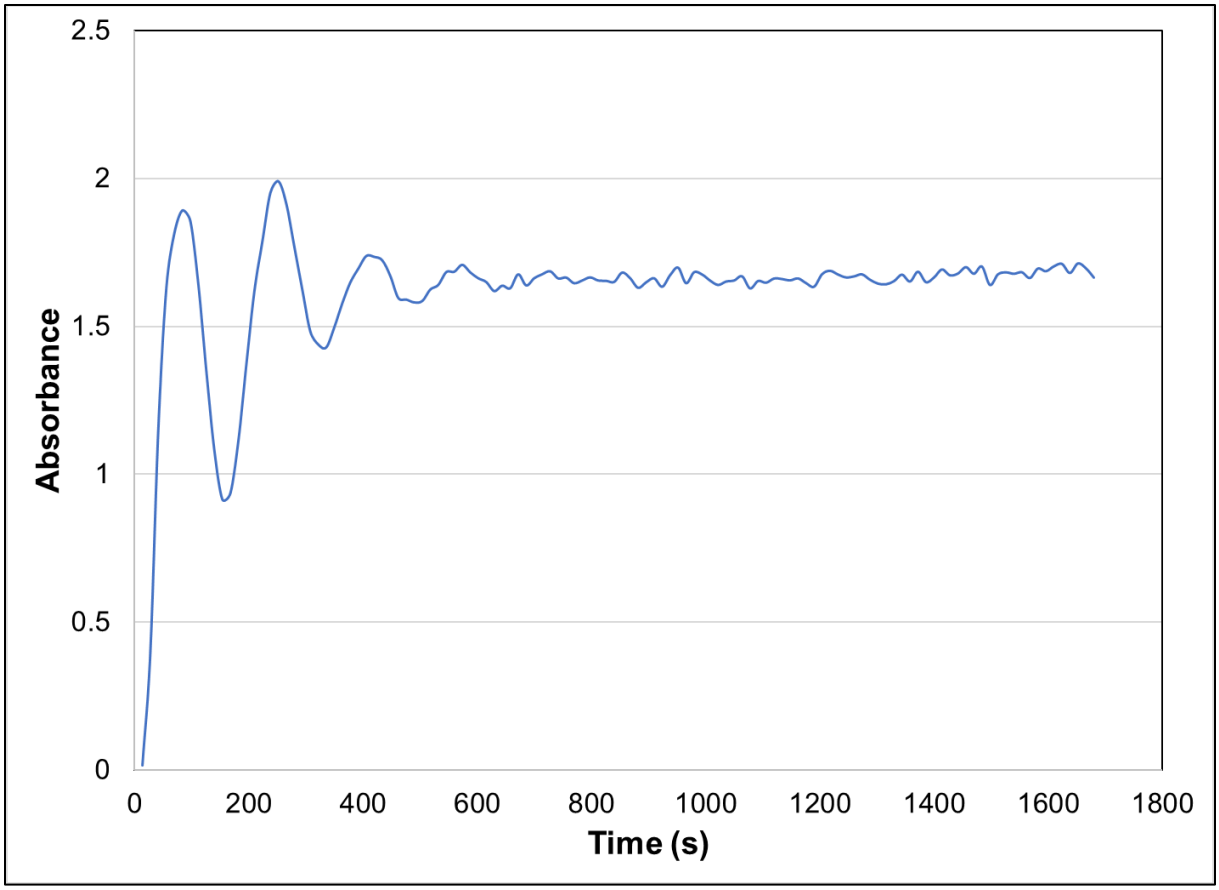


Figure 5-3: Absorbance measured at 752 cm^{-1} for Test 4 displayed oscillation attributable to poor gas mixing.

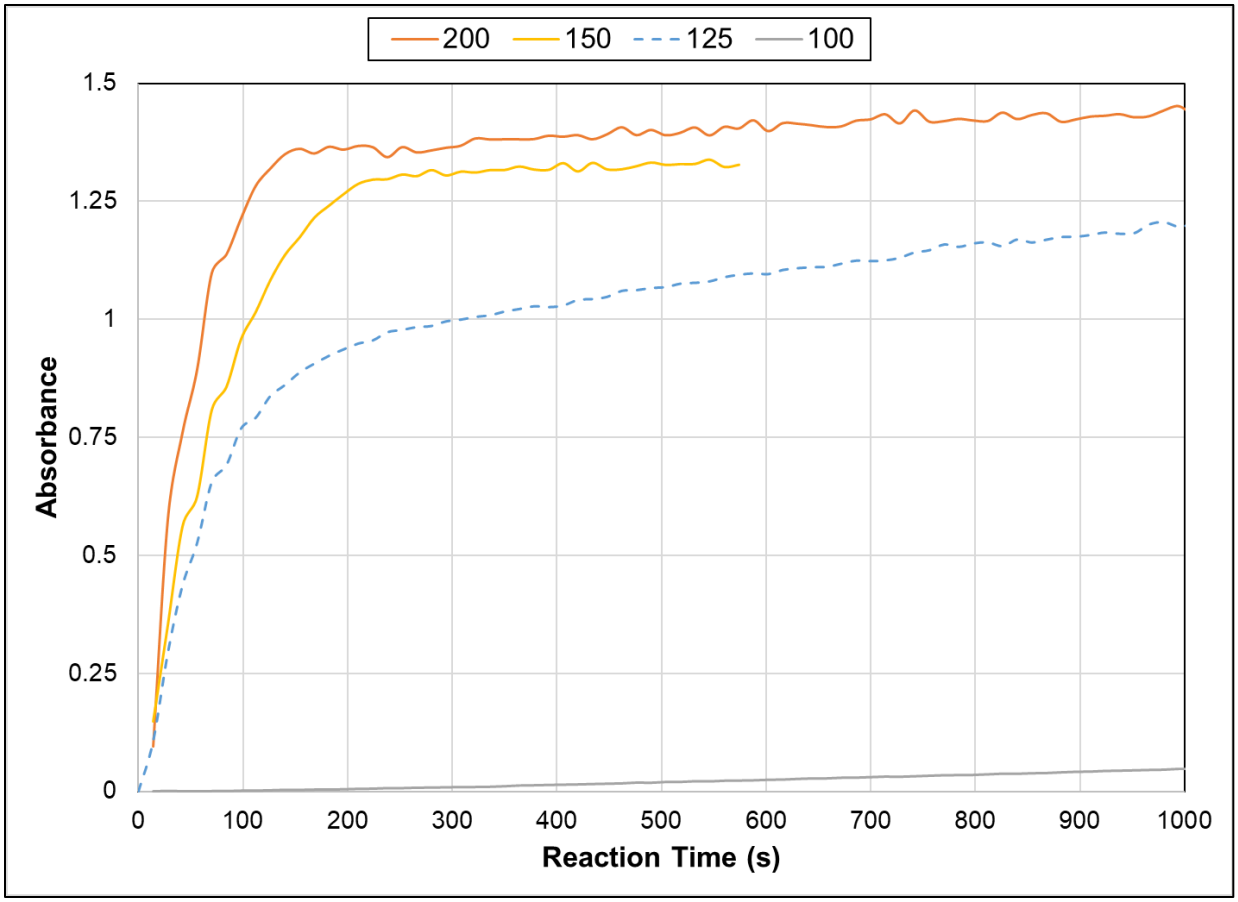


Figure 5-4: Initial TeF_6 production at varying temperatures.

The initial rate of reaction for the period of 0–2 min is shown in Figure 5-5 for temperatures ranging from 125 to 200°C. The 100°C test is off-scale in this case.

The initial rate of the reaction can be determined using:

$$k_{00:14-02:04} = \frac{\Delta ABS_{t_{00:14-02:04}}}{\Delta t_{00:14-02:04}}$$

The initial reaction rate for temperatures ranging from 100 to 200°C is shown in Table 5-1 and represented graphically in Figure 5-6. Test 5, performed at 100°C, had an extremely low reaction rate. While this data may be accurate, an attempt to replicate it was not performed.

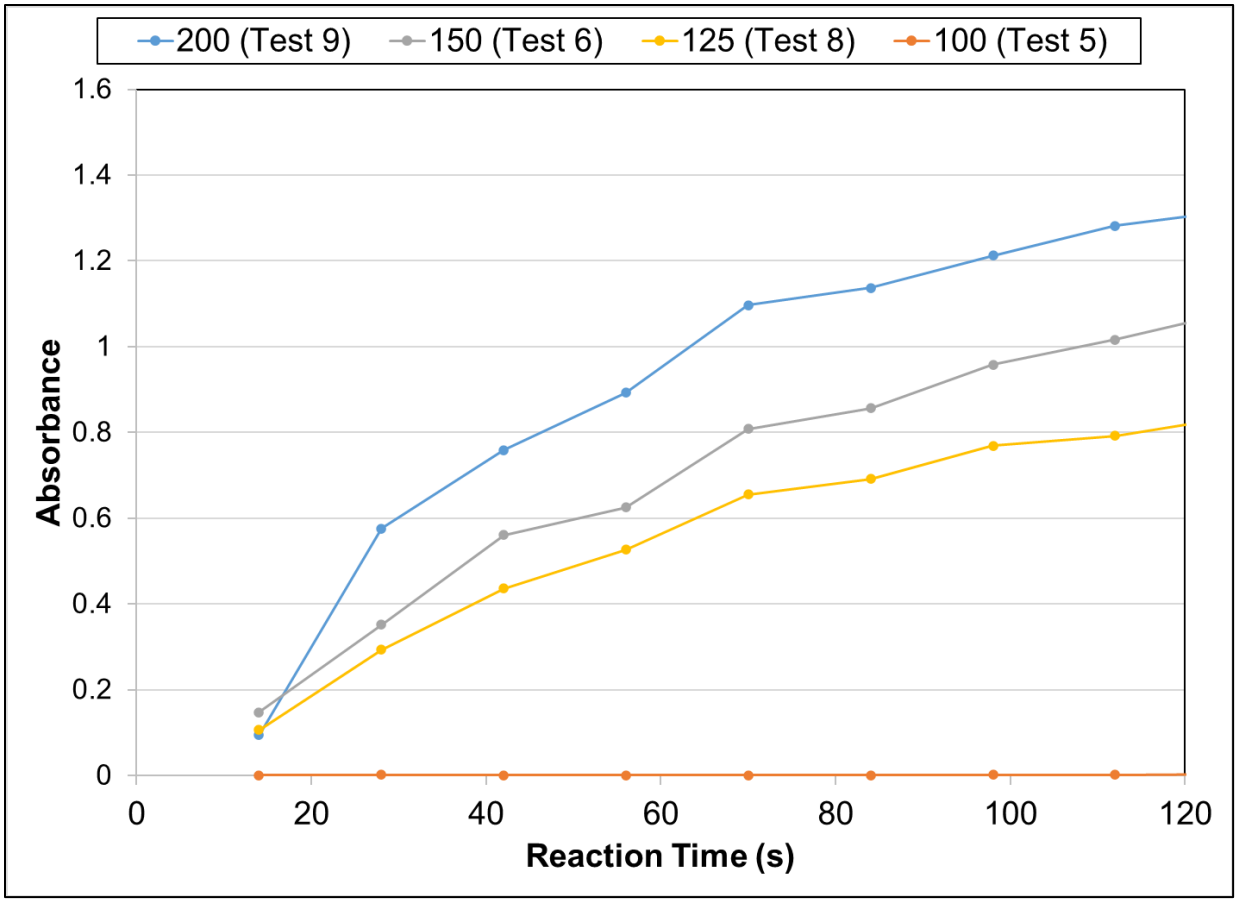


Figure 5-5. Initial reaction rate as a function of temperature.

Table 5-1: Initial rate of reaction at varied test temperatures.

Test	Temperature (°C)	Initial Reaction Rate
5	100	0.002
8	125	0.792
6	150	1.016
9	200	1.282

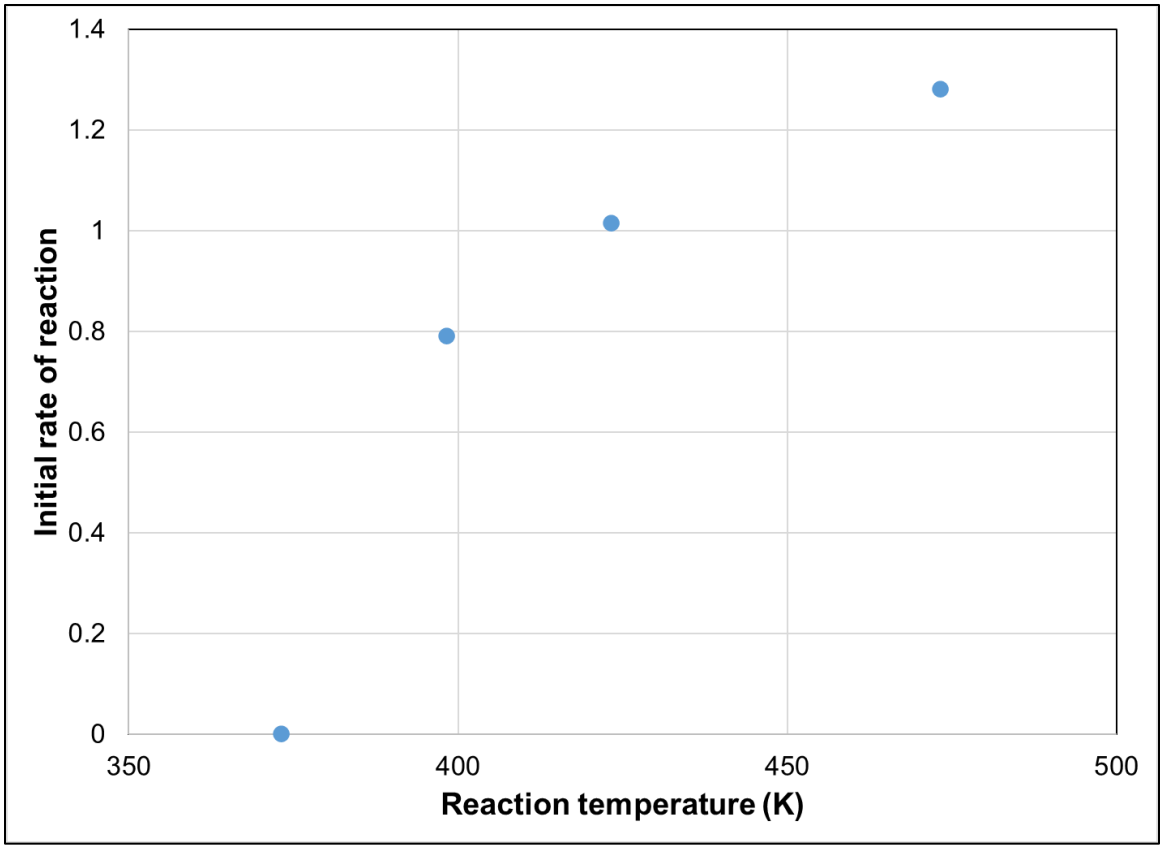


Figure 5-6: Dependence of initial rate of reaction on temperature.

TeF_6 Production as a Function of Particle Size

While testing the two particle size ranges of interest (10–25 and 37–74 µm), these two size ranges were observed to behave differently during the transfer to the nickel plate used for support in the reaction vessel. The smaller size fraction clumped and aggregated together, whereas the larger size fraction poured easily, and individual particles could be individually distinguished visually. For these reasons, the Te metal arrangement on the nickel plate during the reaction was different for the two particle size fractions, mounds of Te metal were observed for the smaller particle size range, and the larger size range more evenly distributed in a flat layer on the plate (Figure 5-7).

TeF_6 production proceeded at 150°C, and the absorbance of the 752 cm^{-1} peak over the course of the two tests is shown in Figure 5-8.

The initial reaction rates are nearly identical, despite the difference in particle size. However, the maximum absorbance is markedly different for the larger particle size, outside of the variability observed for production using 10–25 µm diameter particles. Although larger particle sizes typically reduce the area available for reaction, it is hypothesized in this case that the even distribution of the larger particle sizes on the nickel plate might have resulted in a larger accessible surface area for reaction and a higher fractional conversion of the starting metal to TeF_6. This would indicate also that the initial reaction rate is not surface area limited under these conditions.

One variable that was not controlled for in these experiments was the potential for heating of the Te metal during reaction. Given the exothermic nature of the reaction, it was speculated that there could be a potential for sintering of the metal during the reaction. Any sintering would decrease the surface area available for reaction and could affect the observed reaction progression.

The physical appearance of the recovered Te following each test did not show evidence of sintering. The material appeared ash-like (white and powdery). Vissers and Steindler (1966) also report the formation of a white ash during Te fluorination and identify it as TeF_4, a white solid. Although speciation of the recovered material was not determined in these experiments, TeF_4 should be considered as a possible partially fluorinated product of this work.

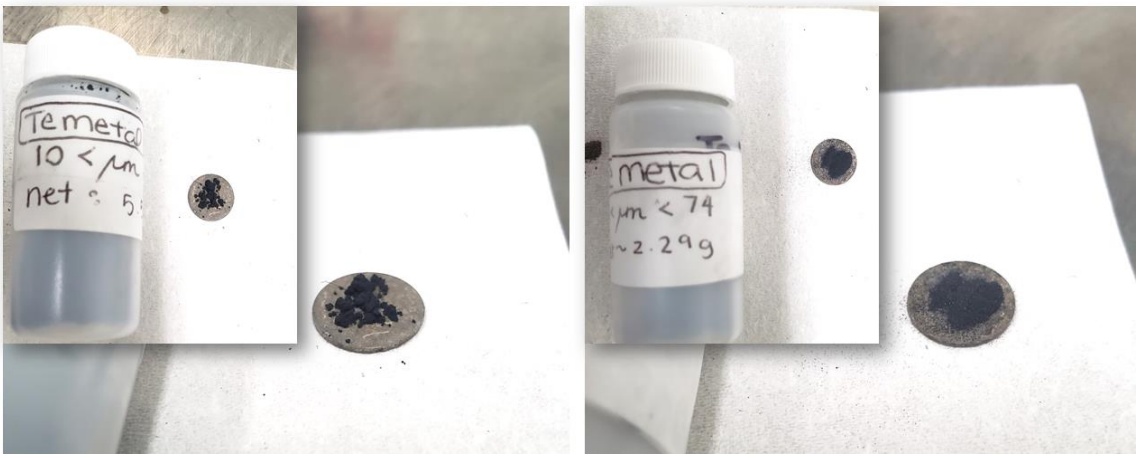


Figure 5-7: Two sizes of Te metal particles located on nickel reaction support plate (10-25 µm, L; 37–74µm, R).

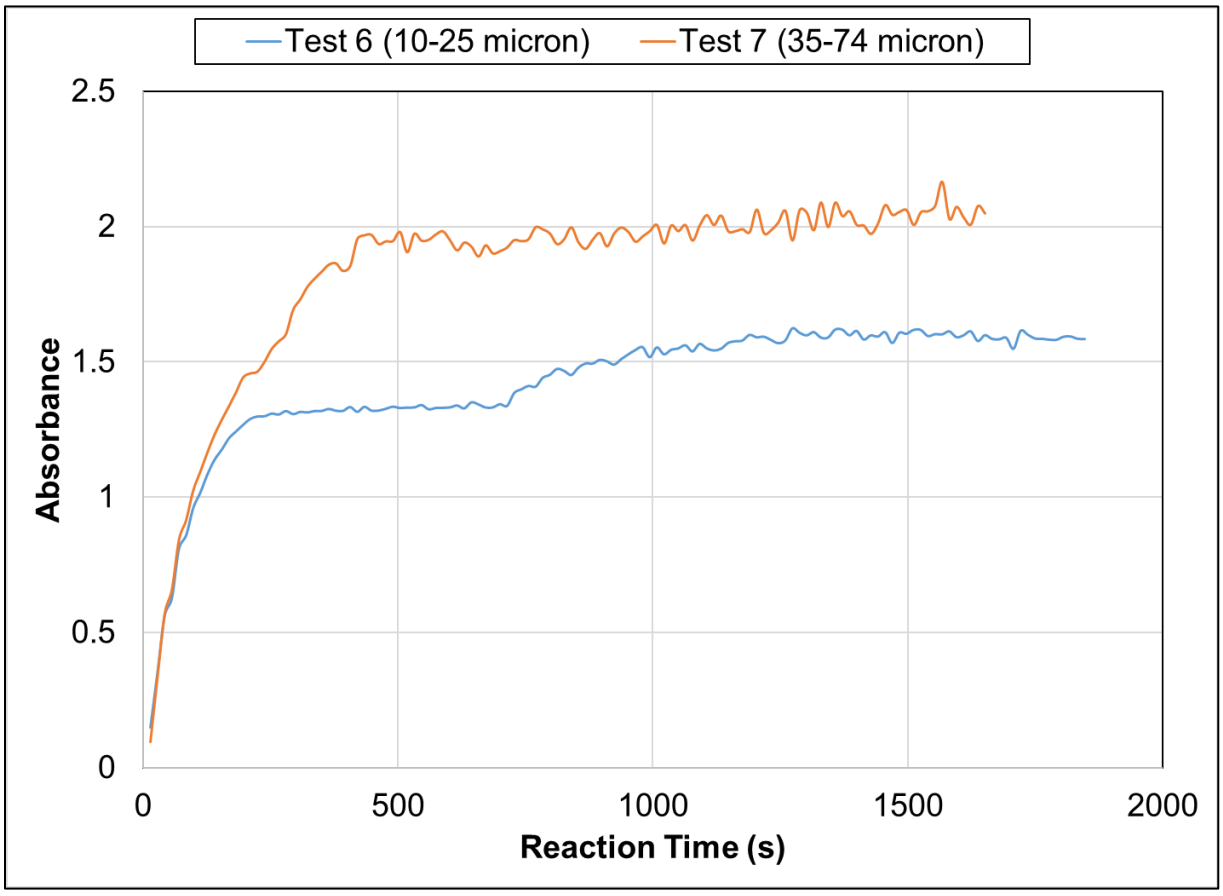


Figure 5-8. Production of TeF_6 from different particle size fractions.

It is recommended that future work consider the experiments that could better explore the effect of surface area on reaction progression. First, continuous weight measurements performed in a thermogravimetric analyzer could allow for modeling the reaction based on the shrinking particle model and for quantifying the dependence of reaction rate on a continually-decreasing surface area. Second, dispersion of the Te metal through a fluidized bed would allow for experiments in which the heat of reaction is quickly and easily dispersed, the reaction temperature profile is more even, and the potential for particle sintering is reduced. It should be noted that common fluidized bed media (including SiO_2 and Al_2O_3) will not be suitable for experiments with F_2. Nickel powder or other fluorine-resistant metals could be considered as potential fluidized bed media but it should also be noted that the gas velocity required to fluidize dense materials is relatively high.

TeF_6 Production as a Function of Fluorine Partial Pressure

A scoping test was performed to evaluate whether increased F_2 partial pressure would result in an increased initial reaction rate. The results shown in Figure 5-9 indicate that the initial rate of reaction increases with an increase of F_2 partial pressure from 20 to 40 Torr and that it is too fast to measure with this experimental system. The oscillations in the curve indicate essentially the pumping frequency of the gas within the system and the volume of the reaction vessel, with a burst of TeF_6 most likely produced as the pump pushed a fresh charge of unreacted fluorine into the reaction vessel.

Te Conversion Fraction

As discussed in Chapter 4, the unreacted solids were recovered from each test and the mass of Te in these solids was determined by the dissolution of the solids and analysis of the solution by ICP-MS for tests 3–10. The amount of Te volatilized as TeF_6 was inferred from the amount of Te recovered from the reaction vessel at the conclusion of each test and was shown in Table 4-3.The amount of recovered solids was about 5 mg for each test that used 10–25 µm diameter Te metal particles. Less material was recovered from Test 7 (using 37–74 µm diameter material) and from tests 9-10.

It was observed that conversion was nearly complete for the larger particle size test, likely to due increased accessible surface as discussed previously. The conversion under the most commonly used reaction conditions (20% fluorine) did not appear to have a temperature dependence and ranged from 80 to 90%.

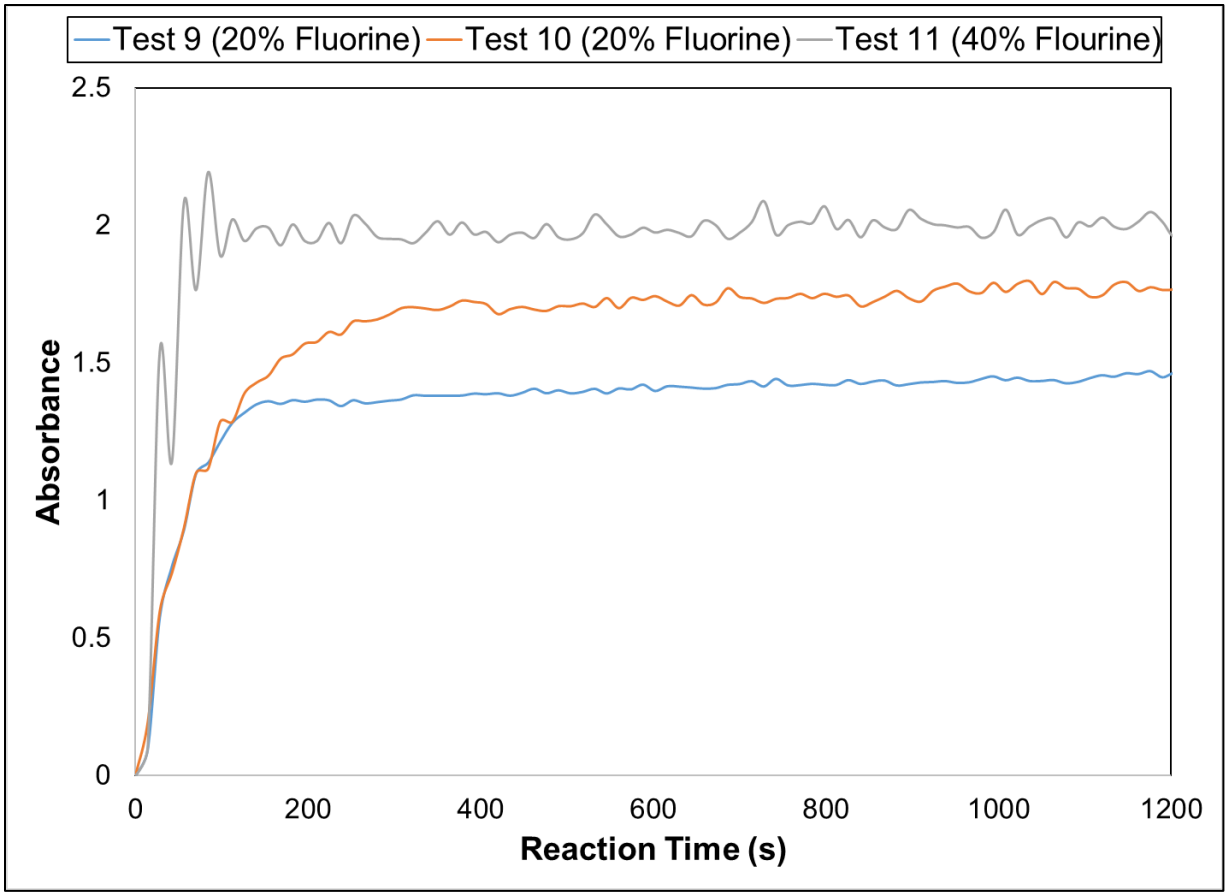


Figure 5-9. Effect of increased F_2 partial pressure on the initial reaction rate.

Analysis of Reaction Curves

Although a formalized rate expression could not be developed the reaction curves were processed and fit to an exponential expression.

Wiley (2007) indicates that a curve rising to a maximum can be fit with an equation of the form shown in Equation 9.

Equation 9 $y = Max(1–e^{-mt}) + C,$

with *m* being a parameter characteristic of the curve and C being a constant value reflecting any measurement offsets.

This equation was modified for the purposes of this work to the form shown in Equation 10.

Equation 10 $A = Abs_{max}(1–e^{-mt}) + C,$

With *m* being designed as the conversion rate, t being equal to reaction time, A being measured absorbance, Abs_{max} being the maximum observed absorbance at steady state, and C being a constant offset reflecting baseline FTIR measurements.

The Microsoft Excel solver function was used to fit this equation, with the solver minimizing the difference between the experimental data and predicted curve through a chi-squared (χ^2) function. Abs_{max} was fixed based on experimental observation. C was allowed to be optimized. This optimization was only performed for tests 6-11, as Tests 3 and 4 did not have steady gas concentrations, Test 5 (100°C) did not reach a maximum steady-state absorbance over the test period, and Test 12 had an intense absorbance that measured off-scale.

The conversion rate determined for each test, along with the χ^2 value of each fit, is shown in Table 5-3. For tests in which temperature was the primary variable, the χ^2 value was fairly good with three of the four tests showing a value < 0.1. However, when manipulating other variables, including fluorine concentration and particle size, the fit did not predict the data quite as closely.

Table 5-2: Fitted parameters for selected tests.

Test	**Characteristic Variable**	**Abs_{max}**	**Conversion rate *m***	**χ^2**
6	Temperature	1.623	0.0127	0.034
7	Particle size	2.170	0.0046	2.005
8	Temperature	1.201	0.0063	0.798
9	Temperature	1.380	0.0274	0.039
10	Temperature	1.750	0.0123	0.077
11	$[F_2]$	1.950	1.1350	0.560

The data and fitted curves for Tests 6-11 are shown in Figure 5-10. During the fitting process, it was observed that one confounding issue is that of the maximum absorbance. As previously discussed, the rate of the reaction is reproducible across test conditions, but the maximum absorbance varies for reasons not understood. As an illustration of how this impacted the curve fitting exercise, note that Tests 9 and 10, which were replicate runs that differed in maximum absorbance, differ significantly in the modeled parameter *m.* The conversion rate *m* is plotted as a function of temperature in Figure 5-11.

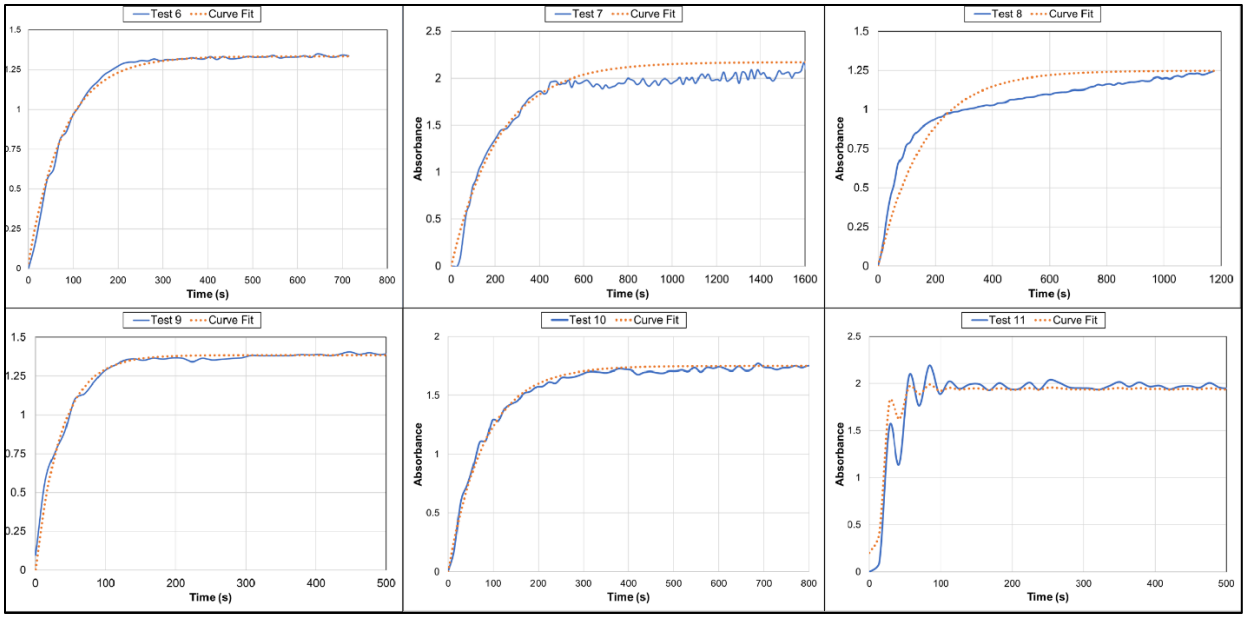


Figure 5-10: Curve fitting for Tests 6-11.

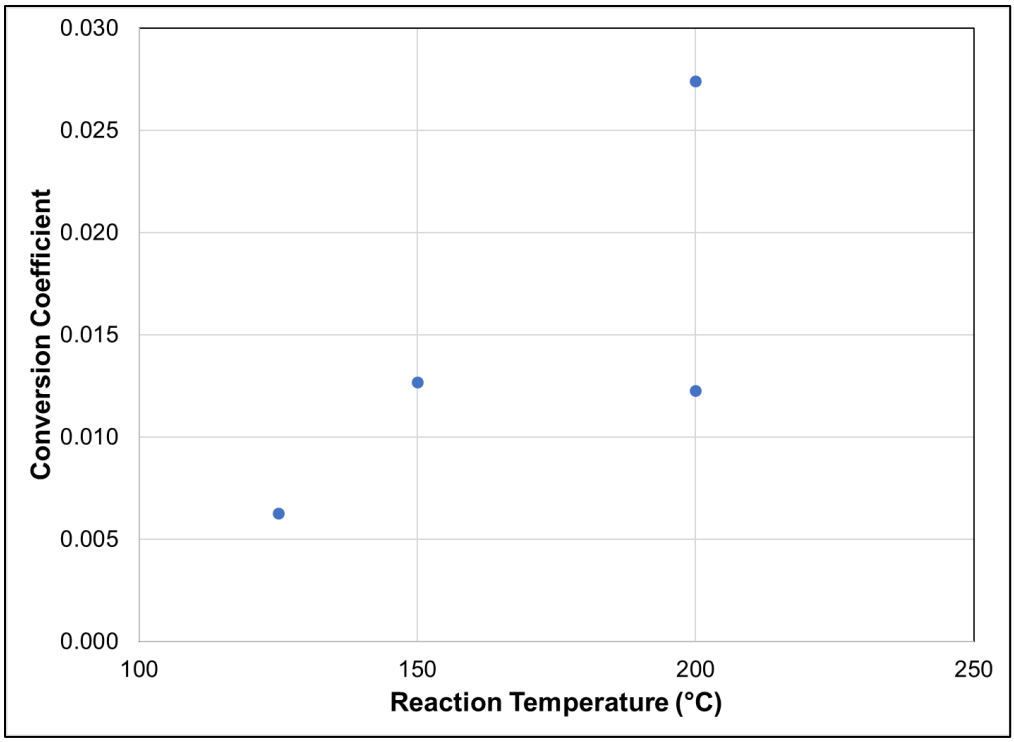


Figure 5-11: Correlation of conversion coefficient with reaction temperature.

CHAPTER SIX TELLURIUM HEXAFLUORIDE SORPTION

The ultimate goal of the project was to begin identifying and testing materials that could remove TeF_6 from gas streams arising from advanced nuclear reactors or advanced nuclear fuel processing. A literature review identified copper and alumina as candidates for scoping tests. Tests 9–13 examined the sorption of TeF_6 by alumina and copper.

Identification of Potential Sorbent Materials

To date, the earliest and most comprehensive evaluation of TeF_6 abatement was conducted by Vissers and Steindler (1968). In that work, the authors tested 13 sorbents: activated alumina, two types of charcoal, two types of molecular sieves, MgF, NaF, soda lime, CuO, and four metallic adsorbents, including Cu, Ni, Te, and Al. Gaseous radiolabeled TeF_6 was used as the TeF_6 source and the sorbent was contained in a 3.25 in. diameter tubular reactor with a maximum bed length of 12 in. All test system materials were nickel. Two types of experiments were conducted: (1) static batch-style sorption experiments and (2) flow-through sorption experiments.

In the batch-style experiments, the sorbent was placed into the heated sorption chamber, and a measured amount of TeF_6 was added into the evacuated chamber. The pressure of the system was monitored to track the pressure reduction, which was assumed to correspond to the sorption of TeF_6 by the sorbent. The excess TeF_6 was pumped off via a mild vacuum, and then the system was placed under a 10^{-2} Torr vacuum to remove any TeF_6 that was reversibly sorbed. These batch-style experiments were used to identify the most promising sorbents, which were then further investigated by flow-through sorption experiments.

The most promising sorbents included activated alumina, charcoal, and molecular sieve 13X. The flow-through sorption experiments indicated that alumina was the most desirable sorbent based on the decontamination factors achieved. Charcoal is no longer considered a desirable sorbent when F_2 is present because of the potential for uncontrolled reactions, and the flow-through experiments conducted in Vissers and Steindler using molecular sieve 13X did not validate the promise of the batch-style experiments.

Thus, a patent on the removal of TeF_6 via activated alumina was submitted (Vissers and Steindler 1970). This patent briefly mentions that excess F_2 can displace adsorbed TeF_6, indicating that the TeF_6 is adsorbed reversibly or that it could require a soaking period to fully immobilize on the adsorbent. Komaki et al. (1973) attempted to better understand TeF_6 sorption by activated alumina, but

the experiments were conducted without excess F_2 and did not address the concern of TeF_6 removal or displacement from alumina.

Thus, the literature shows that activated alumina, the only potential TeF_6 sorbent studied in any detail, is still surrounded by unanswered questions regarding its TeF_6 sorption performance in realistic off-gas streams. First, although alumina may be effective at absorbing TeF_6 in the presence of excess F_2 gas, much of the alumina's capacity would be used by co-adsorbed F_2, increasing the replacement frequency of absorbent cartridges and preventing the recycle of F_2 into the process. Reagent recycle could be especially valuable considering the challenges in obtaining pure fluorine gas. Second, how would F_2 impact the sorption of TeF_6 by alumina?

The current work sought to evaluate TeF_6 sorption by activated alumina in the presence of excess F_2. Additionally, the concept of a TeF_6-selective sorbent was considered, and copper shot was tested for this purpose. Preliminary thermodynamic calculations indicate that progressive temperature ramping of the copper sorbent could promote selective TeF_6 removal by copper, but this had not been investigated until this work. To support an understanding of the concentration of TeF_6 contacting the sorbent beds, a series of preliminary testing identified the TeF_6 production rate and the equilibrium concentration of TeF_6 in the gas stream that contacts the adsorbent.

Sorption by Activated Alumina

Test 9 used nonactivated alumina, which has limited capacities for both F_2 and TeF_6, and those results are not reported here. No TeF_6 adsorption was observed, likely due to saturation of the limited capacity of the alumina with fluorine.

Test 10 used activated alumina. FTIR data from Test 10, shown in Figure 6-1, reflect a sharp TeF_6 production curve to a steady-state absorbance of about 2.0 and a subsequent sharp drop in absorbance to zero as an activated alumina bed is placed in line with the test loop and TeF_6 is absorbed. Sorption of TeF_6 occurs very quickly and is complete. Sorption of F_2 occurs concurrently and all F_2 is removed, as indicated by pressure monitoring on the system.

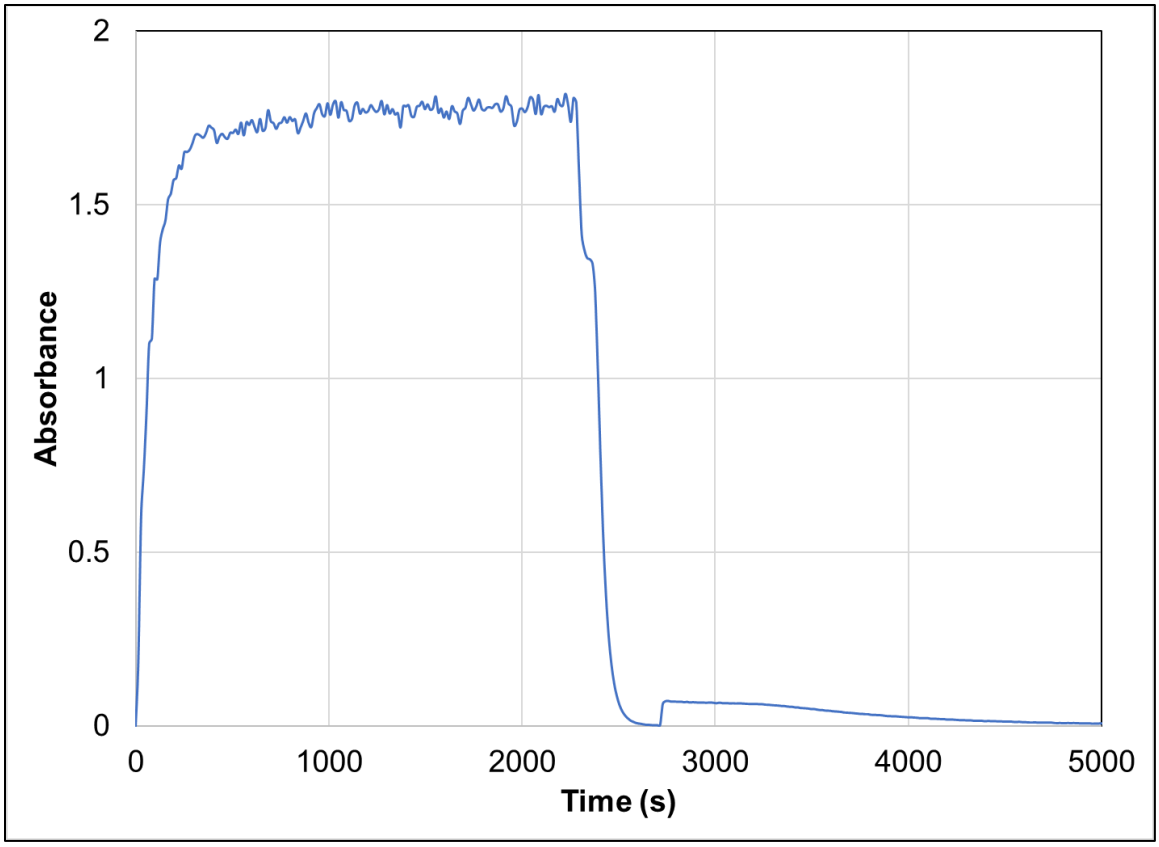


Figure 6-1: Production, steady-state, and sorption phases of Test 10.

To assess how the presence of fluorine could impact the sorption of TeF_6 by alumina, Test 11 contained double the amount of F_2 as test 10 (40 vs. 20 Torr, respectively). The sorption phases of the two tests are compared in Figure 6-2. Although the two sorption curves are not identical, they both show near-complete sorption of TeF_6 within 6 min, and no deleterious effect on TeF_6 sorption was observed in the presence of higher F_2 pressures. In the tests completed here, the number of alumina sites available for reaction dwarfed the amount of TeF_6 and F_2 present. Future work should consider operating at conditions closer to sorbent saturation, but the limitations on F_2 procurement limited the inspection of this element of the work.

Sorption by Copper

Vissers and Steindler (1968) indicated that Cu would absorb TeF_6, but details on sorbent temperatures and other specifics were not provided. Preliminary calculations were performed using HSC Chemistry to assess whether TeF_6 sorption was thermodynamically favorable and whether TeF_6 could be sorbed at different temperatures than F_2. Table 6-1 shows some potential sorption reactions and their free energies (ΔG_{rxn}). Because the potential sorption mechanism and resulting products were unknown, several different reactions were calculated with varying products, including CuTe, TeF_4, and CuF_2. These calculations showed that the decomposition of TeF_6 by Cu was thermodynamically favorable for some reaction pathways. The most favorable reactions, simply based on thermodynamics, were those in which copper fluorides and tellurium metal were formed. However, simply determining free energies of reaction cannot inform as to the kinetics of the sorption process, the potential for unfavorable intermediate states, and whether the process occurs via adsorption, decomposition, or another pathway.

HSC Chemistry was used to generate predominance diagrams by using the three elements of interest: Cu, Te, and F. These predominance diagrams show that CuTe becomes more favored above 300°C as shown in Figure 6-3, Figure 6-4, and Figure 6-5.

Thermodynamic calculations cannot resolve the effects of two competing adsorbates because the reactions will be governed by not only the free energy of the reaction but also the kinetics of the reaction for the competing species' sorption and decomposition—in this case, TeF_6 and F_2. However, these calculations were favorable and suggested completing a scoping test to assess the behavior of TeF_6 in contact with a copper sorbent at varying temperatures.

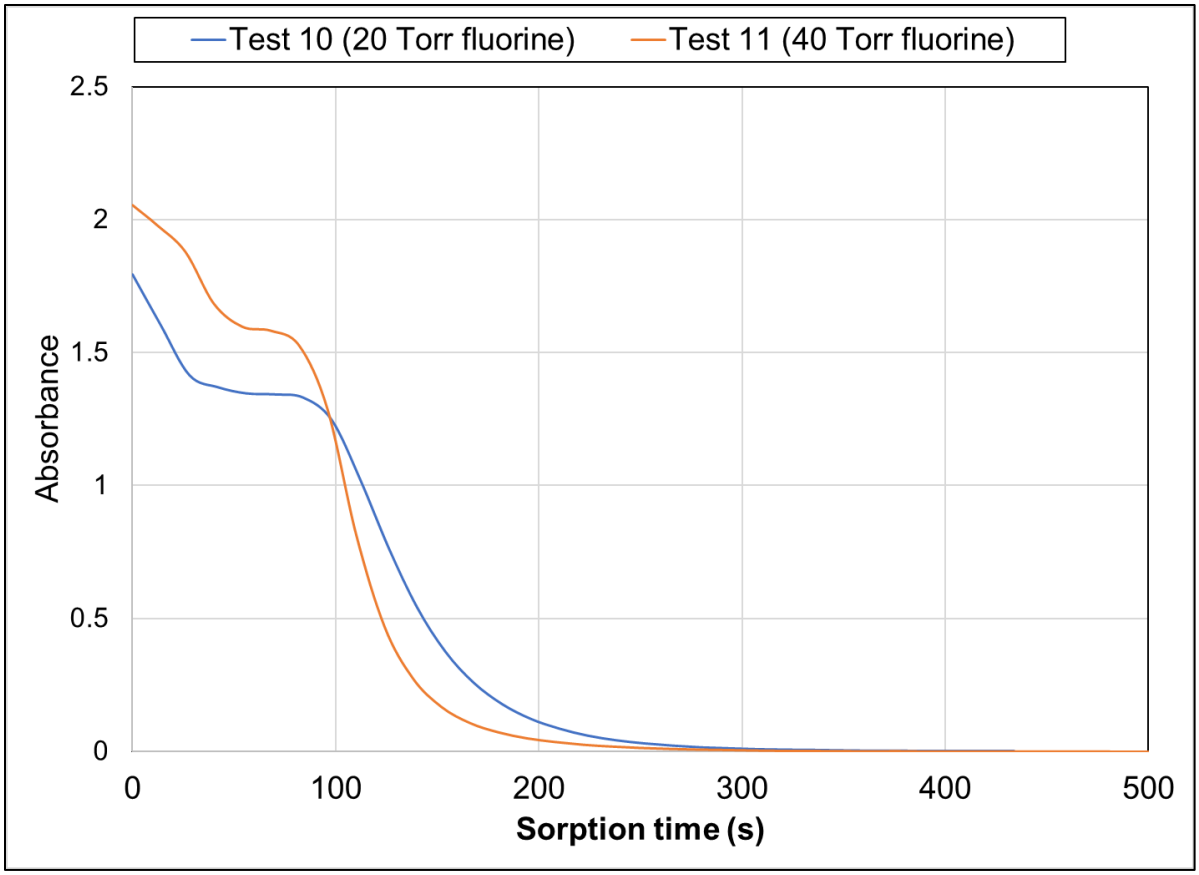


Figure 6-2. Sorption of TeF_6 by activated alumina at two different F_2 pressures.

Table 6-1: Free energies of reaction for selected TeF_6 and F_2 interactions with Cu.

Reaction	ΔG at 100°C (kcal)
$F_2(g) + Cu \rightarrow 2CuF$	-121.6
$F_2(g) + Cu \rightarrow CuF_2$	-115.6
$TeF_6(g) + Cu \rightarrow CuTe + 3F_2(g)$	291.7
$TeF_6(g) + 6Cu \rightarrow Te + 6CuF$	-66.4
$TeF_6(g) + 3Cu \rightarrow 3CuF_2 + Te$	-48.4
$TeF_6(g) + Cu \leftrightarrow TeF_4(g) + CuF_2$	-32.1
$TeF_6(g) + Cu \leftrightarrow TeF_4(s) + CuF_2$	2.7

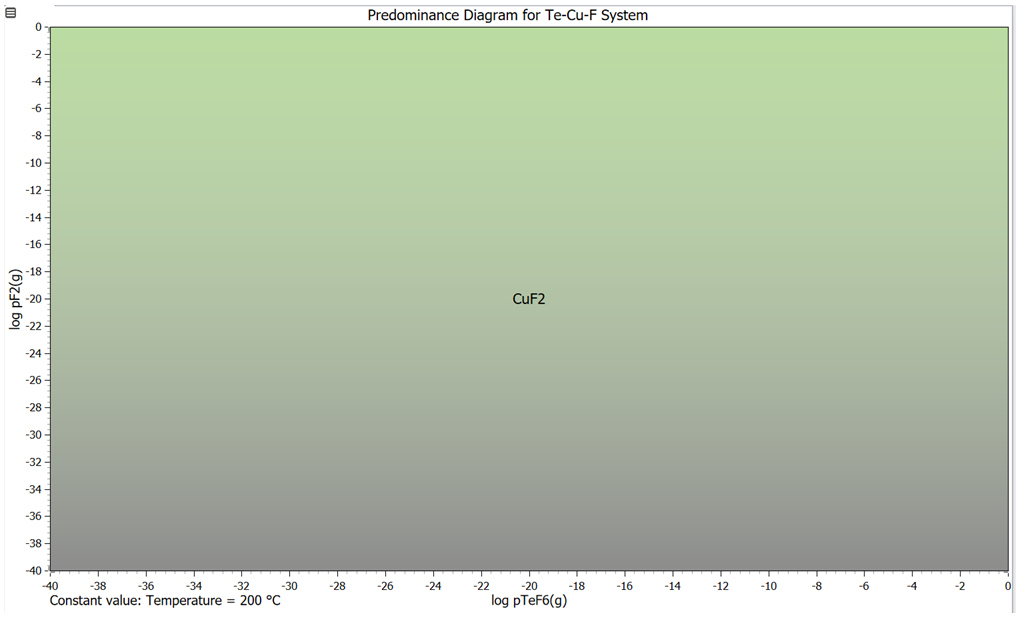


Figure 6-3: Predominance diagram for the Cu-Te-F system at 200°C.

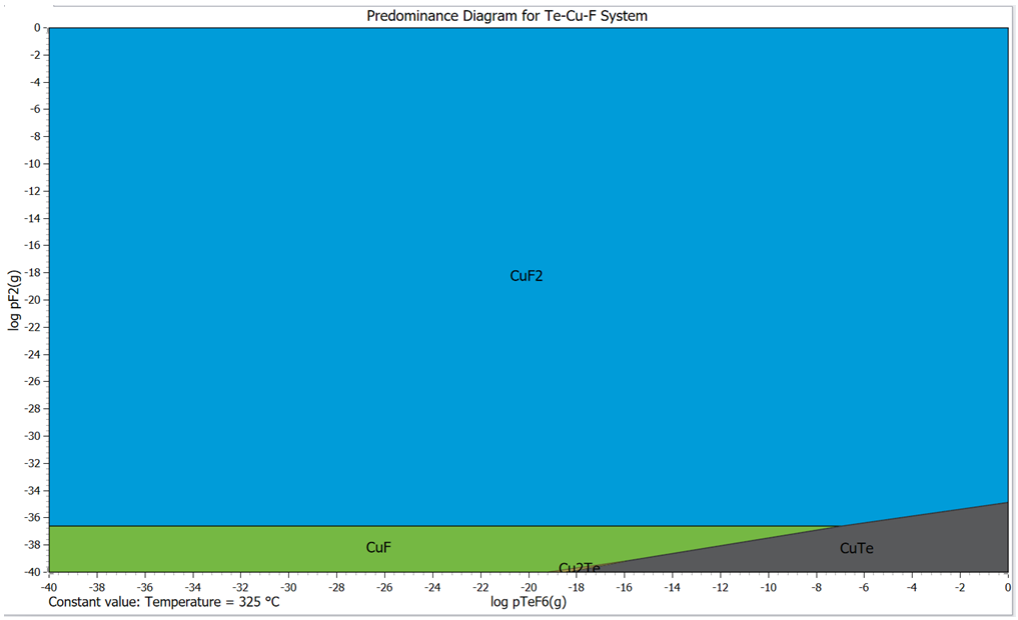


Figure 6-4. Predominance diagram for the Cu-Te-F system at 325°C.

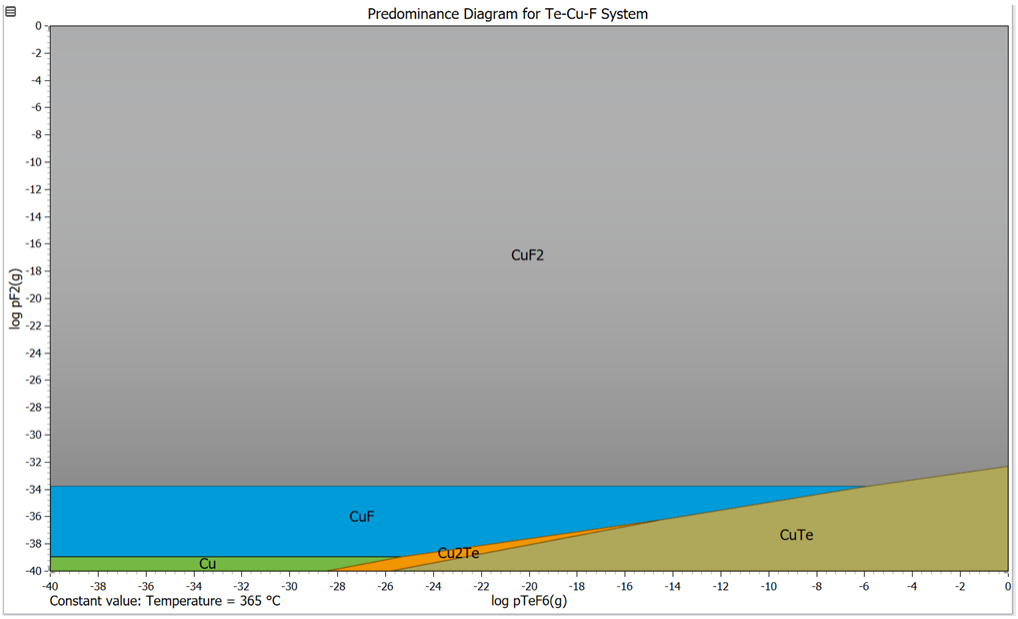


Figure 6-5: Predominance diagram for Cu-F-Te system at 365°C.

Scoping Test 1

This scoping test generated TeF_6 at 200°C and allowed the TeF_6 concentration to plateau. Once this occurred, the recirculating TeF_6/F_2 stream was passed through a copper sorbent bed while the total pressure of the system and the TeF_6 absorbance were monitored. The copper sorbent bed was ramped stepwise with hold times of about 10 min per step (50–335°C). The temperature profiles of the reactor and the copper sorbent tube are shown in Figure 6-6, and each temperature increment is designated with the letters A–K.

The system pressure dropped continuously during sorption testing, but the TeF_6 absorbance remained constant across all temperature steps. This indicates the sorption of F_2 with no sorption of TeF_6. For simplicity, only the FTIR scans for sorption phases A and K are shown in Figure 6-7, which reflect constant TeF_6 absorbances across the test duration.

Scoping Test 2

Based on the results of scoping test 1, it was hypothesized that the copper may have preferentially removed fluorine from the system, with the surface becoming passivated and prevented from interacting with TeF_6. A second scoping test was performed in which TeF_6 was condensed from the gas phase (refer to Section 4) and held in a sealed U-tube while the residual F_2/N_2 in the loop was removed through vacuum. Once the F_2 was removed the loop was refilled with N_2 and TeF_6 was released into the loop, creating a TeF_6/N_2 blend gas.

The copper trap was opened to the recirculation loop while at ambient temperature. The temperature of the copper trap was manually ramped to 367°C while absorbance of TeF_6 was monitored by FTIR. Results are provided in Figure 6-8 and show that at about 300°C, the measured absorbance of TeF_6 began to drop, presumably due to adsorption by the copper media. The temperature ramp continued and the final temperature of the copper sorbent trap was 367°C. TeF_6 adsorption was found to be relatively slow, taking nearly 50 minutes to completely be removed by the copper trap after the maximum temperature was reached.

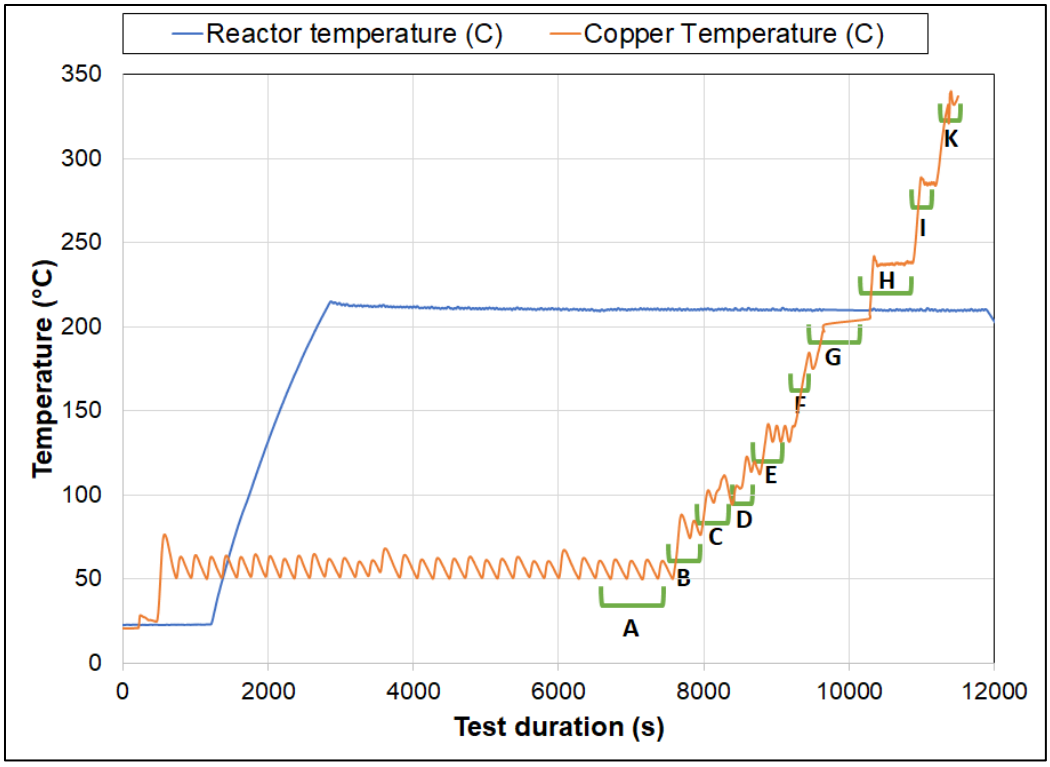


Figure 6-6. Temperature profiles of test 12 with each sorbent temperature hold noted as the letters A–K.

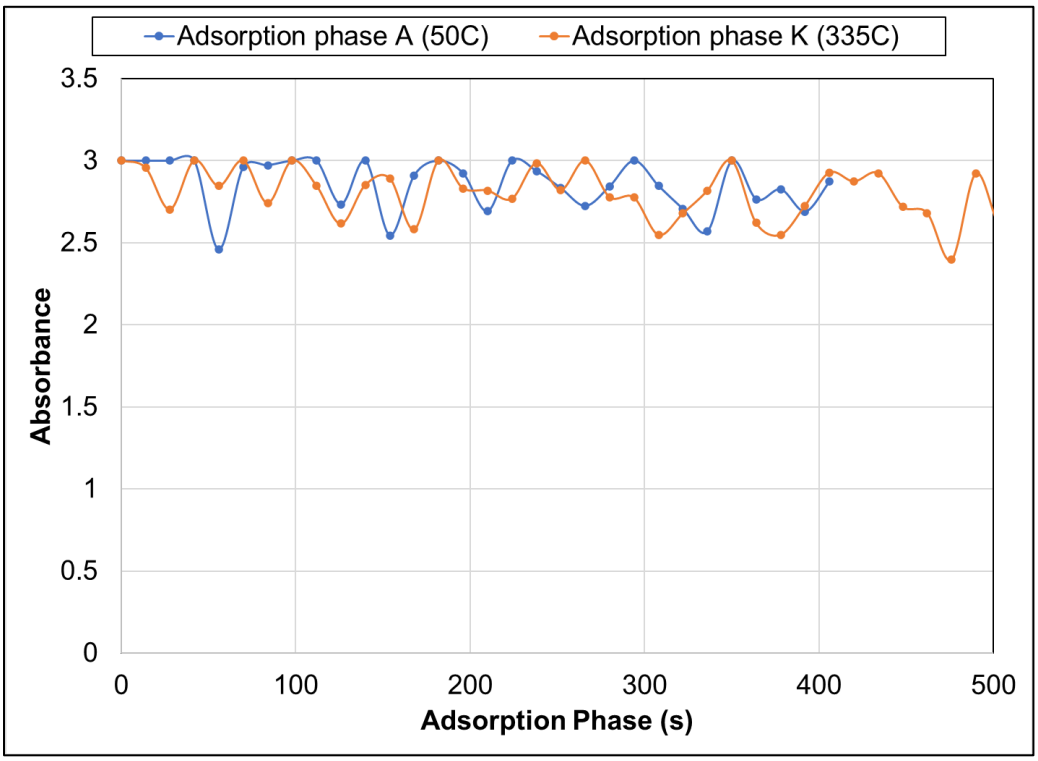


Figure 6-7. Comparison of TeF_6 absorbances during sorption phases A and K.

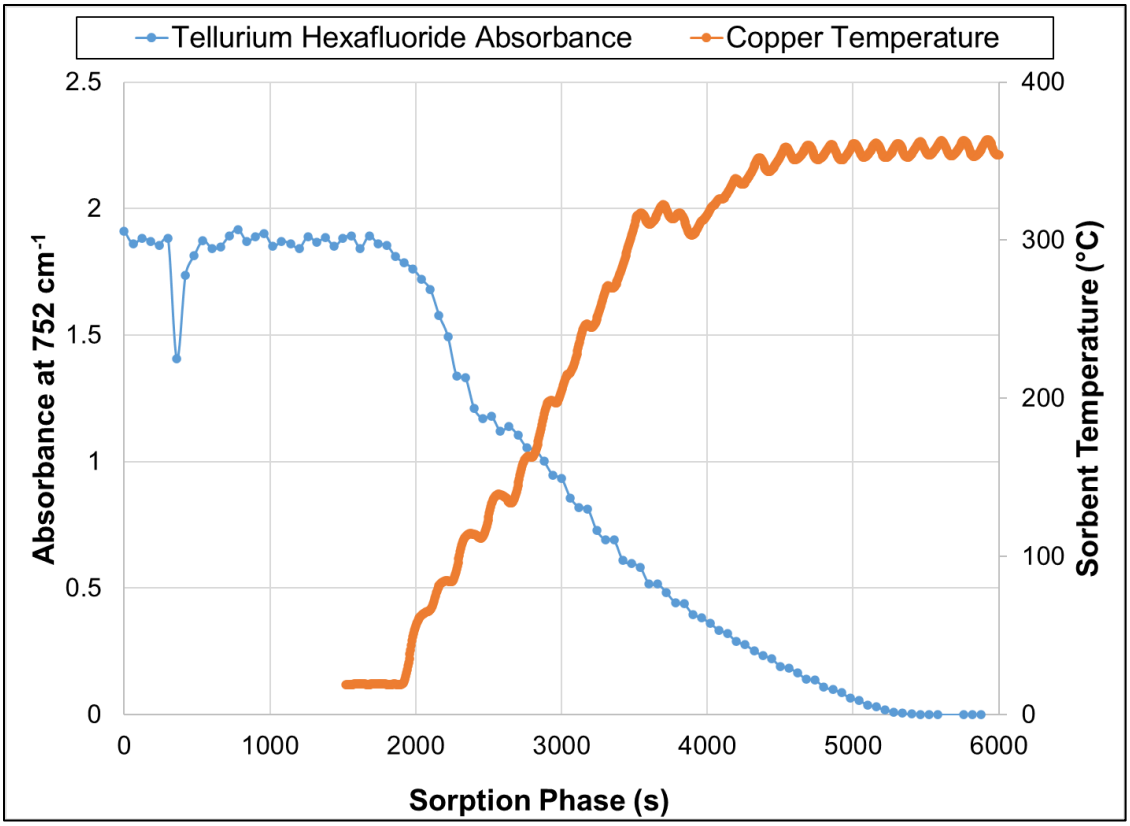


Figure 6-8: Temperature and absorption monitoring for Test 13.

Following testing, the copper was removed from the trap. It was noted that the Inconel (material used to build the trap) had a blue tint, but this is not uncommon with steels exposed to high temperatures. The copper removed from the trap was visually distinct from the copper recovered from Scoping Test 1. Fresh copper and exposed copper from both scoping tests are shown in Figure 6-9.

The results of Scoping Test 2 confirmed the hypothesis that copper is selective for F_2 over TeF_6 and that copper can sorb TeF_6 when F_2 is not present. Scoping Test 2 also confirmed thermodynamic predictions that Te-Cu interactions would be more predominant at higher temperatures, specifically over 300°C.

Scanning Electron Microscopy of Copper Material

Scanning electron microscopy (SEM) coupled with electron dispersion spectroscopy (EDS) was used to analyze the surface of the copper sorbent material before and after testing. The copper materials were not kept in an inert environment after removal from the sorbent tube, so the potential for oxygen interaction was not eliminated.

Fresh copper is compared to the copper recovered from sorbent Test 1 in Figure 6-10. It can be observed that morphology of the fluorine-exposed material is noticeably different than that of fresh copper, with small particles located on the surface of the material. Three spot EDS scans were performed on the fresh copper, showing it to be 100% copper (as expected). On the copper recovered from sorbent test 1, the main surface was found to be copper oxide using a single spot EDS scan. Three spot EDS scans found the formed particles to have an average composition of CuF. Two additional fluorine-exposed copper sorbent samples were analyzed, each with three spot scans. The findings were similar for all three sorbent samples.

A magnification of the surface particles is shown in Figure 6-11. These particles appear to be crystalline in nature.

The copper sorbent material recovered from Scoping Test 2 had a morphology similar to fresh copper (Figure 6-12).

Four particles were examined by SEM-EDS. On each of the first two particles, three spot scans were conducted showing that there was tellurium present on the material. On the second two particles, elemental surface maps were used to reflect a similar finding. The weight % of tellurium from each EDS spectrum is tabulated in Table 6-2.



Figure 6-9: Observe the difference between fresh copper (L), copper exposed to a mixed F_2/TeF_6 stream (middle), and a pure TeF_6 stream (R).

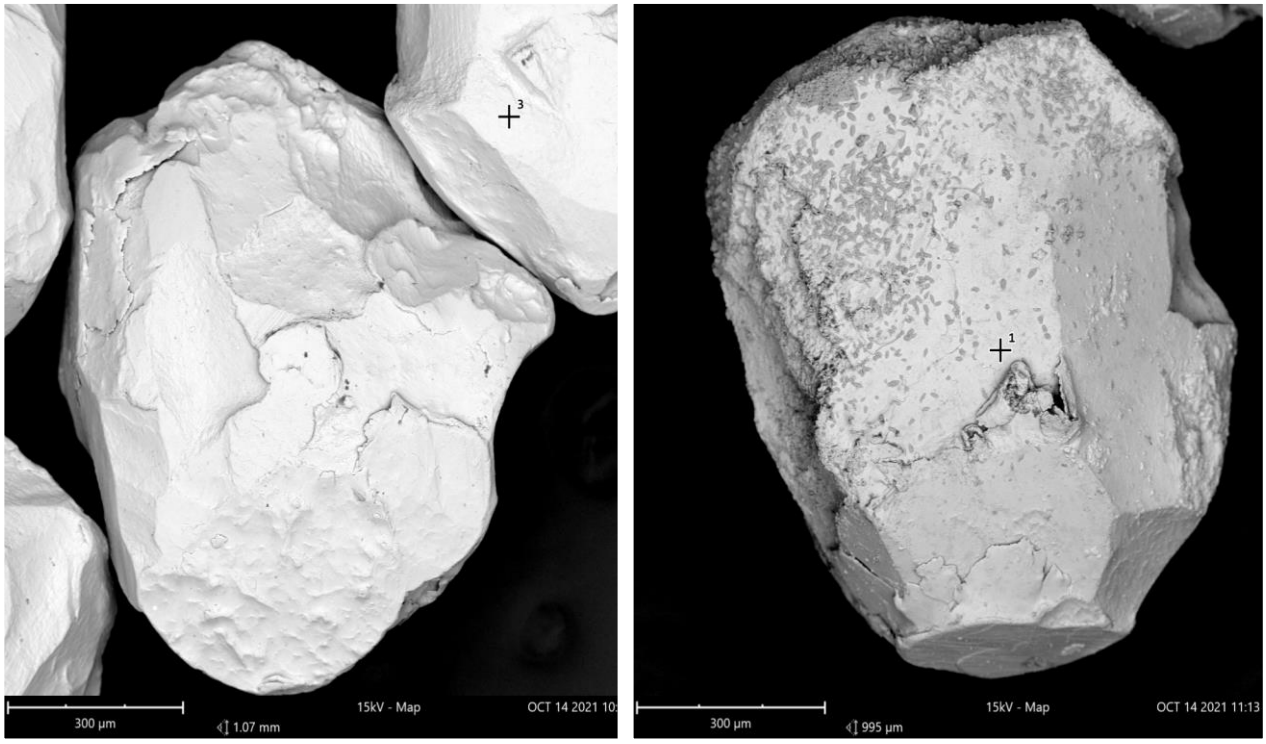


Figure 6-10: Scanning electron microscopy of fresh copper and fluorine-exposed copper.

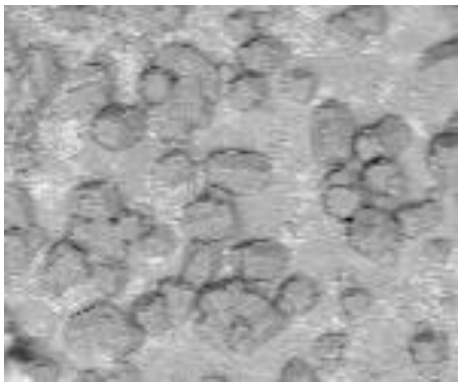


Figure 6-11: Granules formed on copper surface having an average composition of CuF.

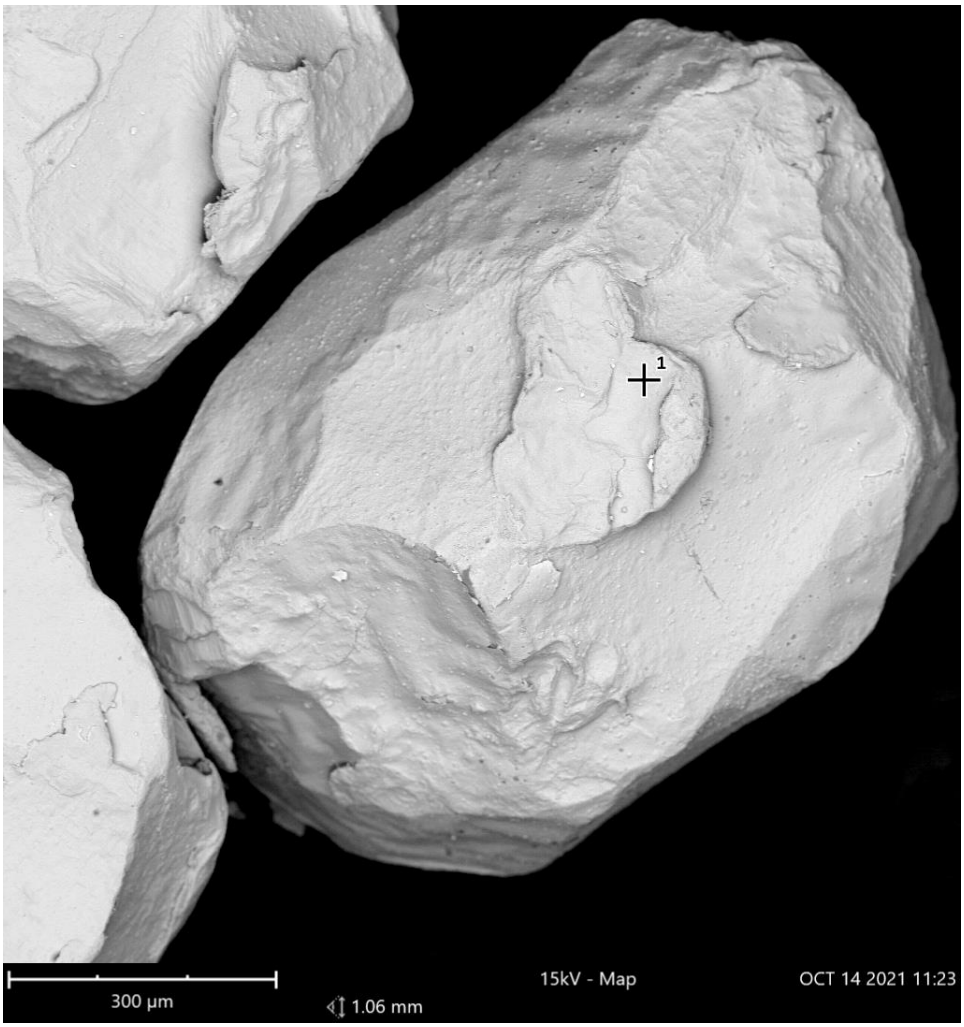


Figure 6-12: SEM of copper sorbent material recovered from Scoping Test 2.

Table 6-2: Tellurium surface concentration on copper sorbent material recovered from Scoping Test 2.

Sample-Spot	Te (weight %)
1-1	3.04
1-2	2.19
1-3	1.26
2-1	0.00
2-2	0.00
2-3	0.00
3-1 (map)	1.73
4-1 (map)	0.50
Average	0.81

The mapped areas used for Sample-Spot 3-1 and 4-1 are shown in Figure 6-13. It can be observed that there are perhaps small particles on the surface of the copper, but the sensitivity of the instrument did not allow for confirmation that these were tellurium-bearing. The EDS of the four samples was largely consistent in that (with the exception of Sample 2) they all showed single-weight percent tellurium on the surface of the copper. Generally, EDS detection limits are such that good practice dictates that numbers below 1 weight % should not be used quantifiably. However, the SEM-EDS performed on the Scoping Test 2 samples can be qualitatively used to confirm that tellurium was present on the samples and that copper does sorb TeF_6 from fluorine-free streams above 300°C.

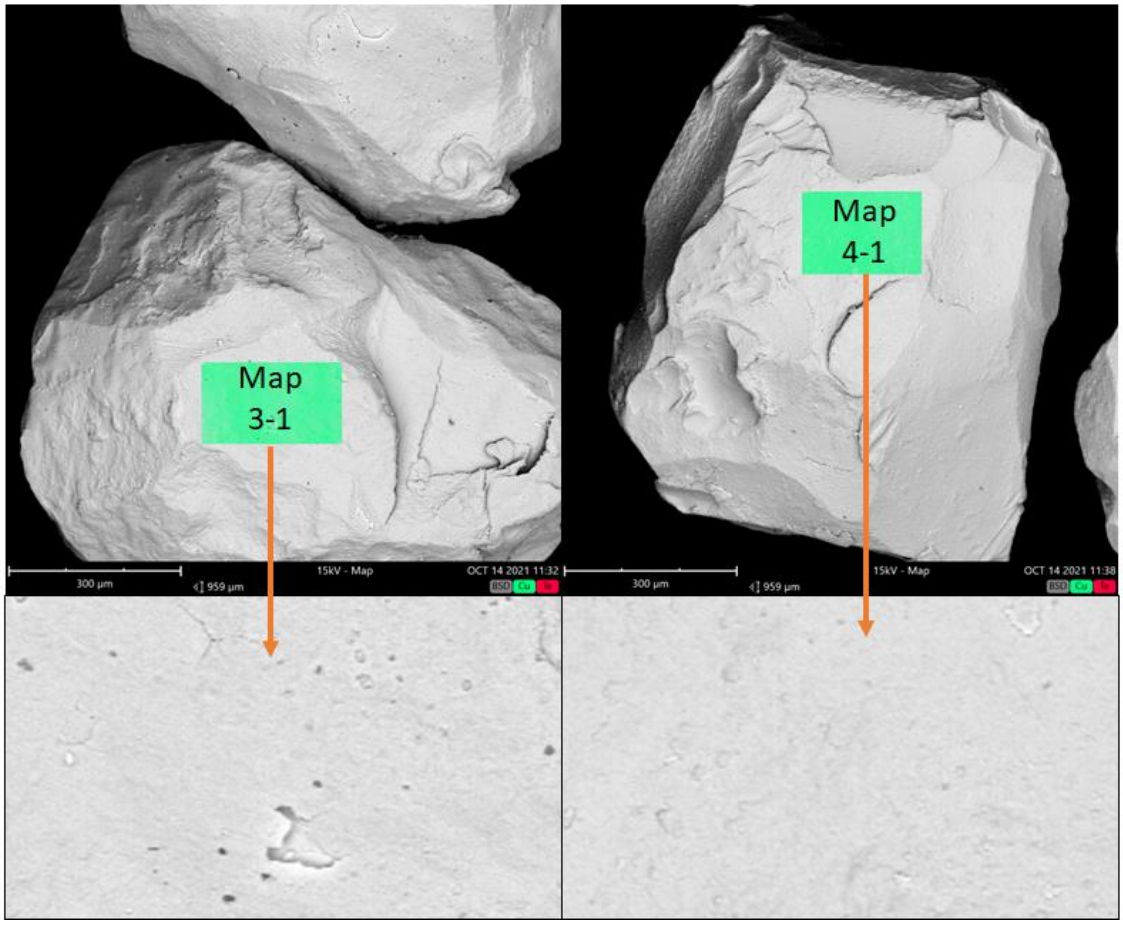


Figure 6-13: SEM of mapped areas for Scoping Test 2, samples 3 and 4.

CHAPTER SEVEN CONCLUSIONS

The experimental effort described here was intended to advance the management of fluoride volatility off-gases through development of TeF_6 production, measurement, and abatement technologies. These objectives were met through (1) the determination of the molar absorptivity coefficient for the primary infrared peak of TeF_6, (2) characterizing the production of TeF_6 from Te metal under varied temperature, particle size, and F_2 concentration, and (3) developing a better understanding of the removal of TeF_6 from a gas stream by copper and activated alumina.

TeF_6 has a primary v_3 stretching band with a wavelength of 752 cm^{-1}, allowing it to be measured through infrared spectroscopy. Although this band was identified decades ago, the only reported molar absorptivity coefficient present in the literature was very low and did not appear to reflect the strong absorptivity of the primary TeF_6 peak. This work systematically used the ideal gas law and Beer's Law to report a new molar absorptivity coefficient of 28.51 ± 1.35 cm^2 $Torr^{-1}$. This molar absorptivity coefficient will allow more accurate online monitoring of TeF_6 peaks across a suite of applications, including in the off-gas monitoring of molten salt-based nuclear reactors and in the off-gas monitoring of fluoride volatility processing.

TeF_6 was produced by the fluorination of Te metal across a temperature range of 100-250°C with a fluorine pressure of 20 Torr. Two particle sizes were used in testing and no significant change in reaction rate was observed for these different particle sizes under the experimental conditions used. When fluorine partial pressure was increased to 40 Torr, the reaction rate was too quick to be measured by this experimental system. It was observed that about 80% of the starting Te metal was converted and that this conversion rate was independent of reaction temperature. From a practical perspective, it can be assumed that nearly all Te will be favored to exist as TeF_6 under any realistic molten salt reactor or fluoride volatility conditions. However, the type of data collected here can help inform future research into TeF_6 chemistry and engineering applications; very little data is available in the literature that was helpful in understanding how to generate a steady TeF_6 source term for use in experimentation.

Finally, TeF_6 was found to be successfully removed from a gas stream by both activated alumina and copper. Sorption of TeF_6 by activated alumina was very fast and complete. In testing with activated alumina, TeF_6 was present in a gas blend with F_2 and N_2. Tests were performed with F_2 pressures of 20 and 40 Torr. No practical differences in TeF_6 sorption were observed across the two F_2 pressures used.

Thermodynamic calculations on the TeF_6-F_2-Cu system indicated that F_2 would preferentially form CuF_2 when copper was used as an sorbent. Experimental testing confirmed this, with no TeF_6 removal observed when a TeF_6/F_2 blend gas was passed through a heated copper sorbent column. However, these same thermodynamic calculations also indicated that the formation of CuTe could occur above 300°C. A second sorption test was conducted with TeF_6 present in N_2 (no F_2 present). TeF_6 was observed to be fully removed by copper when the sorbent was heated above 300°C. Sorption was slow, requiring 50 minutes for full TeF_6 removal. SEM of the discharged copper sorbent confirmed that Te was present on the copper surface.

These findings represent a substantial advancement in the body of knowledge surrounding TeF_6 measurement, production, and sorption. Future work should focus on several key areas. First, the molar absorptivity coefficient should be externally validated, with additional spectral deconvolution of TeF_6 and Te_2F_{10} as a goal. Second, using specialized instrumentation could facilitate direct measurement of Te during a fluorination reaction, allowing a formalized rate expression to be developed along with other key parameters, such as the activation energy of the fluorination reaction. Finally, work to identify a sorbent selective for TeF_6 over F_2 should be pursued; likely a size-based sieving could be a promising approach. These types of experiments will continue to provide the knowledge needed to effectively manage TeF_6 emissions within a fluorine-based nuclear fuel system.

LIST OF REFERENCES

Billo, E. J. (2007). *Excel for scientists and engineers: numerical methods*. John Wiley & Sons.

Bresee, J. C., & Larson, P. R. (1957). Continuous Cold Trap for Fluoride Volatility Processing of Uranium. *Industrial & Engineering Chemistry*, *49*(9), 1349-1354.

Campbell, R., & Robinson, P. L. (1956). 668. The fluorination of tellurium. Ditellurium decafluoride and tellurium oxyfluorides. Journal of the Chemical Society (Resumed), 3454-3458.

Clark, R. A., McNamara, B. K., Barinaga, C. J., Peterson, J. M., Govind, N., Andersen, A., ... & Ballou, N. E. (2015). Electron ionization mass spectrum of tellurium hexafluoride. *Inorganic chemistry*, *54*(10), 4821-4826.

Collins, E. D., et al. *State-of-the-Art Report on the Progress of Nuclear Fuel Cycle Chemistry* (No. NEA--7267). Organisation for Economic Co-Operation and Development. 2018

Davis, M. E., & Davis, R. J. (2012). *Fundamentals of chemical reaction engineering*. Courier Corporation.

Fedunik-Hofman, L., Bayon, A., & Donne, S. W. (2019). Kinetics of solid-gas reactions and their application to carbonate looping systems. *Energies*, *12*(15), 2981.

Fukasawa, T., Hoshino, K., Watanabe, D., & Sasahira, A. (2020). Application of fluoride volatility method to the spent fuel reprocessing. *Journal of Nuclear Science and Technology*, *57*(1), 49-56.

Harrison, J. J. (2020). New infrared absorption cross sections for infrared limb sounding of sulfur hexafluoride. *Journal of Quantitative Spectroscopy and Radiative Transfer*, *254*, 107202.
Haynes, W. M. (2016). *CRC Handbook of chemistry and physics: A ready reference book*. CRC Press: Boca Raton, FL, USA.

Homma, S., Ogata, S., Koga, J., & Matsumoto, S. (2005). Gas–solid reaction model for a shrinking spherical particle with unreacted shrinking core. *Chemical Engineering Science*, *60*(18), 4971-4980.

Komaki, Y., M. Iwasaki, and S. Tsujimura. “Removal of Volatile Tellurium Fluoride in Low Concentrations by Activated Alumina.” *Journal of Nuclear Science and Technology* 10, no. 6 (1973): 385–387.

McDowell, R. S., R. F. Holland, W. H. McCulla, G. K. Anderson, and M. J. Reisfeld. “Infrared Spectroscopy of TeF_6.” *Journal of Molecular Structure* 145, no. 3-4 (1986): 243–256.

Milford, R. P. (1957). Engineering design features of the ORNL fluoride volatility pilot plant. (No. CF-57-4-18). Oak Ridge National Lab. (ORNL), Oak Ridge, TN (United States).

Outotec, H. S. C. “Chemistry Software.” Version 9, 1974–2018.

Shimanouchi, T. (1973). *Tables of molecular vibrational frequencies*. US Government Printing Office.

Steindler, M., and Vissers, D. (1966). Laboratory investigations in support of fluid-bed fluoride volatility processes. Part X- A literature survey on the properties of tellurium, its oxygen and fluorine compounds (Physical and chemical properties of tellurium, tellurium oxides, tellurium fluorides, and tellurium oxyfluorides for use in support of fluid bed fluoride volatility processes). ANL-7142, Argonne National Laboratory.

Uhlíř, J., Mareček, M., & Škarohlíd, J. (2012). Current progress in R&D of fluoride volatility method. *Procedia Chemistry*, *7*, 110-115.

Vissers, D. R., and M. J. Steindler. “Removal of Tellurium Hexafluoride from Gaseous Systems by Solid Reagents.” *Industrial & Engineering Chemistry Process Design and Development* 7, no. 4 (1968): 496–502

Vissers, D. R., M. J. Steindler, and J. T. Holmes. 1970. Tellurium hexafluoride removal method. US Patent 3,491,513, filed October, 22, 1970, and issued January 27, 1970.

Vyazovkin, S; Wight, C. A. Kinetics in solids. Annu. Rev. Phys. Chem. 1997, 48, 125–149.

Watanabe, D., Kani, Y., Sasahira, A., Hoshino, K., & Kawamura, F. (2016). Experimental study on elemental behaviors in fluorination of nuclear spent fuel with flame reactor. *Journal of Nuclear Science and Technology*, *53*(4), 513-520.

Wright, M. R. (2005). *Introduction to chemical kinetics*. John Wiley & Sons.

CHAPTER EIGHT APPENDIX A: REACTION DATA

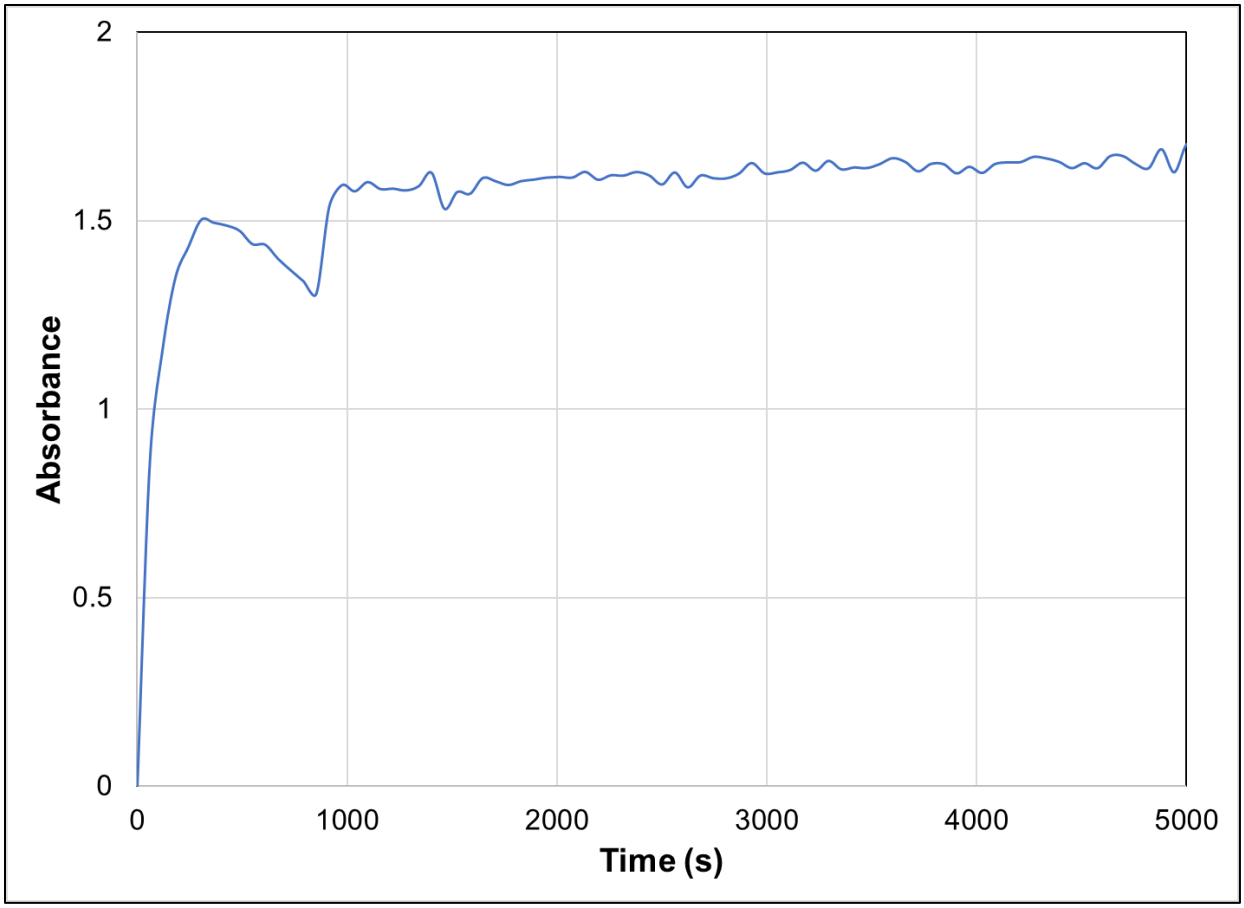


Figure 8-1: Test 3 measured absorbance at 752 cm^{-1} across test duration.

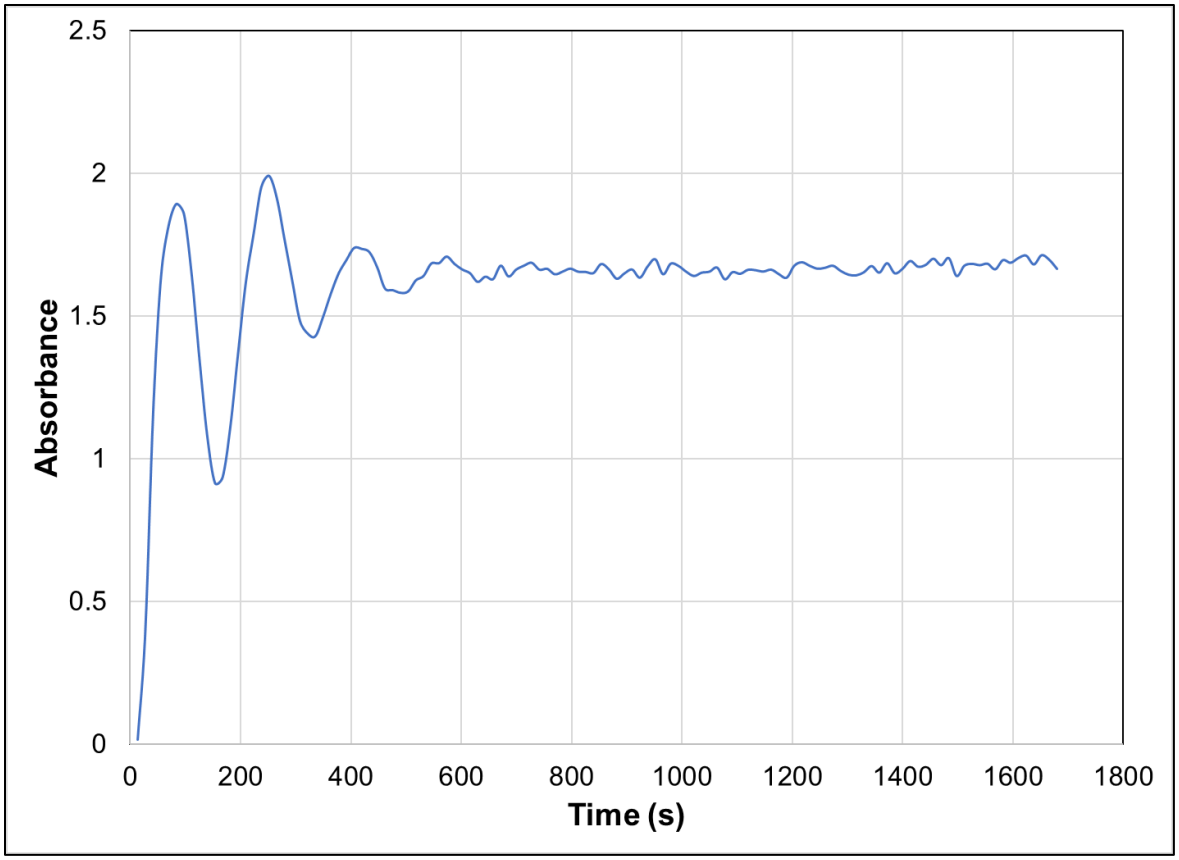


Figure 8-2: Test 4 measured absorbance at 752 cm^{-1} across test duration.

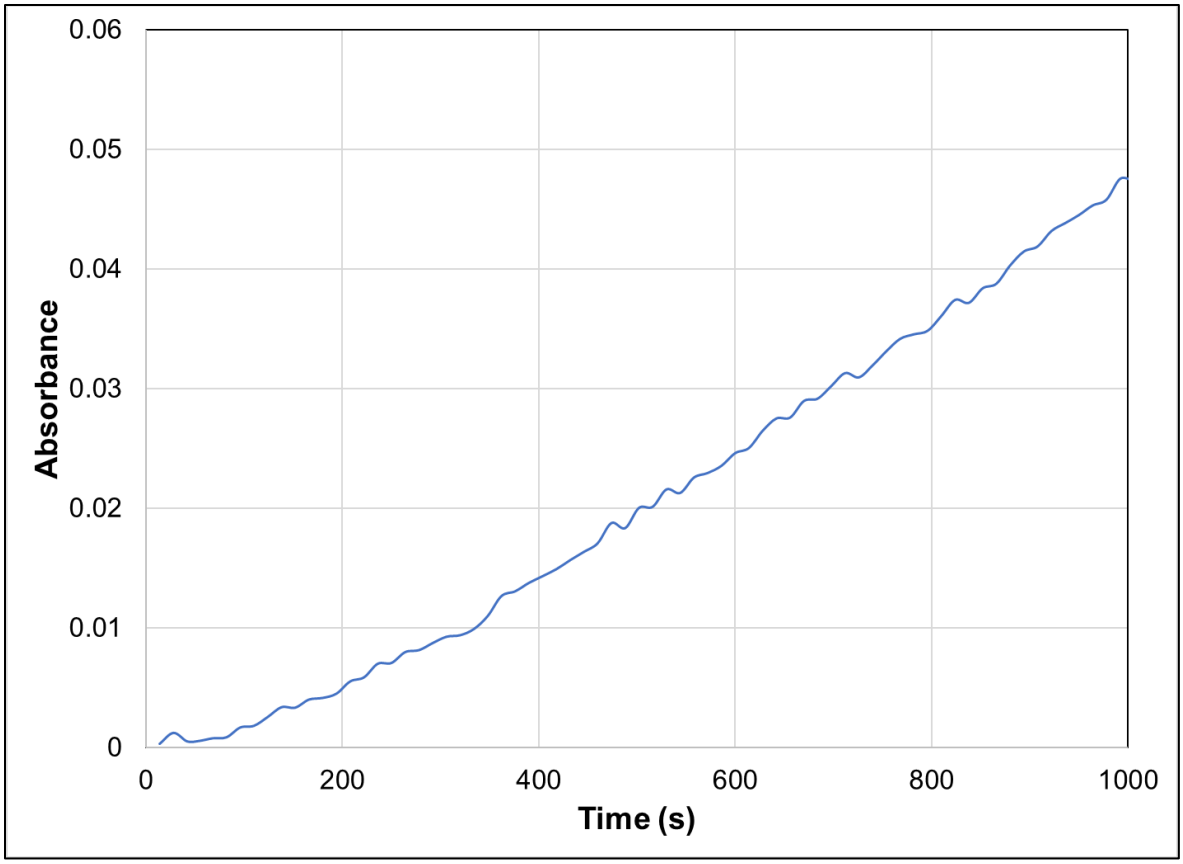


Figure 8-3: Test 5 measured absorbance at 752 cm^{-1} across test duration.

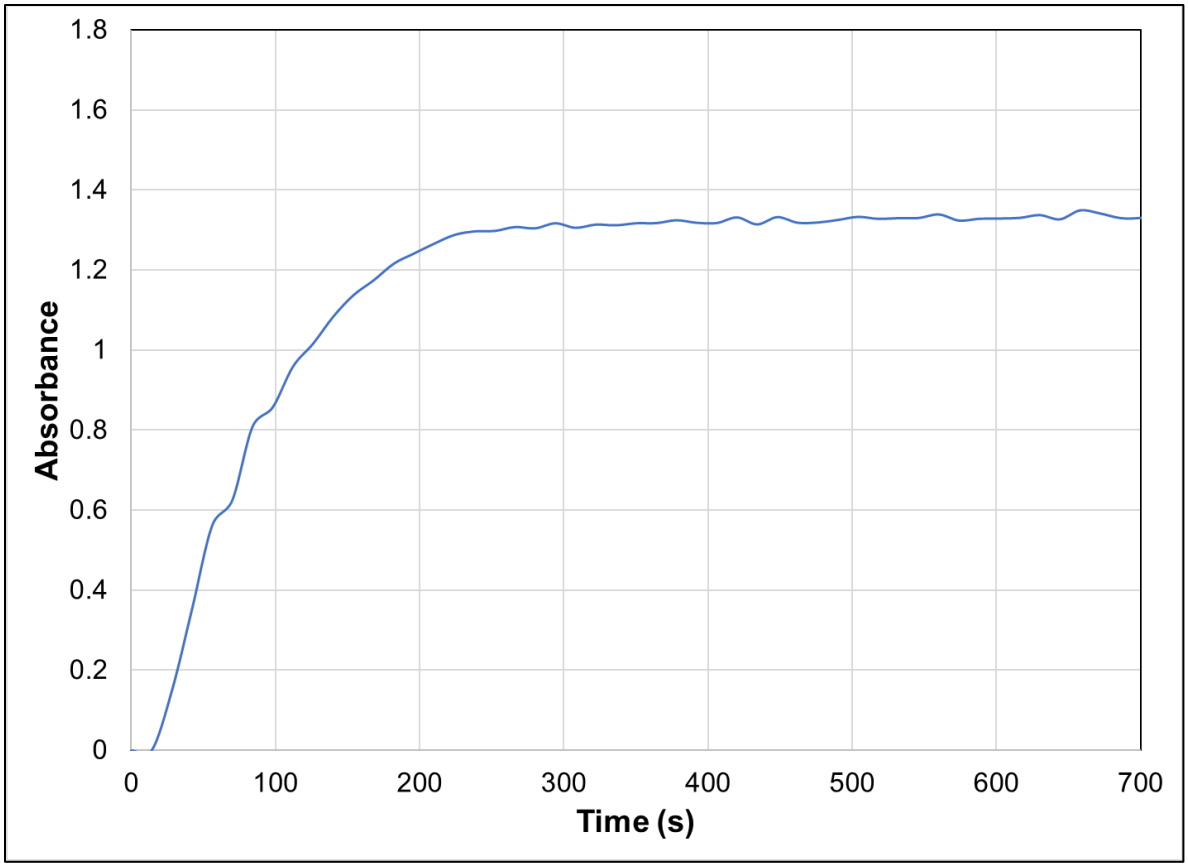


Figure 8-4: Test 6 measured absorbance at 752 cm^{-1} across test duration.

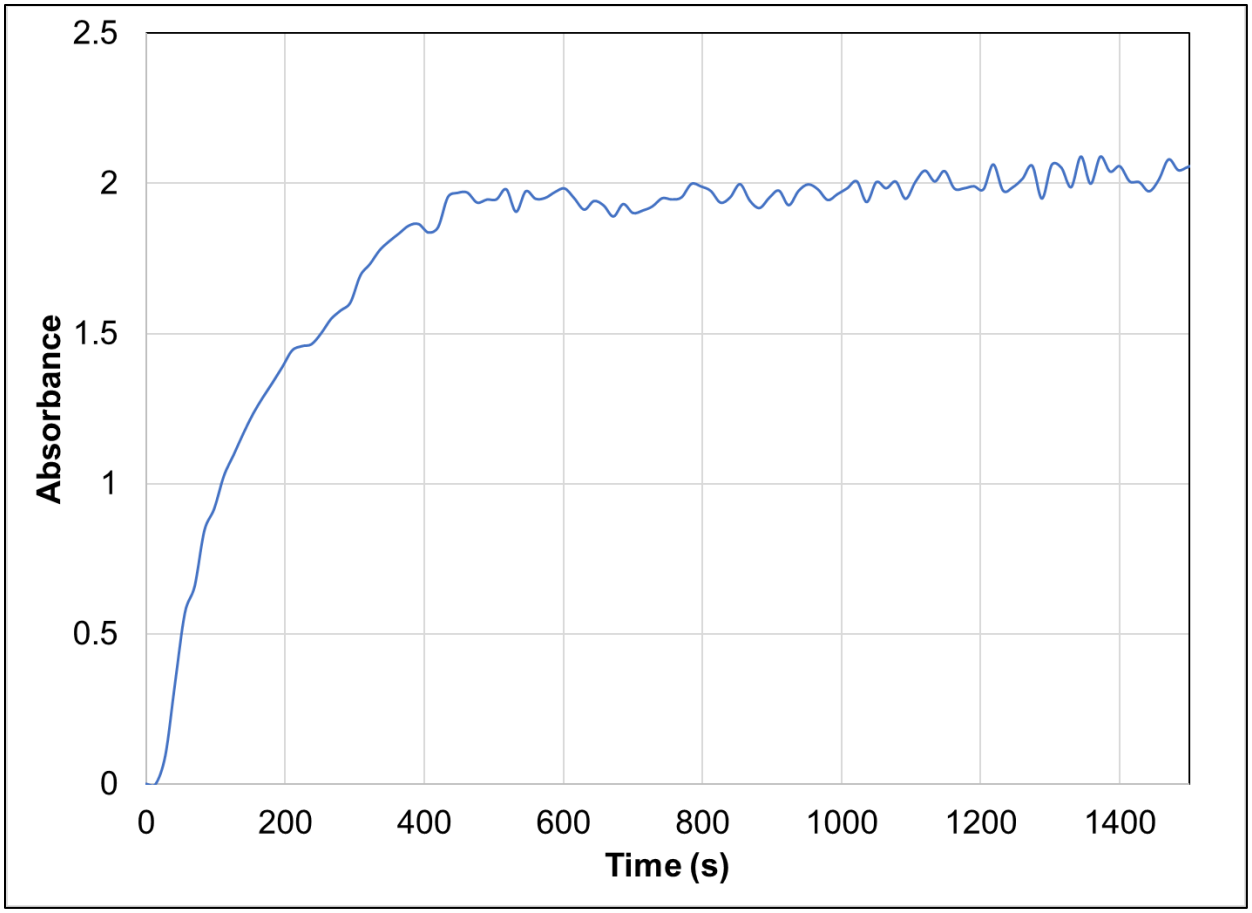


Figure 8-5: Test 7 measured absorbance at 752 cm^{-1} across test duration.

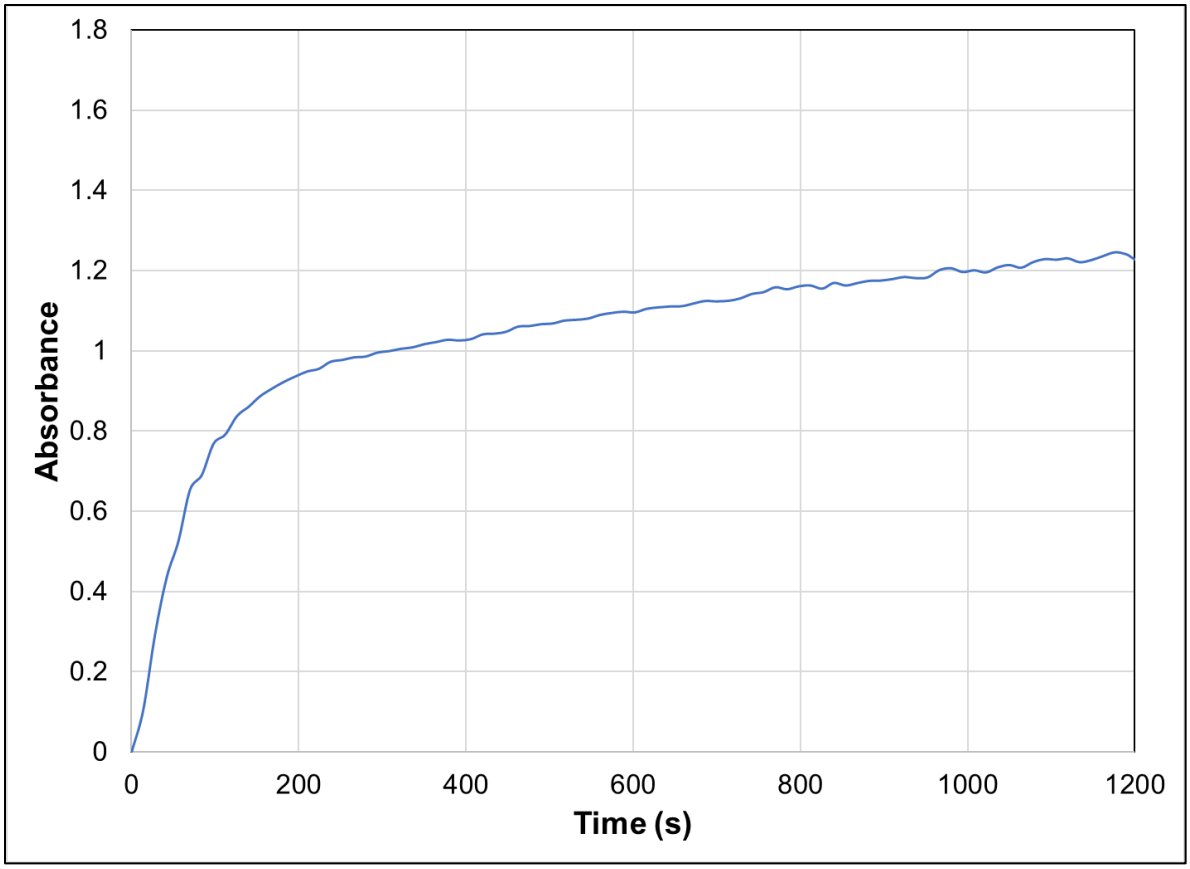


Figure 8-6: Test 8 measured absorbance at 752 cm^{-1} across test duration.

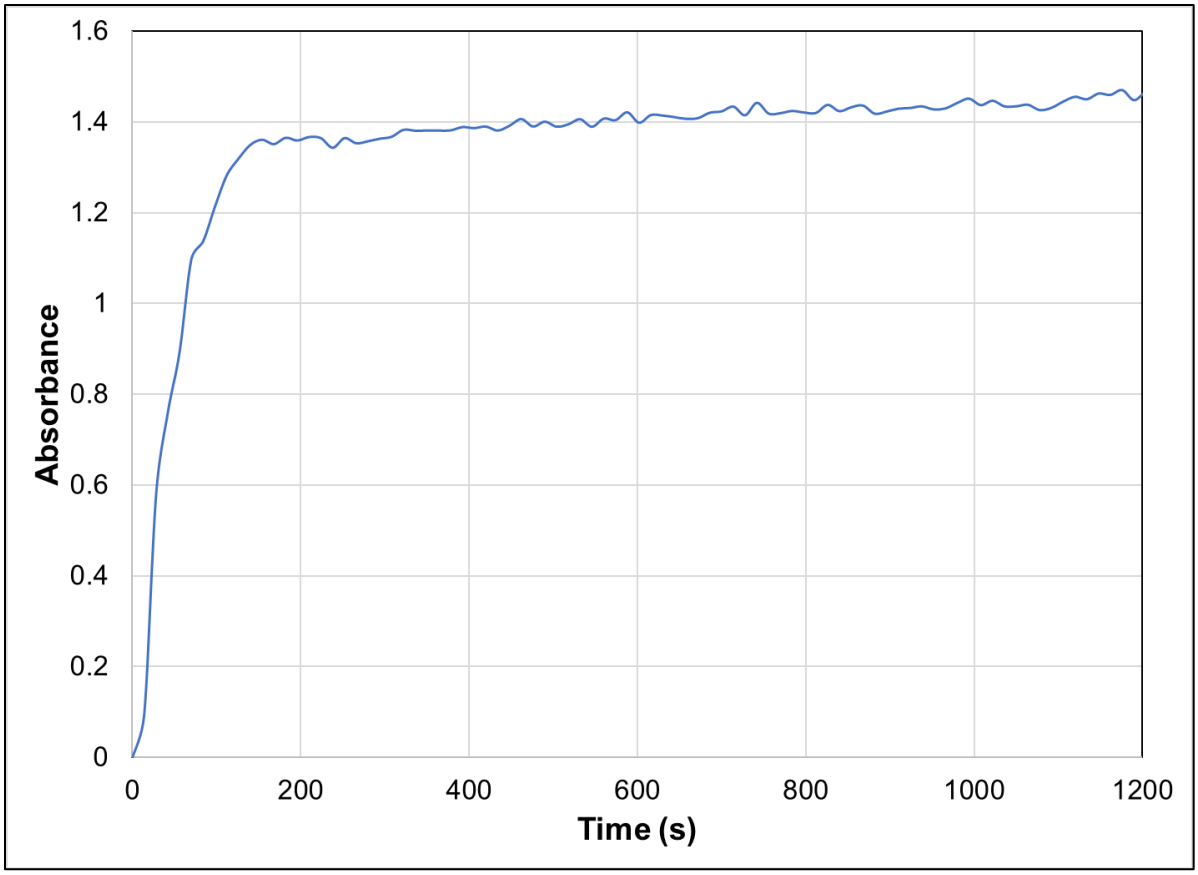


Figure 8-7: Test 9 measured absorbance at 752 cm^{-1} across test duration.

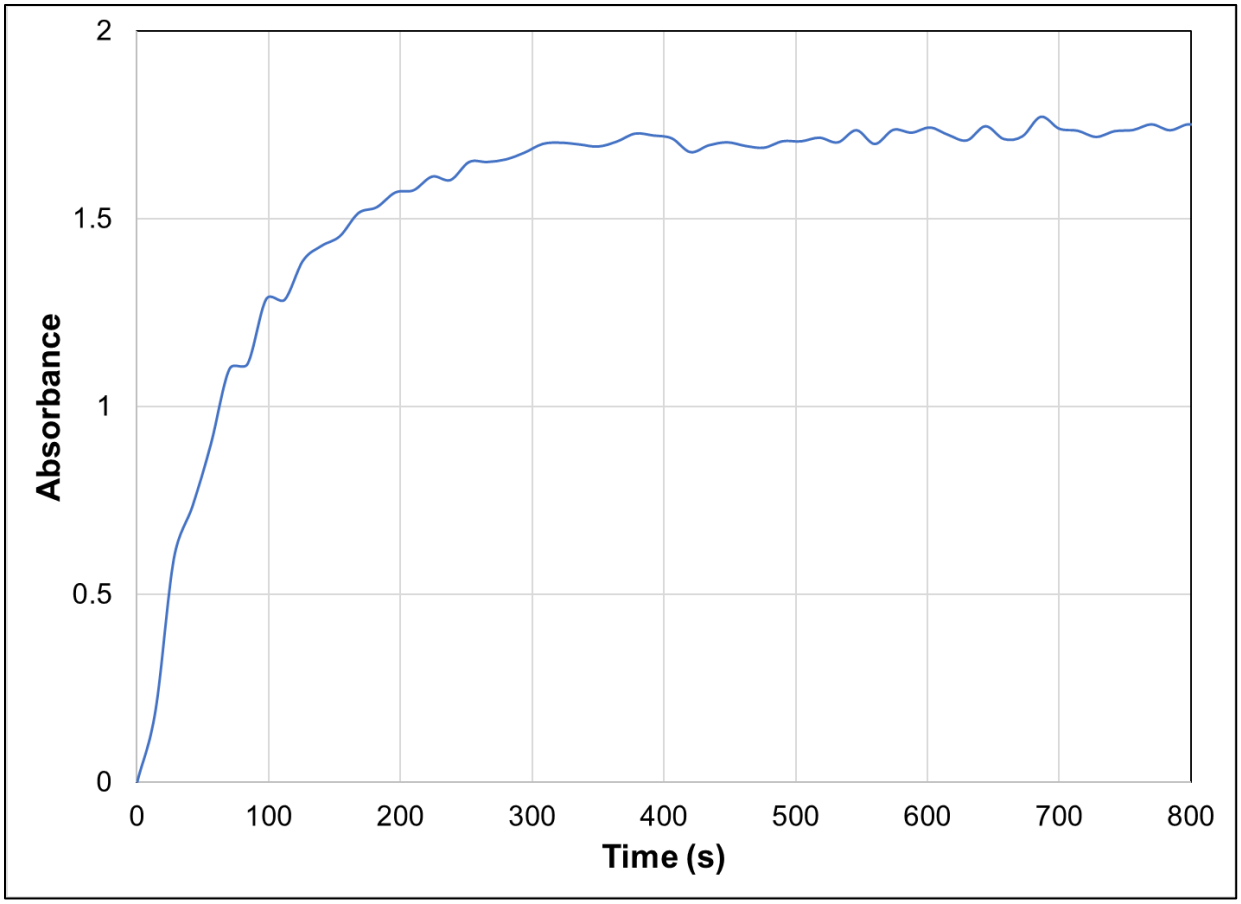


Figure 8-8: Test 10 measured absorbance at 752 cm^{-1} across test duration.

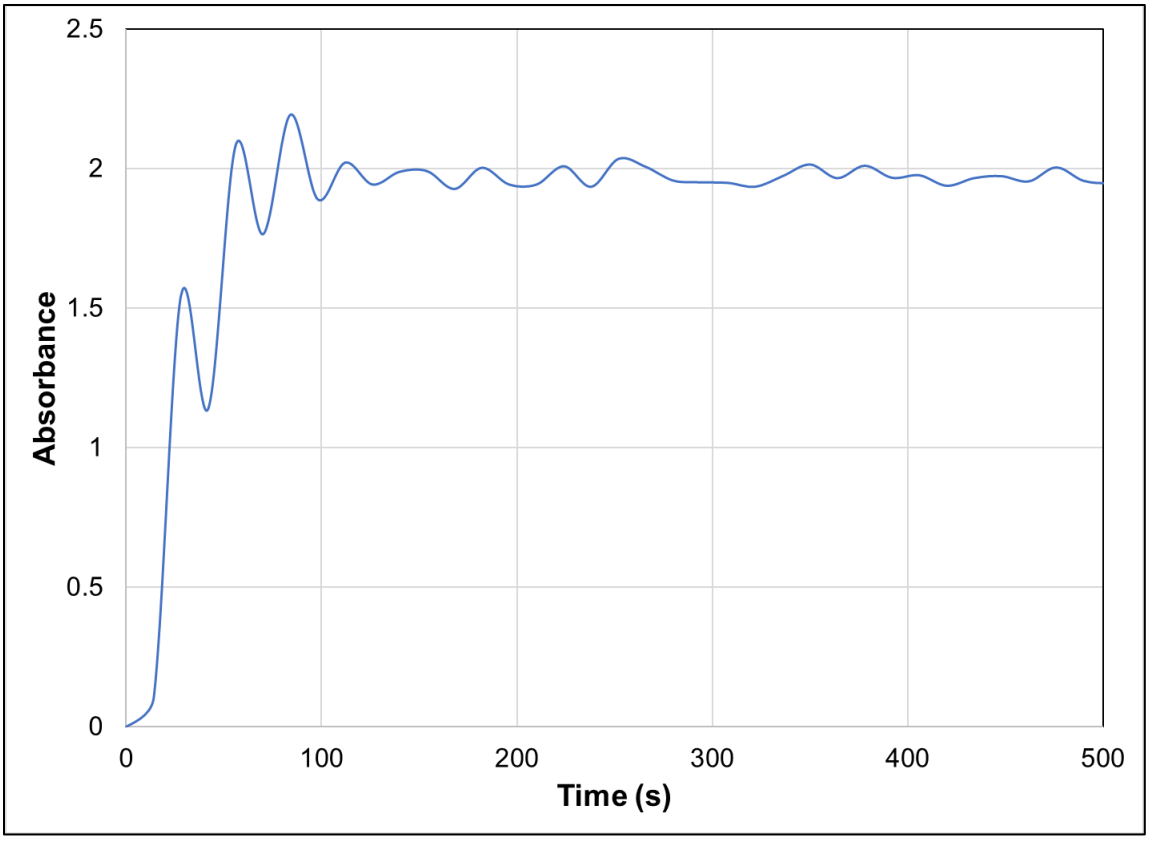


Figure 8-9: Test 11 measured absorbance at 752 cm^{-1} across test duration.

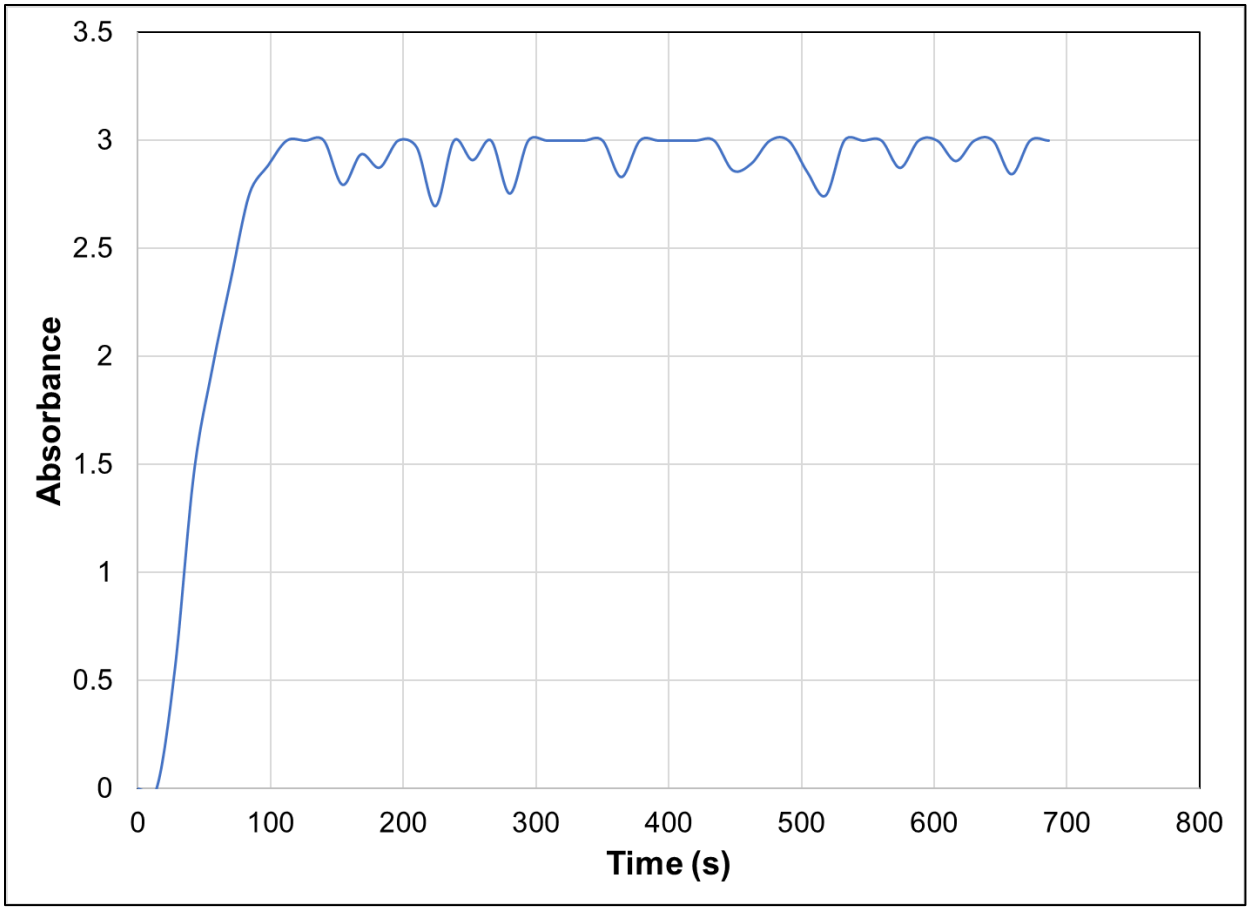


Figure 8-10: Test 12 measured absorbance at 752 cm^{-1} across test duration.

VITA

Stephanie Holbrook Bruffey received a B.S. in Chemistry from Tennessee Technological University in 2007, and a M.S. in Chemistry from Washington State University in 2009. Stephanie has 12 years of research and development experience, with an emphasis on the processing and disposition of spent nuclear fuel. Stephanie is especially recognized for her contributions in the field of radioactive off-gas management.